

# **Investigating the role of nuclear BNIP3 in regulation of cellular proliferation**

by

**Amandeep Singh**

A Thesis submitted to the Faculty of Graduate Studies of  
The University of Manitoba  
in partial fulfillment of the requirements of the degree of

**Master of Science**

Department of Biochemistry and Medical Genetics  
University of Manitoba  
Winnipeg, Manitoba

Copyright © 2018 by Amandeep Singh

## **Abstract**

BNIP3 is a member of BCL-2 family of cell death regulating proteins. When overexpressed in the cytoplasm under stress conditions such as hypoxia, BNIP3 localizes to the mitochondria and promotes cell death through mitochondrial dysfunction. Moreover, cytoplasmic (and mitochondrial) BNIP3 has also been shown to promote autophagy and autophagic cell death. However, when expressed in the nucleus, BNIP3 promotes cell survival by inhibiting transcription of certain cell death proteins. Interestingly, *Bnip3*-knockout mice show increased cellularity in the brain. Cell proliferation studies on MEF, primary mouse astrocytes and HEK293 cells confirmed that cells lacking BNIP3 are more proliferative than cells expressing nuclear BNIP3, indicating a novel role of nuclear BNIP3 in regulating cell proliferation. Furthermore, cells lacking BNIP3 also show increased activation of RAS-MAPK cell proliferation pathway, as well as increased expression of cell cycle proteins, Ki67 and Cyclin D1. Investigations into the mechanism through which BNIP3 may affect proliferation identified three target genes, however their expression differences between cells expressing or lacking BNIP3 were inconclusive. In summary, nuclear expression of BNIP3 plays a role in repressing cell proliferation.

“Never give up on a dream just because of the time it will take to accomplish it. The time will pass anyway.”

— Earl Nightingale

## Acknowledgements

I would first like to thank my supervisor, Dr. Spencer Gibson, for providing me the opportunity to join his lab as a graduate student and his continued mentorship, guidance and support at every stage throughout my graduate training. I am also very grateful for his understanding and support of my career goals.

I would also like to thank my committee members, Dr. Tamra Werbowetski-Ogilvie and Dr. Sachin Katyal, for their guidance, time, constructive criticism and help during my graduate training. They went above and beyond in their help with the progress of this research.

I am also grateful for the welcoming and friendly environment in the Gibson lab. I would like to thank Elizabeth Henson, my lab manager and cheerleader for teaching me all the lab techniques, for her enthusiasm and encouragement no matter how many times the experiments failed, and for sharing my interest in video games. I would like to thank all the past and present members of the Gibson lab as well. I have learned a lot from everyone, and have shared great memories over the years. I am thankful for all the great people I have met and friends I have made during this journey.

A special thanks to Chris Taylor from Central Animal Care Services for his help with maintaining the mice required for this research (and sorry for making you work overtime Chris). I would also like to thank the Katyal lab for their help with reagents and equipment used in this research.

I would also like to acknowledge the financial support from NSERC through studentship funding and University of Manitoba through GETS funding.

Finally, I would also like to thank my family and friends for their continued love, support and encouragement. This was all so much easier with them and I could not have done this without them.

# Table of Contents

---

Abstract .....	i
Acknowledgements .....	iii
Table of Contents .....	iv
List of Tables.....	viii
List of Figures .....	ix
List of Abbreviations.....	x

<b>Chapter 1: Introduction .....</b>	<b>1</b>
1.1 Cell fate .....	1
1.1.1 Cell proliferation .....	1
1.1.2 Regulation of cell cycle.....	4
1.1.2.1 Cell cycle transition through different phases.....	4
1.1.2.2 Cell cycle checkpoints .....	6
1.1.3 Cell cycle regulation and Cancer .....	9
1.1.4 Programmed cell death (apoptosis).....	10
1.1.4.1 Extrinsic pathway.....	11
1.1.4.2 Intrinsic pathway.....	12
1.1.5 Necrotic and Autophagic cell death .....	14
1.2 BCL-2 family of proteins .....	15
1.2.1 Pro-survival/anti-apoptosis BCL-2 family proteins .....	15
1.2.2 Multi-domain Pro-apoptotic BCL-2 family proteins .....	15
1.2.3 BH3-domain only BCL-2 family proteins .....	16
1.2.3.1 BNIP subfamily of BH3-only proteins .....	17
1.2.4 BCL-2 family proteins in development.....	18
1.2.5 BCL-2 family members in Cancer .....	19
1.3 BNIP3.....	19
1.3.1 BNIP3 structure .....	19
1.3.2 Regulation of BNIP3.....	22
1.3.2.1 Induction of <i>Bnip3</i> .....	22
1.3.2.2 Repression of <i>Bnip3</i> .....	24
1.3.2.3 Post-translational modification of BNIP3 .....	24

1.3.2.4 Degradation of BNIP3 .....	25
1.3.2.5 Subcellular localization of BNIP3 .....	25
1.4 Functions of BNIP3.....	25
1.4.1 Mechanism of BNIP3-mediated mitochondrial dysfunction .....	26
1.4.2 BNIP3-mediated cell death .....	27
1.4.2.1 BNIP3-mediated apoptosis .....	27
1.4.2.2 BNIP3-mediated necrosis .....	27
1.4.2.3 BNIP3-mediated autophagy .....	28
1.4.3 Nuclear BNIP3 and its role in transcriptional repression.....	30
1.4.4 BNIP3 in human diseases .....	31
1.4.4.1 BNIP3 in myocardial infarction .....	32
1.4.4.2 BNIP3 in cancer .....	32
1.4.5 BNIP3 in development.....	33
1.5 Thesis Rationale, Hypothesis and Aims.....	36
1.5.1 Rationale .....	36
1.5.2 Hypothesis.....	36
1.5.3 Research Aims and Objectives .....	37
<b>Chapter 2: Material and Methods .....</b>	<b>38</b>
2.1 Reagents .....	38
2.2 Cell culture .....	38
2.2.1 Mouse embryonic fibroblasts.....	38
2.2.2 Primary mouse astrocytes .....	38
2.2.3 Human embryonic kidney cells, HEK293 .....	39
2.2.4 Cell culture plates and flasks .....	39
2.2.5 Cell passaging .....	39
2.2.6 Cell preservation .....	40
2.2.7 Thawing and culturing of frozen cells .....	40
2.2.8 Incubation in hypoxia.....	40
2.3 Western blot .....	41
2.3.1 Preparation of protein lysates.....	41
2.3.2 Protein Quantification, Gel Electrophoresis and Western Blotting .....	42

2.4 Reverse Transcription and Quantitative Real-time Polymerase Chain Reaction (RT-qPCR) .....	45
2.5 Cell proliferation assays .....	46
2.5.1 Edu cell proliferation assay and Flow cytometry analysis .....	46
2.5.2 Real time cellular analysis (RTCA) .....	47
2.5.3 Cytation 5 cell counting .....	48
2.6 Site-directed mutagenesis.....	49
2.7 Transient <i>Bnip3</i> overexpression in HEK293 cells .....	51
2.9 Wildtype and <i>Bnip3</i> -null mice .....	51
2.9.1 Genotyping.....	51
2.9.2 Isolation of embryonic fibroblasts .....	52
2.9.3 Isolation of primary astrocytes.....	52
2.10 Immunofluorescence on cover slips .....	53
2.11 Immunofluorescence on paraffin-embedded tissue sections.....	54
2.12 Statistical Analysis .....	55
<b>Chapter 3: Results .....</b>	<b>56</b>
3.1 AIM 1: To determine whether BNIP3 knockout cells are more proliferative than wildtype cells .....	56
3.1.1 Rationale for AIM 1 .....	56
3.1.2 Evaluation of purity of Primary Astrocytes cultures.....	56
3.1.3 Validation of wildtype and <i>Bnip3</i> -knockout MEFs and Primary Astrocytes.....	58
3.1.4 Optimization of cell proliferation assays .....	60
3.1.5 <i>Bnip3</i> -knockout cells are more proliferative than <i>Bnip3</i> -expressing cells.....	63
3.1.6 HEK293 cells overexpressing nuclear <i>Bnip3</i> have lower proliferation capacity than cells lacking <i>Bnip3</i> expression. ....	66
3.1.7 <i>Bnip3</i> -KO mice brain show increased levels of Ki-67 protein compared to wildtype brain. ....	68
3.1.8 Summary of AIM 1 .....	69
3.2 AIM 2: To identify potential target genes through which BNIP3 may be repressing proliferation.....	69
3.2.1 Rationale for AIM 2 .....	69
3.2.2 <i>Bnip3</i> -knockout MEFs have increased expression and/or activation of proliferation proteins compared to wildtype MEFs. ....	70

3.2.2 <i>Bnip3</i> -KO astrocytes have altered expression of cell cycle and proliferation genes which could be involved in the observed increase in proliferation in these cells.....	72
3.2.3 RT-qPCR of identified target genes shows differences in expression that are not consistent with RNA-Seq data.....	73
3.2.4 Determination of levels of proteins encoded by identified target genes.....	75
3.2.5 Summary of AIM 2 .....	77
<b>Chapter 4: Discussion and Conclusion .....</b>	<b>78</b>
4.1 Discussion .....	78
4.2 Conclusion .....	85
<b>Chapter 5: Future Directions .....</b>	<b>86</b>
<b>Chapter 6: References .....</b>	<b>87</b>

## **List of Tables**

Table 2. 1 Composition of lysis buffers used for different cells and tissues. ....	41
Table 2. 2 Primary antibodies used for western blot and immunofluorescence. ....	44
Table 2. 3 Secondary antibodies ..... .....	44
Table 2. 4 Amplicon context sequence and expected product size of Bio-Rad primers. ....	45
Table 3. 1 Purity of Astrocytes cultures as a percentage of GFAP positive cells.....	58
Table 3. 2 Three potential target genes identified through IPA of RNA-Seq data. ....	73

# List of Figures

Figure 1. 1 An overview of eukaryotic cell cycle.....	1
Figure 1. 2 An overview of mitosis.....	2
Figure 1. 3 Cyclin-CDK complexes active during different stages of cell cycle.....	5
Figure 1. 4 Mechanism of two DNA damage checkpoints regulated by ATM and ATR.....	8
Figure 1. 5 Extrinsic and Intrinsic pathways of apoptosis.....	13
Figure 1. 6 BCL-2 family of cell death regulating proteins.....	17
Figure 1. 7 Structure of BNIP3.....	19
Figure 1. 8 An overview of BNIP3 function in macroautophagy.....	29
Figure 1. 9 Summary of BNIP3 functions.....	31
Figure 1. 10 Cell count differences in wildtype and <i>Bnip3</i> -KO mice brain.....	35
Figure 2. 1 Copper catalyzed azide-alkyne cycloaddition- “Click” chemistry.....	46
Figure 2. 2 Overview of changes in impedance of electrical current by adherent cells.....	48
Figure 2. 3 Cell counting analysis performed by Gen 5 software.....	49
Figure 3. 1 A representative image of immunofluorescence of primary astrocytes to assess culture purity.....	57
Figure 3. 2 Validation of mouse embryonic fibroblasts (MEFs).....	59
Figure 3. 3 Optimization of the three cell proliferation assays that were used in this study.....	62
Figure 3. 4 <i>Bnip3</i> -knockout cells are more proliferative than wildtype cells expressing BNIP3.....	65
Figure 3. 5 HEK293 cells overexpressing nuclear <i>Bnip3</i> have lower proliferation capacity than cells lacking <i>Bnip3</i> .....	67
Figure 3. 6 .....	68
Figure 3. 7 <i>Bnip3</i> -KO MEFs show higher activation of MAPK compared to wildtype MEFs....	70
Figure 3. 8 MEF cells lacking BNIP3 show higher levels of Cyclin D1 compared to cells expressing BNIP3.....	71
Figure 3. 9 MEF cells lacking BNIP3 have diminished levels of Cyclin D1 compared to MEF cells expressing BNIP3 after cell cycle synchronization.....	72
Figure 3. 10 RT-qPCR analysis of primary astrocytes to quantify the expression of identified target genes.....	74
Figure 3. 11 Western blot analysis of identified target proteins in both mice whole brain and primary astrocytes lysates.....	76

## List of Abbreviations

AIF	Apoptosis inducing factor
AML	Acute myeloid leukemia
APAF1	Apoptosis protease activating factor 1
ATG	Autophagy-related genes
ATM	Ataxia-telangiectasia-mutated
ATP	Adenosine triphosphate
ATR	Ataxia telangiectasia and Rad3-related
BAD	BCL-2 associated agonist of cell death
BAK	BCL-2 antagonist/killer
BAX	BCL-2 associated X
BCA	Bicinchoninic acid
BCL-2	B-cell CLL/lymphoma 2
BCL-xL	B cell lymphoma-extra-large
BH3	BCL-2 homology 3
BID	BH3-interacting domain death agonist
BIM	BCL-2 mediator of cell death
BNIP	BCL-2 and adenovirus E1B nineteen kilodalton interacting protein
BSA	Bovine serum albumin
CD	Conserved domain
CDK	Cyclin-dependent kinase
Chk1/2	Checkpoint kinase 1/2
CNS	Central nervous system
COX	Cyclooxygenase
CV	Coefficient Variance
DCIS	Ductal carcinoma <i>in situ</i>
DIABLO	Direct IAP binding protein with low PI

DISC	Death inducing signalling complex
DLX1	Distal-less Homeobox 1
DMEM	Dulbecco's Modified Eagle Medium
DMSO	Dimethyl sulfoxide
DR5	Death receptor 5
DRP1	Dynamin-related protein 1
ECL	Enhanced Chemiluminescence
EDTA	Ethylenediaminetetraacetic acid
Edu	5-ethynyl-2'-deoxyuridine
EGF	Epidermal growth factor
EndoG	Endonuclease G
ER	Endoplasmic reticulum
ERK	Extracellular signal-regulated kinase
FADD	Fas-associated death domain
FasL	Fas-ligand
FBS	Fetal bovine serum
FOXM1	Forkhead box M1
FOXO3a	Forkhead box O3a
GAPDH	Glyceraldehyde 3-phosphate dehydrogenase
GFAP	Glial fibrillary acidic protein
GlcNac	N-acetylglucosamine
HDAC1	Histone deacetylase 1
HEK293	Human embryonic kidney 293 cells
HIF1	Hypoxia inducible factor 1
HRE	HIF-1 response element
HRP	Horseradish peroxidase
I/R	Ischemia and reperfusion
IAP	Inhibitor of apoptosis proteins

IGF	Insulin-like growth factor
IGF2BP1	Insulin-like growth factor 2 mRNA binding protein 1
IgG	Immunoglobulin G
IPA	Ingenuity pathway analysis
kDa	Kilodalton
KO	Knockout
LC3	Light chain 3 protein
LIR	LC3-interacting region
MAPK	Mitogen-activated protein kinase
MCL-1	Myeloid cell leukemia 1
MEK	Mitogen activated protein kinase kinase
MEF	Mouse embryonic fibroblast
MOMP	Mitochondrial outer membrane permeabilization
MPF	Maturation promoting factor
MPTP	Mitochondrial permeability transition pore
MRN	Mre11, Rad50 and Nbs1
mTORC1	Mammalian target of rapamycin complex
NaCl	Sodium chloride
neo <sup>r</sup>	neomycin-resistance
NFκB	Nuclear factor kappa-light-chain-enhance of activated B-cells
NIX	BNIP3/NIP3 like protein X
NLS	Nuclear localization signal
NO	Nitric Oxide
OMM	Outer mitochondrial membrane
OPA1	Optic atrophy protein 1
PAGE	Polyacrylamide gel electrophoresis
PAS	Phagophore assembly site
PBS	Phosphate buffered saline

PBST	Phosphate buffered saline with Tween 20
PCR	Polymerase chain reaction
PE	Phosphatidylethanolamine
PEST	Proline- glutamic acid- serine- threonine sequence
PHD2	Prolyl-4-hydroxylase domain 2
PI3K	Phosphatidylinositol 3-kinase
PLAGL2	Pleomorphic adenoma gene-like 2
PMSF	Phenylmethanesulfonylfluoride
PNS	Peripheral nervous system
PSF	PTB-associated splicing factor
PTGS2	Prostaglandin-endoperoxidase synthase 2
PTB	Polypyrimidine tract-binding protein
PUMA	p53 upregulated mediator of apoptosis
RHEB	Ras homolog enriched in brain
ROS	Reactive oxygen species
RTCA	Real time cellular analysis
RT-qPCR	Reverse transcription and quantitative real-time polymerase chain reaction
S100A4	S100 calcium binding protein A4
SDS	Sodium dodecyl sulfate
SIM2s	Single-minded homolog 2-short isoform
Smac	Second mitochondria-derived activator of caspases
TM	Transmembrane
TNF	Tumor necrosis factor
TRADD	TNFR1-associated death domain
TRAIL	TNF-related apoptosis inducing ligand
ULK1	UNC-51-like kinase 1
UTR	Untranslated region
UV	Ultraviolet

VHL von Hippel Lindau

WT Wildtype

# Chapter 1: Introduction

---

## 1.1 Cell fate

A fine balance between cell proliferation and cell death is required for normal functioning of any organ, and in turn, of any living organism. A plethora of research has determined the molecular pathways that regulate these two mechanisms, and determine if a cell will survive to proliferate into daughter cells, or die through controlled cell death mechanisms. This section covers the basic mechanisms of cell proliferation and cell death, focusing on key signalling pathways involved.

### 1.1.1 Cell proliferation

Cell growth and division occurs through a highly conserved order of events, called the “Cell cycle”. First described in 1951, cell cycle is tightly controlled at both the transcriptional and translational levels<sup>1</sup>.

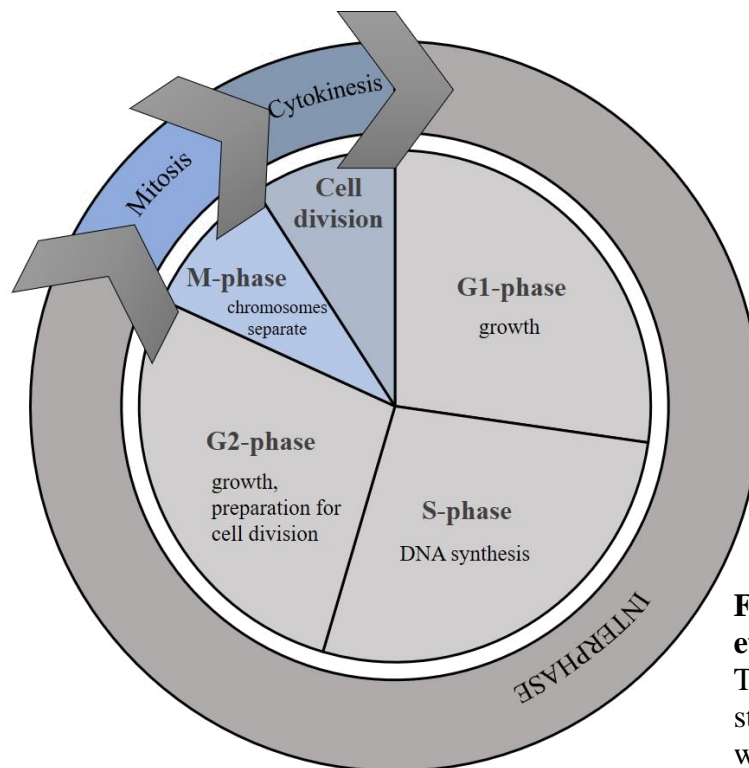


**Figure 1. 1 An overview of eukaryotic cell cycle.**

This diagram shows the different stages of cell cycle, and the order in which events occur.

During Interphase, cells continue with their various metabolic functions. This phase exists between cell divisions, and can span days, weeks or even years depending on cell type. Whether a cell will stay in interphase or divide into daughter cells, is determined by growth promoting stimuli they receive. A mature cell that is arrested in interphase and will never proliferate, which describes the majority of cells in the body, is said to be in G0 state<sup>2,3,4</sup>. For cells that may enter cell cycle, Interphase can further be divided into G1 (gap 1), S (DNA synthesis) and G2 (gap 2) phases. Cells in the G1 phase continue to grow and carry out their normal metabolic functions until they are ready to begin DNA synthesis<sup>2,3,4</sup>. Cells then enter the S phase of cell cycle where duplication of chromosomes and nuclear proteins, such as histones, occurs. Once DNA synthesis has occurred, cells enter the G2 phase of cell cycle where they continue to grow in preparation for cell division. Once ready, cells in G2 phase enter Mitosis (M-phase). Mitosis refers to the process by which duplicated chromosomes are separated into two daughter nuclei<sup>2,3,4</sup>.

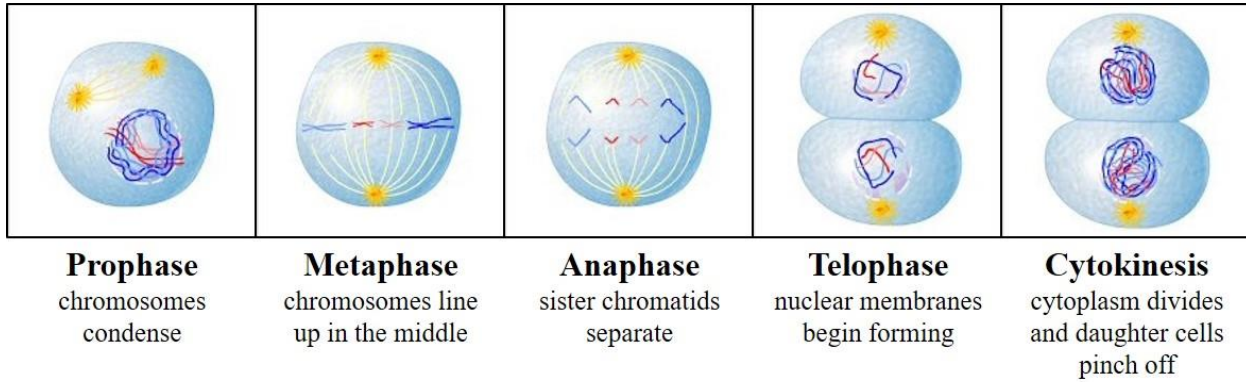


**Figure 1. 2 An overview of mitosis.**

Mitosis is divided into 4 major phases, based on the events that occur during each phase. During prophase, the chromosomes condense and mitotic spindles start forming. Metaphase involves lining up of chromosomes at the center, while the chromosome centromeres are attached to spindles at kinetochores. During anaphase, the sister chromatids are pulled to either side of the cell to ensure each daughter cell gets all the genetic information. Telophase and Cytokinesis occur simultaneously. The nuclear membranes form around separated chromosomes in telophase, while the cytoplasm pinches off during cytokinesis to form two daughter cells.

Mitosis is categorized into distinct phases: Prophase, Metaphase, Anaphase and Telophase. Sometimes Prophase is studied as two distinct stages, Early Prophase and Prometaphase<sup>2,3,4</sup>. These phases occur in sequential order, and define the events that occur inside the cell. Cells in late G2 phase consist of duplicated chromosomes, with two sister arms or chromatids. However, individual chromosomes are hard to distinguish under a microscope as they are still in their decondensed, long string-like form. During early Prophase, the chromosomes start to condense. Condensed chromosomes can be seen under the microscope as distinct X-shapes during this stage of cell cycle. Specialized organelles called Centrosomes begin to form mitotic spindles, microtubular fibres that will attach to and separate the sister chromatids. These spindles begin forming on opposite poles and start connecting to and organizing chromosomes during late prophase, or Prometaphase. The spindles attach to chromosomes via Kinetochores, proteins present at Centromeres (regions where sister chromatids are most strongly attached). During Metaphase, chromosomes are firmly lined up along a plane, often referred to as metaphase plate. Each sister chromatid at this stage is attached to spindles from opposite poles. This stage is called the Spindle checkpoint as the cell performs a check to ensure all sister chromatids are properly attached to spindles at kinetochores, and the chromosomes are lined up along the metaphase plate<sup>5</sup>. In case of any aberrations, a cell will not proceed to Anaphase until the problems are fixed. Checkpoints are explained in more detail in section 1.1.2.2. The sister chromatids are then pulled to opposite ends of the cell during Anaphase. During Telophase, the spindle microtubules break into monomers and the chromosomes start decondensing while nuclear membranes form around them on each end of the cell. Cytokinesis begins during telophase, where the cytoplasm is pinched towards the middle by formation of a cleavage furrow, an actin ring. This ultimately leads to the cell dividing into two daughter cells, each with a membrane bound nucleus containing complete genetic information from the parent

cell. Following cell division, cells re-enter interphase and continue with their programmed functions<sup>2,3,4</sup>.

### **1.1.2 Regulation of cell cycle**

#### **1.1.2.1 Cell cycle transition through different phases**

Cell cycle regulating proteins were initially identified in yeast. It was shown that a maturation promoting factor (MPF) was required to transition cells into the M-phase of cell cycle. MPF was shown to consist of two subunits- (1) a kinase subunit capable of phosphorylating other proteins, and (2) a regulatory cyclin subunit that binds to and activates the enzymatic kinase subunit<sup>2,4</sup>.

Cyclins were named as such because their levels increased during cell cycle, and decreased post-mitosis. These protein complexes were later named Cyclin-dependent kinases (CDKs). Further studies identified the role of CDKs in regulating transition through all stages of the cell cycle. Cyclins bind to the catalytic subunit of CDKs, and cause a conformational change that exposes the active site of respective kinases, and allows them to phosphorylate their target proteins. In mammalian cells, different Cyclin-CDK complexes are active during different phases of the cell cycle, where they regulate different substrates to promote transition through these phases<sup>2,6</sup>. An overview of different cyclin-CDK complexes is shown in Figure 1.3.

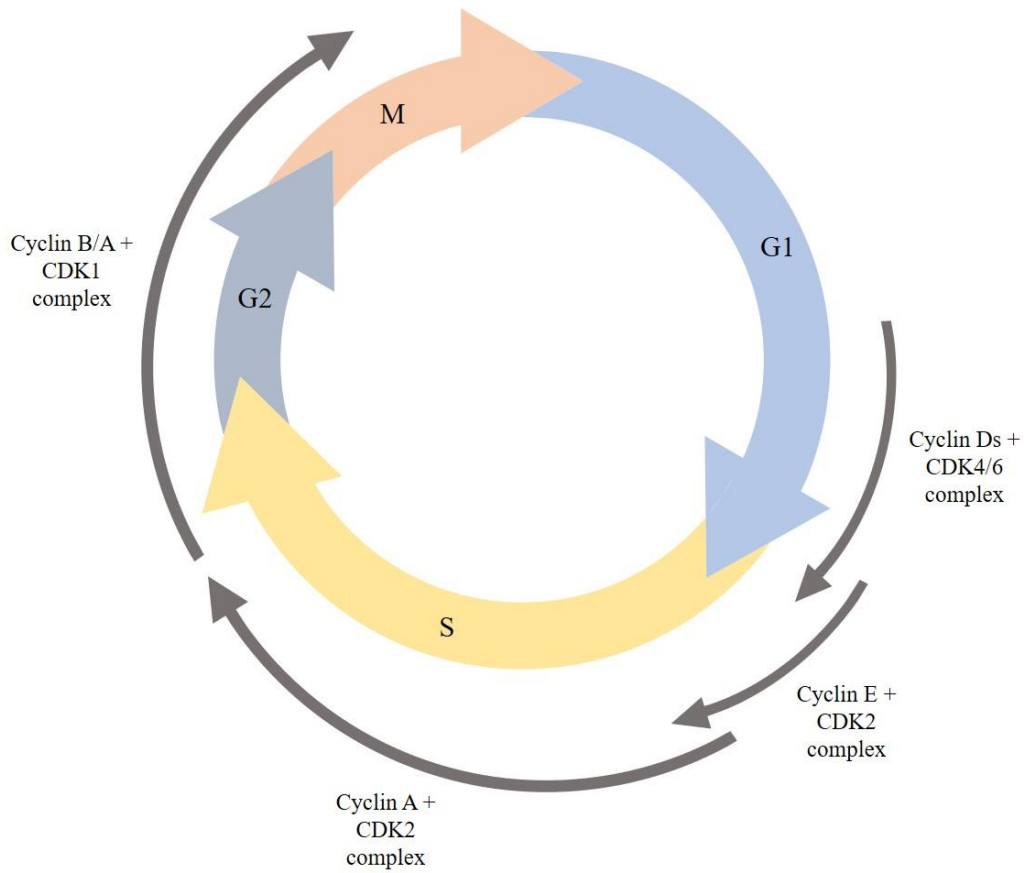


**Figure 1. 3 Cyclin-CDK complexes active during different stages of cell cycle.**

CDK activity is very low during early-G1, but complexes between CDK4 and 6 are seen with Cyclin Ds (D1, D2 and D3) beginning mid-G1. Retinoblastoma (Rb) is an important target of these kinases as phosphorylated Rb transcriptionally activates expression of proteins such as Cyclins E and A, CDK1 and proteins involved in replication. The G1-S transition is controlled by complexes between Cyclin E and CDK2, and Cyclin A and CDK2. Successive activity of Cyclin A-CDK2 and Cyclin B-CDK1 complexes regulates the G2-M transition. These kinase complexes phosphorylate several nuclear envelope proteins, histones as well as cytoskeletal proteins.

Most eukaryotes have four basic types of Cyclins, grouped by the phases during which they are expressed and/or mostly needed: G1 cyclins, G1/S cyclins, S cyclins and M cyclins<sup>7</sup>. Of these, G1 cyclins are first expressed during G1 phase, however they are needed for most of the cell cycle. The G1/S cyclins are required for the transition of the cell cycle. The S cyclins are first expressed during S phase, but maintain expression during G2 phase as well. Similarly, the expression of M

phase cyclins begins in G2 phase, however their expression peaks in M phase where they are needed to promote various events of mitosis<sup>7</sup>. Unlike Cyclins, CDKs are expressed constitutively during the cell cycle, however they remain inactive until bound by their respective cyclins<sup>2,4</sup>. As shown in figure 1.3, a CDK can be activated by multiple Cyclins. Hence, the activity of CDKs and their target proteins is controlled by the Cyclins that are being expressed at any given stage of cell cycle.

### **1.1.2.2 Cell cycle checkpoints**

There are regulatory checkpoints at the transition of each cell cycle phase which arrest cell cycle if (1) chromosomal DNA is damaged, or (2) critical cell cycle processes such as DNA replication or chromosomal separation are not correctly completed. It is important to validate the integrity of dividing cells as defective cells, when left unchecked, can lead to diseases such as cancer. Many checkpoint response proteins are not involved in normal cell cycle events, and are only activated if DNA damage or other complications are detected by sensory proteins<sup>2,8,9</sup>.

Cell cycle is regulated at various stages but there are three main checkpoints: (1) G1 checkpoint (G1/S transition), (2) G2 checkpoint (G2/M transition), and (3) aforementioned spindle checkpoint (Metaphase/Anaphase transition)<sup>2,4</sup>. At G1 checkpoint, a cell checks both its internal and external environment to decide if it should divide. Some examples of conditions checked include nutrients/energy available for division, DNA damage, size of the cell, and external growth factors or other proliferation cues. If the cell fails to pass this checkpoint, it enters the G0 phase of cell cycle. However, once a cell passes G1 checkpoint, it is irreversibly committed to dividing<sup>2,4</sup>. The G2 checkpoint allows the cell to check for DNA damage and completeness of DNA replication. In case of DNA defects, the cell cycle is paused and the cell tries to fix the problems, either by completing DNA replication or by repairing DNA damage<sup>2,4,8,9</sup>.

Ataxia-telangiectasia-mutated (ATM) and ataxia telangiectasia and Rad3-related (ATR) protein kinases are key proteins in maintaining genome integrity in eukaryotes<sup>2,8</sup>. ATM and ATR are activated in response to double-strand and single-strand DNA breaks, respectively. ATM is recruited to the site of DNA damage by the MRN protein complex (Mre11, Rad50 and Nbs1) that initially detects the double-strand break. ATR, on the other hand, localizes to sites of single-strand breaks by detecting protein-coated single-strand DNA. In the accompanying figure 1.4, ATM is activated in the G1 phase due to double-strand breaks caused by ionizing radiation. Activated ATM phosphorylates and activates Checkpoint kinase 2 (Chk2), which phosphorylates transcription factor p53. Phosphorylation of p53 stabilizes the protein which in-turn allows it to activate transcription of p21, a CDK inhibitor. Inhibition of CDKs by p21 leads to cell cycle arrest in G1<sup>2,10</sup>. Similar to ATM, activated ATR due to single-strand DNA breaks in G2 phase phosphorylates and activates Chk1, another checkpoint kinase protein. Activated Chk1 phosphorylates Cdc25, a key phosphatase enzyme required for removal of inhibitory phosphates from CDK1. Phosphorylation of Cdc25 enables it to bind an adaptor protein in the cytoplasm, preventing the phosphatase activity of the protein. Cells with inactive CDK1 fail to transition from G2 to M phase, leading to cell cycle arrest in G2<sup>2,10</sup>.

Although cells have the ability to detect and fix many cellular problems, the damage response pathways are not always successful. In case the cell is not able to fix problems such as DNA damage, it undergoes programmed cell death (apoptosis) to prevent propagation of incorrect genetic information to the daughter cells. Programmed cell death is explained in more detail in section 1.1.4.

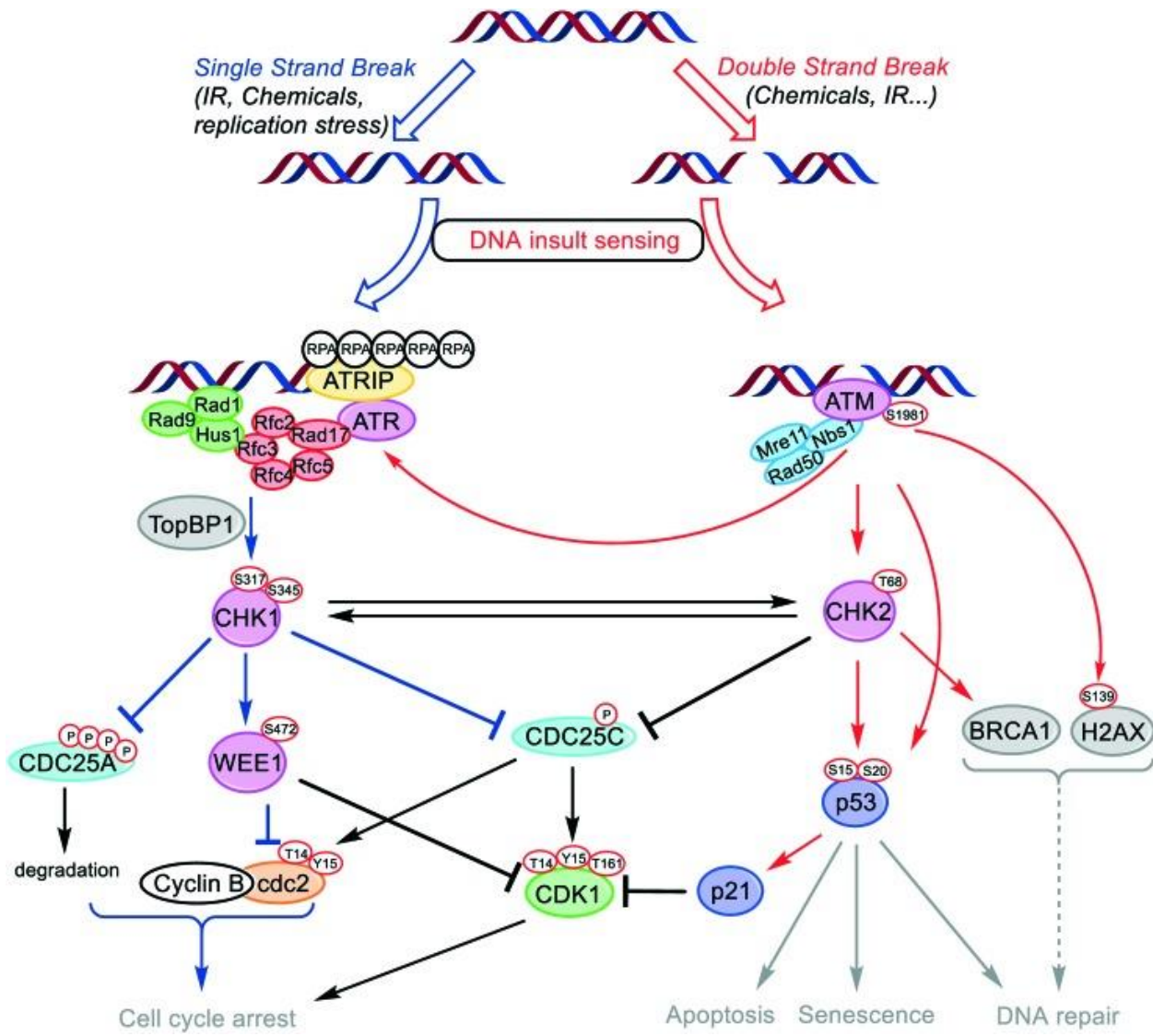


**Figure 1. 4 Mechanism of two DNA damage checkpoints regulated by ATM and ATR.**

DNA damage causes cell cycle arrest by activating DNA repair pathways as a checkpoint response. ATM and ATR are two important protein kinases involved in this response. ATM is activated by double strand breaks, whereas ATR is activated by protein bound to single stranded DNA, for example, during replication defects. Once activated, these kinases phosphorylate and activate downstream checkpoint proteins causing a cascade of events that ultimately leads to inactivation of certain CDKs and eventual cell cycle arrest. (Image taken from Royal Society of Chemistry<sup>10</sup>, through permission from Copyright Clearance Center's RightsLink® Service.)

### **1.1.3 Cell cycle regulation and Cancer**

Cancer is a very complex disease, with many underlying cellular defects and altered signalling pathways<sup>11</sup>. However, simplistically, cancer is a disease of uncontrolled cell division. Although different types of cancers have many different types of mutations and genetic alterations<sup>11</sup>, this section will focus on mutations in cell cycle regulators that may promote cancer development.

Mutations in cell cycle regulators can functionally be grouped into two types: (1) overactivation of cell cycle promoters, and (2) inactivation of cell cycle inhibitors. Cell cycle promoters are essential for growth and division of normal cells. However, some of these positive regulators, termed proto-oncogenes in normal cells, become overactive in cancer cells due to certain genetic mutations, where they promote uncontrolled growth of cancer cells. These overactive genes are referred to as oncogenes<sup>12-14</sup>. Oncogenes code for many proteins responsible for transmitting growth factor signals<sup>15</sup>, such as Ras. In normal cells, growth factor mediated activation of respective growth factor receptors leads to activation of Ras, a G-protein. Active Ras can activate several downstream pathways that promote cell proliferation and cell survival. The Erk1/2 or MAPK pathway is a key signalling pathway that promotes cellular proliferation. Ras activation as a result of growth factor signalling in turn activates its downstream target, RAF kinase protein. RAF kinase phosphorylates and activates MEK (mitogen-activated protein kinase kinase, 1 and 2). MEK then phosphorylates and activates MAPK (mitogen-activated protein kinase), also known as ERK (extracellular signal-regulated kinase). The downstream targets of MAPK include several transcription factors such as c-Jun, c-Myc and c-Fos<sup>16,17</sup>. These transcription factors control transcription of important cell cycle genes such as Cyclin D1 which is required for G1 to S transition. In normal cells, Ras is inactive in the absence of growth factor signalling. However,

cancer cells may express a mutated form of Ras which is always active. Hence, the MAPK signalling may remain active in cancer cells leading to uncontrolled cell growth.

Along with oncogenes, cells also possess negative regulators of the cell cycle which are often inactive or active at low levels in cancer cells. These genes are called tumor suppressors. Tumor suppressor genes, when active in normal cells, lead to cell cycle arrest and abolish growth<sup>12,13</sup>. One of the most studied tumor suppressor protein is p53. As mentioned in section 1.1.2.2, p53 plays an important role in the DNA damage response, as it arrests the cell cycle at the G1 checkpoint by activating the production of a cell cycle inhibitor, p21. Most cancers either lack p53 expression, or express a mutated form of the protein that is either non-functional or less active than normal p53. Inactive p53 in cancer cells fails to prevent cell cycle progression, and hence leads to uncontrolled tumor growth<sup>15,18</sup>.

#### **1.1.4 Programmed cell death (apoptosis)**

Cellular machinery consists of countless complex molecules and biochemical reactions working together to survive while carrying out their biological function. Any defect in one of these critical processes could lead to abnormal function. Cells can initiate death mechanisms in response to extreme stress or as part of their normal development, to prevent accumulation or proliferation of defective cells as seen in several diseases such as cancer. Programmed cell death, or apoptosis, is an orderly series of events that is characterized by shrinkage of cell and its nucleus, loss of adhesion to surrounding cells, blebbing of plasma membrane, fragmentation of chromatin into smaller fragments and packaging of “dead” cargo into vesicles (apoptotic bodies) for removal<sup>19,20</sup>.

Apoptosis plays a very important role in early development as well. For example, apoptotic cell death of tissues interconnecting digits during embryogenesis allows for normal development of

Hands<sup>21</sup>. Apoptotic cell death of extra neurons that lack any meaningful neuronal connections is required for normal development of brain<sup>21,22</sup>.

A key defining feature of apoptosis involves activation of cysteine-aspartic proteases, Caspases, which cleave cytoskeletal proteins. First initiator caspases (2, 8, 9 and 10) are activated through upstream signals, followed by activation of effector caspases (3, 6 and 7) by the initiators. Caspases can be activated through two different pathways- Extrinsic or Intrinsic<sup>23,24</sup>.

#### **1.1.4.1 Extrinsic pathway**

The extrinsic apoptotic pathway is activated by tumor necrosis factor (TNF) family proteins by binding to their respective cells-surface “death receptors”<sup>24</sup>. TNF was first named for its ability to kill tumor cells<sup>25</sup>. This extracellular messenger protein is produced by immune cells in response to hostile environmental conditions, such as radiation, viral infection, high temperatures or toxic chemicals such as chemotherapeutic agents<sup>26</sup>. Many TNF-like members are now known that bind their own specific receptors. For example, TNF-related apoptosis inducing ligand (TRAIL) binds death receptors DR4 and DR5 (or TRAILR1 and TRAILR2), whereas Fas (CD95 or APO1) is activated by Fas-ligand (FasL or CD95L). Activation of receptors induces trimerization and recruitment of adaptor proteins- TNFR1-associated death domain (TRADD) and Fas-associated death domain (FADD), which in turn recruits procaspase-8 to form a multimeric death inducing signalling complex (DISC). FADD and procaspase-8 interact via death effector domains present in both proteins. Once activated, procaspase-8 is cleaved into active caspase-8 consisting of four polypeptides<sup>23,27</sup>. Caspase-8 is an initiator caspase that in turn activates effector caspase, Caspase 3<sup>26</sup>.

#### **1.1.4.2 Intrinsic pathway**

The intrinsic apoptotic pathway is triggered by internal stimuli, such as hypoxia, irreparable DNA damage, high cytoplasmic  $\text{Ca}^{2+}$  (Calcium ions) or severe oxidative stress from reactive oxygen species (ROS)<sup>26</sup>. The intrinsic cell death response begins with permeabilization of mitochondrial membrane and loss of mitochondrial membrane potential, along with release of mitochondrial proteins, most notably cytochrome c<sup>24,28</sup>. Release of cytochrome c is considered a “point of no return” in apoptotic cells<sup>26</sup>. Cytochrome c forms a multimeric complex called apoptosome with APAF1 (apoptosis protease activating factor 1) and several molecules of procaspase-9. Procaspsase-9 is activated into Caspase-9 inside the apoptosome, which in turn activates the effector Caspase 3<sup>23,24</sup>.

Other apoptotic mitochondrial proteins that may be released upon membrane permeabilization include Smac/DIABLO (second mitochondria-derived activator of caspases/Direct IAP binding protein with low PI), endoG (endonuclease G) and AIF (apoptosis inducing factor). Smac/DIABLO block activity of IAPs (inhibitor of apoptosis proteins) and allow for activation of caspases. EndoG and AIF induce caspase-independent cell death by translocating to nucleus and mediating DNA fragmentation<sup>23,24</sup>.

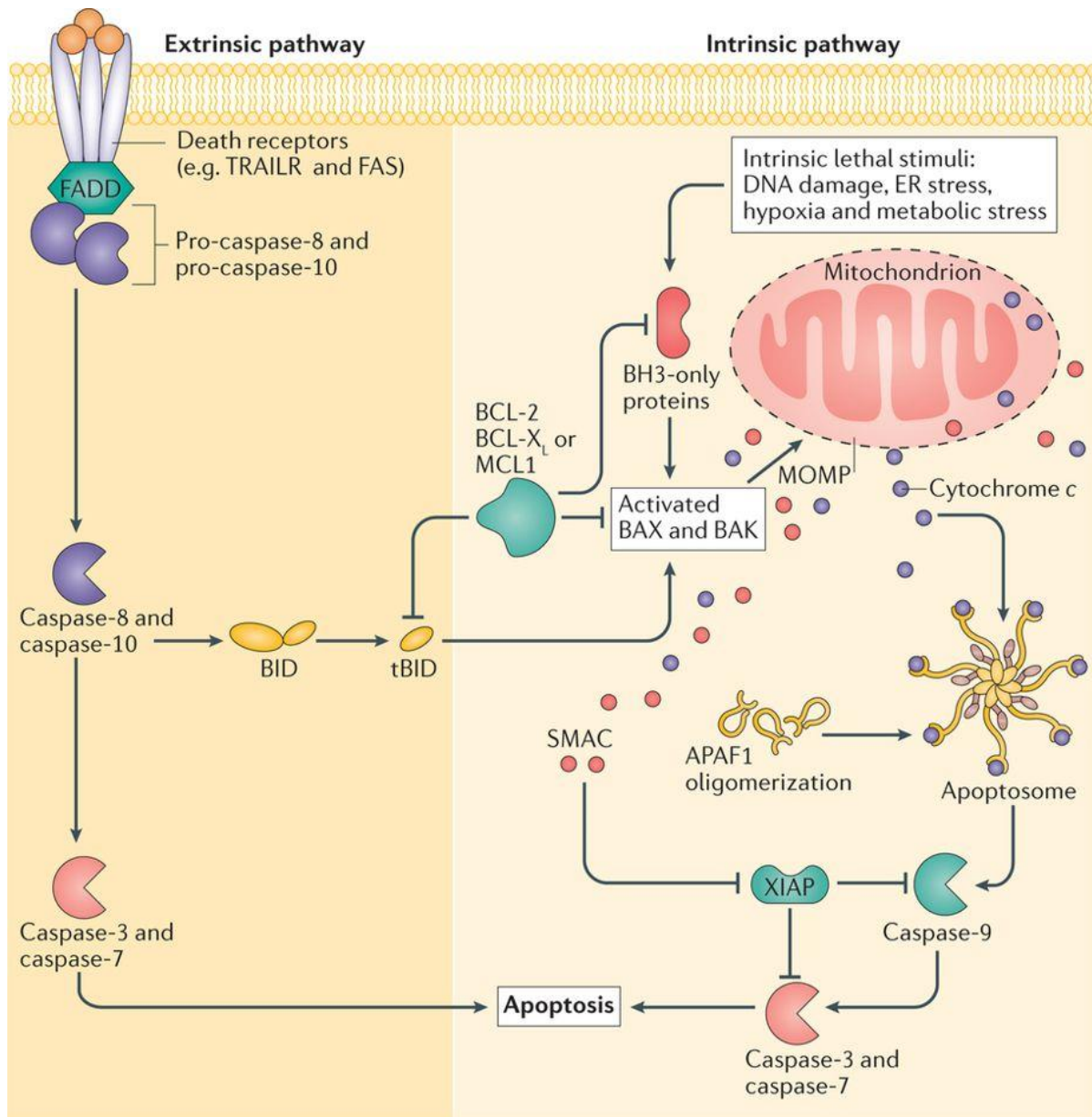


**Figure 1.5 Extrinsic and Intrinsic pathways of apoptosis.**

The extrinsic pathway involves activation of TNF superfamily of death receptor proteins, which induces activation of initiator Caspase-8 through formation of multimeric death inducing signalling complex (DISC) consisting of adaptor Fas-associated death domain (FADD) protein and inactive procaspase-8. The intrinsic pathway can be activated by several stress stimuli, which leads to mitochondrial dysfunction through pro-apoptotic BCL-2 family proteins BAX and BAK, and BH-3 only proteins. Disruption of mitochondria leads to release of cytochrome c, which binds to apoptotic protease activating factor 1 (APAF1). This complex binds to inactive initiator pro-caspase 9 to form apoptosome which then activates Caspase-9. Activated initiator caspases 8 and 9 can then activate effector Caspase 3 and 7, which are responsible for cleavage of many important cellular substrates and ultimately lead to apoptotic cell death. (Image taken from Nature Reviews Cancer<sup>29</sup>, through permission from Copyright Clearance Center's RightsLink® Service)

The crucial initial step of mitochondrial membrane permeabilization is a result of cross-talk between anti-apoptotic and pro-apoptotic members of BCL-2 family of proteins<sup>30</sup> as described in detail in section 1.2.

### **1.1.5 Necrotic and Autophagic cell death**

Necrosis and Autophagy are two other well established cell death mechanisms. Unlike apoptosis, necrosis has long been considered uncontrolled cell death as it is usually caused by unexpected stressors in the cell such as toxins and infection<sup>23,31,32</sup>. Necrosis results in swelling and rupture of organelles, depletion of adenosine triphosphate (ATP), loss of membrane integrity and ultimately the release of cellular contents into the extracellular space<sup>19,20</sup>. This unregulated release of cellular components often leads to inflammation of neighbouring cells<sup>33</sup>. However, recently advancements in necrosis research have identified programmed necrotic mechanisms in normal development and physiology, mediated by calcium and ROS. Programmed necrosis occurs as a cross-talk between several biochemical and molecular pathways, and further insights into the mechanism of these pathways may unveil a potential mechanism to kill apoptosis-resistant tumor cells<sup>31,34</sup>.

On the other hand, autophagy is a programmed cellular recycling process. It involves the breakdown of damaged cellular components in a controlled manner inside the lysosome<sup>35,36</sup>. Specific mechanisms of autophagy will be discussed later in section 1.4.2.3. In summary, low basal levels of autophagy are maintained in many cells, through which cells are able to recycle damaged organelles and other cellular cargo. This often promotes survival in case of acute stress such as lack of nutrients. However, under chronic stress, prolonged autophagy often leads to autophagic cell death. Unlike apoptosis, DNA and cytoskeleton integrity is initially maintained in autophagic cell death, whereas the cellular organelles are degraded such that normal metabolic functions would not be possible<sup>19,20</sup>.

## **1.2 BCL-2 family of proteins**

The B-cell CLL/lymphoma 2 (BCL-2) family of proteins consist of evolutionarily conserved proteins that mediate programmed cell death. The BCL-2 family proteins consist of one to four Bcl-2 homology (BH) domains and are grouped according to their functions in cell death. There are three distinct groups (Figure 1.6)- (1) Pro-survival/anti-apoptosis group consisting of multi-domain proteins such as BCL-2, myeloid cell leukemia 1 (MCL1), (2) Pro-apoptosis group consisting of multi-domain proteins such as BCL-2 antagonist/killer (BAK) and BCL-2 associated X (BAX), and (3) Pro-apoptotic BH3 domain-only proteins such as BCL-2 interacting mediator of cell death (BIM), BCL-2 associated agonist of cell death (BAD) and BH3-interacting domain death agonist (BID)<sup>30,37-39</sup>. The ultimate cell fate of survival or death is decided by the interactions and balance between the pro-survival and pro-death proteins.

Although BCL-2 family proteins were initially studied for their role in apoptotic cell death, several studies have also established their role in regulating autophagic cell death<sup>30,40,41</sup>.

### **1.2.1 Pro-survival/anti-apoptosis BCL-2 family proteins**

The pro-survival BCL-2 family members contain three to four BH-domains (BH1-4) and can effectively block apoptosis when they are overexpressed. Some notable members of the family include BCL-2, B cell lymphoma-extra-large (BCL-xL), BCL-2 related protein A1 (A1) and MCL-1. These proteins are integrated within outer mitochondrial membrane (OMM) where they inhibit pro-apoptotic BCL-2 members by direct binding<sup>30</sup>.

### **1.2.2 Multi-domain Pro-apoptotic BCL-2 family proteins**

Multi-domain BCL-2 family proteins are effectors of cell death and consist of BH domains 1, 2 and 3, along with a modified BH4 domain with a conserved BH4 motif. BAK and BAX are the

two well-known effector members in this subgroup. These proteins homo-oligomerize when activated and form pores in the OMM to cause mitochondrial outer membrane permeabilization (MOMP) and release of several pro-apoptosis factors, which ultimately causes apoptosis<sup>30,42</sup>.

### **1.2.3 BH3-domain only BCL-2 family proteins**

As the name implies, these proteins only contain BH3 domain and are the least homologous members of BCL2 family. Unlike multi-domain pro-death members, BH3-only proteins do not cause cell death directly. Instead, these proteins work by interacting with other pro-survival proteins like BCL-2 or effector proteins like BAK and BAX, and based on these interactions they can either be classified as either sensitizers and/or derepressors or direct activators, respectively. Direct activators like BID and BIM interact with pro-death effectors like BAK and BAX through their BH3 domain to cause effector oligomerization which ultimately leads to MOMP and cell death. Sensitizer proteins like p53 upregulated mediator of apoptosis (PUMA) interact and associate with anti-apoptotic proteins like BCL-2, which prevents anti-apoptotic proteins from binding direct activators like BIM, and allows BIM to activate effectors that cause death. Derepressors work similar to sensitizers by associating with anti-apoptotic proteins, but instead of binding to empty anti-apoptotic proteins, they help release activators that have been sequestered by anti-apoptotic proteins. For example, BAD can help release activated BID that is bound by BCL-2, which can then directly activate effector proteins<sup>30,42</sup>.

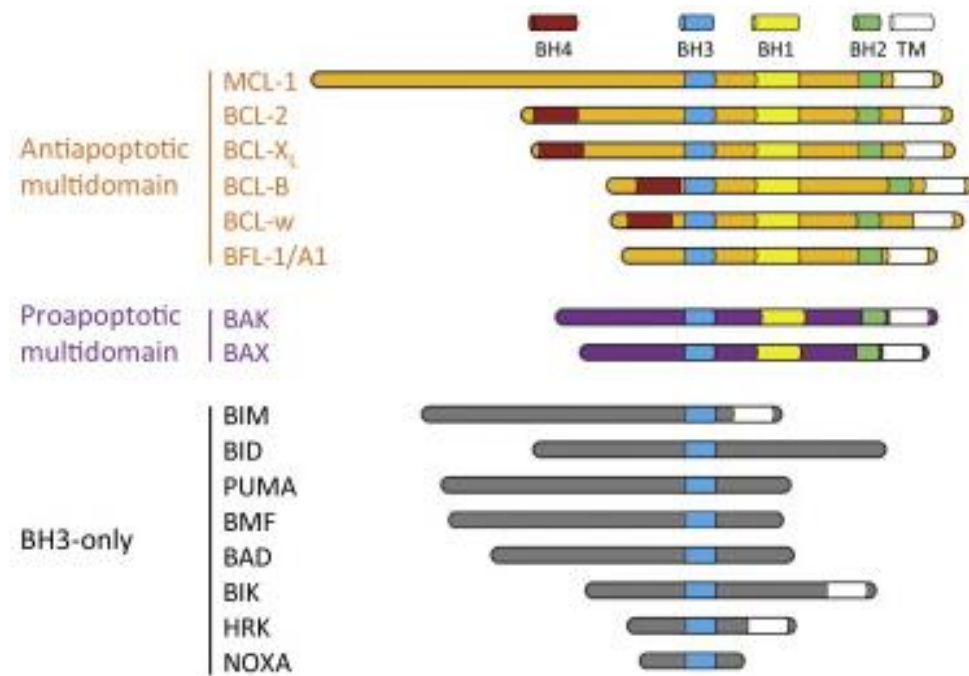


**Figure 1. 6 BCL-2 family of cell death regulating proteins.**

Image shows the structural features of different BCL-2 family proteins, grouped by their function in cell death. Multidomain anti- and pro-apoptotic proteins possess BCL-2 homology (BH) domains 1, 2 and 3 with some members also containing a conserved BH4 domain. BH3-only subfamily of pro-apoptotic proteins only contains the BH3 domain. Many members of BCL-2 family contain a C-terminal transmembrane (TM) domain which allows these proteins to anchor at intracellular membranes. (Image taken from Trends in Endocrinology & Metabolism<sup>43</sup>, through permission from Copyright Clearance Center's RightsLink® Service)

### 1.2.3.1 BNIP subfamily of BH3-only proteins

Another subgroup that exists within the BH3-only subfamily of proteins is the BNIPs. The BNIP proteins have limited sequence homology with other BH3-only proteins in their BH3 domains and the C-terminal transmembrane domain<sup>44</sup>. This subgroup consists of proteins BNIP1 (BCL2 and adenovirus E1B 19 kilodalton interacting protein 1), BNIP2, BNIP3 and BNIP3L (BNIP3 like protein X, or NIX). The BNIP proteins were originally found interacting with BCL2 and adenovirus E1B 19 kilodalton (kDa) proteins in a yeast two-hybrid screen<sup>45</sup>. E1B 19 kDa is an anti-apoptotic protein that protects cells from death after adenovirus infection. Mutated anti-apoptotic BCL2 and E1B 19 kDa proteins that cannot interact with BNIP proteins, also fail to

suppress cell death. Hence, BNIP proteins are pro-apoptotic proteins similar to other BH3-only members which can be suppressed by anti-apoptotic BCL2<sup>46</sup>. BNIP1 and 2 have been shown to localize to nuclear envelope and endoplasmic reticulum, whereas overexpressed BNIP3 localizes to mitochondria<sup>45</sup>. BNIP3 is the most well studied member of BNIP subgroup and is the focus of this study.

#### **1.2.4 BCL-2 family proteins in development**

The importance of apoptosis in development was mentioned briefly in section 1.1.4. Research has identified the role of pro-apoptotic BCL-2 members, BAX and BAK, in developmental apoptosis, for example, in retinal development in mice<sup>47,57</sup>. However, BAX and BAK double-knockout mice are born in sub-mendelian ratios without any defects in early embryogenesis. Interestingly, cell death is still seen in these developing mice, indicating that other compensatory mechanisms exist to eliminate cells during development<sup>48,57</sup>. In addition to apoptosis, cell survival promoted by anti-apoptotic BCL-2 members is also essential for development. For example, increased BCL-2 expression is seen during early neurulation (E4.5-8) where an increase in number of neurons occurs in both CNS and PNS<sup>49-51,57</sup>. BCL-xL expression increases after neural tube formation (E10-11), and stays high throughout neuronal development<sup>50,51,57</sup>. Loss of BCL-xL results in increased apoptosis in both nervous and hematopoietic systems and leads to embryonic death by E13.5. Increased apoptosis in developing post-mitotic immature neurons suggests that BCL-xL is required for survival of immature cells during development<sup>52,57</sup>. Another pro-survival member MCL-1 is critical during both neuronal and hematopoietic development as well<sup>57</sup>. Additionally, BCL-2 deficient mice suffer from polycystic kidney disease, and die by 4-16 weeks of age<sup>53</sup>. These mice also display a loss of pigmentation over 5-6 weeks after birth due to an increased death of melanocytes<sup>53,54</sup>. Mice lacking BCL-W suffer from testicular degeneration due to apoptosis of

Sertoli cells after weaning. Leydig cells also undergo apoptosis past 3 months of age, resulting in sterile mice<sup>55</sup>. Targeted deletion of *Mcl-1* in late embryogenesis was shown to cause fatal cardiomyopathy<sup>56</sup>.

### **1.2.5 BCL-2 family members in Cancer**

Cancer is a disease of unregulated cell growth, as mentioned in section 1.1.3. In addition to increased cell growth, cancer cells may also have defective apoptosis which provides increased survival<sup>58</sup>. These defects are often the result of deregulation of BCL-2 family proteins. Pro-survival BCL-2 members have been shown to act as oncogenes whereas pro-death proteins are characterized as tumor suppressors<sup>59</sup>. For example, BCL-2 was first identified involved in chromosomal translocation in non-Hodgkin's lymphoma<sup>60</sup>. Moreover, pro-death BCL-2 family proteins BAX, BID, PUMA and NOXA are transcriptional targets of tumor suppressor p53<sup>59</sup>.

## **1.3 BNIP3**

*Bnip3* is located at human chromosome 10q26.3<sup>61</sup> and consists of six exons<sup>62</sup>. The encoded BNIP3 protein has been shown to play a role in apoptosis and autophagy. Overexpression of BNIP3 has also been associated with pathogenesis of diseases such as cardiovascular disease and cancer.

### **1.3.1 BNIP3 structure**

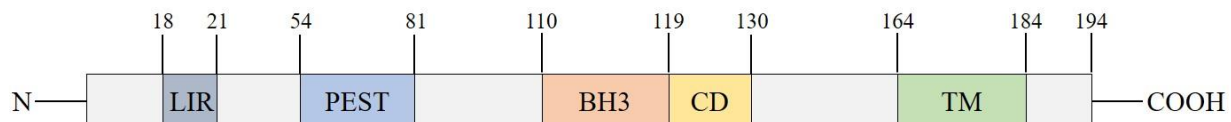


**Figure 1. 7 Structure of BNIP3.**

BNIP3 protein consists of several notable regions. The N-terminal of protein has a short LC3-interacting region (LIR) which allows mitochondrial BNIP3 to interact with LC3-containing autophagosomes and mediates the engulfment of mitochondria for mitophagy. The PEST domain is associated with targeting of proteins for proteasomal degradation, however its mechanism in degradation of BNIP3 is not well studied. The conserved BCL-2 homology 3 (BH3) domain allows interaction with other BCL-2 proteins. The conserved domain (CD) is conserved from *C. elegans* to humans, however its exact function is not known. The C-terminal transmembrane (TM) domain is required for both homodimerization and mitochondrial localization of BNIP3, and hence is necessary for cell death function of BNIP3. The amino acids are indicated on top of the diagram.

BNIP3 protein is 194 amino acids long<sup>45,63</sup> and has a predicted molecular weight of 21.5 kDa. However, the protein migrates on an SDS-PAGE (Sodium dodecyl sulfate-Polyacrylamide gel electrophoresis) gel as a 30 kDa monomer and a 60 kDa homodimer<sup>63,64</sup>. BNIP3 homodimer is resistant to both reducing conditions of β-mercaptoethanol (BME) and denaturation by SDS detergent<sup>63,65</sup>. BNIP3 dimerizes at its C-terminal (amino acids 164-184) transmembrane (TM) domain<sup>66</sup>. This TM domain is essential for the apoptotic function of BNIP3 as it is involved in targeting BNIP3 to mitochondria, homodimerization as well as heterodimerization with other BCL2-family proteins<sup>67-71</sup>.

The stable dimerization at TM domain is due to the amino acid residues that comprise the C-terminal of the protein. The two TM domains in a homodimer form a right-handed parallel helix-helix structure of hydrophilic amino acids that spans a lipid bilayer with the help of a stretch of external hydrophobic residues. The helix structure comprises of a glycine zipper motif A<sup>176</sup>XXXG<sup>180</sup>XXXG<sup>184</sup> (Alanine 176, Glycine 180, Glycine 184) and two critical polar residues, Ser172 (Serine) and His173 (Histidine), that form intermonomer hydrogen bonds in the dimeric interface. Several other backbone residues and polar side chains also aid in the stabilization of the dimers<sup>65,66,69,70</sup>. Dimeric BNIP3 in mitochondria localizes at the OMM. The node formed between polar side chains of Ser172 and His173 through hydrogen bonding as well as the series of internal hydrophilic amino acids present along the lipid bilayer form an acid-sensitive hydrophilic channel that has been proposed to allow conductance of ions through the OMM<sup>72</sup>. Therefore, BNIP3 dimers could directly cause depolarization of mitochondria leading to opening of mitochondrial permeability transition pore (MPTP) which would ultimately cause cell death. The mechanism of BNIP3 mediated cell death will be covered later in section 1.2.3.

Although most of dimeric stability is through TM domain, several other interactions across the protein further contribute to the dimeric stability. A conserved Cysteine residue (Cys 64) in the N-terminal domain forms disulfide bonds in the homodimer<sup>66,73</sup>. The dimer is further stabilized, albeit weakly, by aromatic rings of phenylalanine (Phe 157, Phe 161 and Phe 165) in the N-terminal region which form a hydrophobic cluster through inter- and intramonomeric pi-stacking interactions<sup>72</sup>. Thus, the dimerization of BNIP3 is facilitated by several key interactions which together form the basis for BNIP3's functions.

As a member of the BH3-only subfamily proteins, BNIP3 possesses a BH3 domain that spans amino acid residues 110-118<sup>67</sup>. Although other BH3-only proteins require BH3 domain for their cell death function by heterodimerization with anti-apoptotic proteins<sup>38</sup>, the cell death function of BNIP3 is through its TM domain<sup>68</sup>. Studies have shown that replacing BH3 domain of BNIP3 fails to affect the cell death activity of the protein, but deletion of TM domain disrupts the mitochondrial localization and cell death<sup>68</sup>. An intact BH3 domain is however required for growth factor protection against BNIP3-induced cell death in hypoxia<sup>74</sup>.

The BH3 domain is adjacent to a conserved domain (CD) spanning amino acid residues 119-130<sup>67</sup>. The exact function of CD domain is currently not known, but deletion of CD domain does not affect the activity of BNIP3. The CD domain has been conserved from *Caenorhabditis elegans* to humans<sup>68,75</sup>. Several other features of BNIP3 such as presence of putative BH3 domain, TM domain and a N-terminal PEST domain (discussed later) are also conserved from *Caenorhabditis elegans* to humans with differences in amino acids that form these domains<sup>76</sup>.

Apart from several residues involved in homodimerization of BNIP3, the N-terminal region contains a LC3 (light chain 3)-interacting region (LIR), required for BNIP3 and LC3 interactions to promote mitophagy<sup>77</sup>. The N-terminal domain also contains a PEST domain (amino acids 54-

81), a sequence rich in proline, glutamic acid, serine and threonine flanked by histidine and arginine/lysine residues, which is known to target proteins for proteasomal degradation and leads to short half-life for proteins<sup>63,78,79</sup>.

### **1.3.2 Regulation of BNIP3**

#### **1.3.2.1 Induction of *Bnip3***

*Bnip3* is expressed at some level in most tissues<sup>80,81</sup>, with basal levels of the protein present in skeletal muscle, heart and nucleus of glial cells<sup>44,78,82,83</sup>. The expression of BNIP3 is known to be upregulated under stress conditions. One of the most studied stress conditions that upregulate BNIP3 expression is hypoxia (low oxygen conditions)<sup>74,83,84</sup>. The oxygen levels in hypoxia are well below the normal cellular oxygen levels of 5-10%<sup>85</sup>. Hence, hypoxia requires a strong metabolic response in order for cells to survive. One of the key regulators of the hypoxic response in cells is the transcription factor Hypoxia Inducible Factor 1 (HIF1). HIF1 is a heterodimeric protein consisting of two subunits- alpha (HIF1 $\alpha$ ) subunit which make up the chief transcription regulation unit, and a beta (HIF1 $\beta$ ) subunit that is responsible for nuclear localization of the protein<sup>84,86</sup>. Although HIF1 is constitutively expressed in cells, HIF1 $\alpha$  is rapidly degraded under normal oxygen conditions. Prolyl-4-hydroxylase domain 2 (PHD2) is a HIF-specific enzyme that hydroxylates HIF1 $\alpha$  at specific proline residues in the oxygen-dependent degradation domain, which targets it for recognition and ubiquitination by von Hippel Lindau protein (pVHL), a component of E3 ubiquitin ligase. Ubiquitinated HIF1 $\alpha$  is ultimately degraded by the 26S proteasome. Some key cosubstrates for enzymatic activity of PHD2 include O<sub>2</sub> and 2-oxoglutarate (intermediate of the tricarboxylic acid cycle), which are both diminished under hypoxia. Thus, PHD2 is functionally inhibited under hypoxia which leads to stabilization of HIF1 $\alpha$ <sup>86,87</sup>. Stabilized

HIF1 $\alpha$  regulates expression of multiple genes involved in metabolism, angiogenesis and migration<sup>84,87</sup>.

The *Bnip3* promoter contains a HIF-1 response element (HRE), a highly conserved sequence between rat, mouse and human genome that targets genes to be regulated by HIF1 $\alpha$ . Under hypoxia, stabilization of HIF1 $\alpha$  allows it to bind to HRE in the proximal promoter of *Bnip3*, and induce *Bnip3* expression<sup>74,84</sup>. In addition to hypoxia, Cyanide also stabilizes HIF1 $\alpha$ , thus promoting HRE activation and *Bnip3* expression<sup>88</sup>.

In addition to HIF1 $\alpha$ , several other transcription factors have been identified that induce *Bnip3* expression. The transcription factor E2F-1, which plays an important role in regulation of cell cycle, has been shown to activate intrinsic apoptotic pathway in rat ventricular myocytes through transcriptional activation of *Bnip3* expression<sup>89</sup>. Pleomorphic adenoma gene-like 2 (PLAGL2) is another transcriptional that activates *Bnip3* expression in hypoxia. PLAGL2 has been shown to bind on a different site in *Bnip3* promoter than HIF1 $\alpha$  in mouse fibroblasts and neuroblastoma cells<sup>90</sup>. In addition, *Bnip3* expression has also been shown to be regulated by forkhead box O3a (FOXO3a), a transcription factor involved in regulating cellular energy stress. FOXO3a regulated BNIP3 is involved in promoting autophagy as well as moderating mitochondrial dynamics and function during cardiac stress<sup>91,92</sup>.

Some other stimuli are also known to promote *Bnip3* expression, though the exact mechanism may be unknown. For example, Nitric Oxide (NO) has been shown to induce *Bnip3* expression through RAS signalling pathway<sup>93</sup>. Neurotoxin Manganese causes mitochondrial dysfunction and cell death in neurons by promoting expression of *Bnip3*<sup>94</sup>. Arsenic trioxide, ceramide and amyloid- $\beta$  are some other toxic stimuli that promote *Bnip3* expression<sup>95,96,97</sup>.

### **1.3.2.2 Repression of *Bnip3***

Expression of *Bnip3* has to be tightly regulated due to its pro-death activity. Under normal, non-stressful conditions, nuclear factor kappa-light-chain-enhancer of activated B-cells (NFκB) has been shown to constitutively silence *Bnip3* by competing with E2F-1 for *Bnip3* promoter binding in rat ventricular myocytes<sup>98</sup>. Several other mechanisms of *Bnip3* repression have been studied in cancer cells. In pancreatic ductal adenocarcinoma cells, S100 calcium binding protein A4 (S100A4), a regulator of cell cycle progression and differentiation, was shown to inhibit *Bnip3* expression *in vitro*<sup>99</sup>. Single-minded homolog 2-short isoform (SIM2s) represses *Bnip3* expression by binding at the HRE promoter region, and preventing induction via HIF1α<sup>100</sup>. Furthermore, expression of *Bnip3* is inhibited by pRb-E2F mediated transcriptional repression during development, which is necessary to prevent unwarranted cell death as the embryo normally experiences hypoxic stress<sup>101</sup>. In pancreatic<sup>102</sup>, hematopoietic<sup>103</sup> and colorectal<sup>104</sup> cancers, silencing of *Bnip3* promoter by hypermethylation has been observed to repress *Bnip3* expression.

### **1.3.2.3 Post-translational modification of BNIP3**

There are two known post-translational modifications of BNIP3: O-linked glycosylation and phosphorylation. Increased O-linked glycosylation of BNIP3 by N-acetylglucosamine (GlcNAc) was shown in breast cancer cells that had metastasized to lung<sup>105</sup>. Hence, O-linked glycosylation of BNIP3 may be linked to metastatic dissemination. Furthermore, this modification was not present in the same breast cancer cells recovered from kidney, therefore, this O-linked glycosylation may be involved in organ tropism during metastasis<sup>105</sup>.

Additionally, BNIP3 has a few phosphorylation sites that are important in regulating the function of the protein and can control whether BNIP3 promotes cell death or autophagy. Phosphorylation of serine/threonine residues in C-terminal tail has been shown to prevent mitochondrial

dysfunction and cell death<sup>106</sup>, which is consistent with the importance of C-terminal domain of BNIP3 in regulating apoptosis. Whereas, phosphorylation of serine residues on either side of LC3-interacting region promotes mitophagy through increased interaction between BNIP3 and LC3<sup>77</sup>.

#### **1.3.2.4 Degradation of BNIP3**

As previously discussed, the N-terminal domain of BNIP3 contains a PEST domain which is known to target proteins for ubiquitination and proteasomal degradation. However, the exact mechanism of degradation is currently not known<sup>64</sup>. Moreover, BNIP3 has been shown to be eliminated by both proteasomal degradation and autophagy *in vitro* when cells were incubated in hypoxia accompanied by amino acid starvation. The autophagic removal of BNIP3 was regulated by ULK1 (UNC-51-like Kinase 1) via MTOR-AMPK pathway<sup>107</sup>.

#### **1.3.2.5 Subcellular localization of BNIP3**

The subcellular localization of BNIP3 is dependent on cells and their environment, and plays a major role in determining the functional effects of BNIP3. In summary, BNIP3 is expressed at varying levels under normal conditions in most tissues, with high levels of protein in brain and skeletal muscle. When induced under stress, expression of BNIP3 is predominantly cytoplasmic where it often localizes to the mitochondria<sup>64</sup>. However heavy nuclear localization is also seen in several cancers<sup>82,108,109</sup> and other pathophysiological conditions<sup>110</sup>. The link between localization of BNIP3 and its function is discussed in the next section.

### **1.4 Functions of BNIP3**

As a pro-death member of BCL-2 family, BNIP3 was initially extensively studied for its role in apoptotic cell death. However, its role in other forms of cell death, namely necrosis and autophagic cell death, has also been established over the years. In addition to cell death, BNIP3 has also been

implicated to play a role in cell survival. The various functions of BNIP3 and respective mechanisms are discussed in this section.

#### **1.4.1 Mechanism of BNIP3-mediated mitochondrial dysfunction**

Unlike other BH3-only proteins, BNIP3 can directly alter mitochondrial potential without interacting with other BCL-2 family proteins<sup>72</sup>. When overexpressed, the C-terminal tails of BNIP3 (consisting of TM domains) can homodimerize and translocate to mitochondria where the dimer can insert itself in the OMM via the TM domains<sup>63</sup>. Here, the TM domain can promote mitochondrial dysfunction in several different ways depending on cell type. In isolated mitochondria, TM domains in OMM directly cause opening of mitochondrial transition pore and loss of mitochondrial potential by interacting either with other members of permeability transition pore or other mitochondrial proteins<sup>111</sup>. However, in murine fibroblasts, BNIP3 mediated mitochondrial dysfunction required other BCL-2 proteins, BAK and BAX<sup>112</sup>. Moreover, BNIP3 has also been shown to interact with Optic atrophy protein 1 (OPA1), a dynamin-like GTPase present on inner mitochondrial membrane that is involved in mitochondrial fusion, oxidative phosphorylation and apoptosis. The interactions between C-terminal tails of BNIP3 dimers in OMM with OPA1 inhibits the fusion activity of OPA1. Disruption of OPA1-complex can lead to mitochondrial fragmentation and apoptosis in a BAK/BAX dependent manner<sup>113</sup>. In cardiac myocytes, mitochondria-localized BNIP3 induces mitochondrial translocation of dynamin-related protein 1 (DRP1) which is involved in mitochondrial fission. This increased fission correlates with increased mitophagy, autophagic removal of mitochondria<sup>114</sup>.

## **1.4.2 BNIP3-mediated cell death**

Although BNIP3 was first described as a pro-apoptotic BH3-only protein, research into the function of BNIP3 has revealed several different ways in which BNIP3 may induce cell death. The different forms of cell death caused by BNIP3 are also cell-type specific. Regardless, BNIP3-mediated mitochondrial dysfunction is essential to cell death function of BNIP3.

### **1.4.2.1 BNIP3-mediated apoptosis**

BNIP3 has been shown to induce apoptotic cell death in cardiomyocytes, where mitochondrial localization of overexpressed BNIP3 causes loss of mitochondrial potential, ROS production, DNA condensation, activation of BAK and BAX, cytochrome c release and caspase activation- a classic apoptotic cell death response. Overexpression of BNIP3 in wild-type MEFs also led to increased cell death through loss of mitochondrial membrane potential and release of cytochrome c<sup>112,115</sup>. *In vivo* mouse studies identified BNIP3-mediated post-ischemic apoptosis as a major determinant of ventricular remodelling. Apoptosis was reduced in myocardium of *Bnip3* knockout mice after surgical ischemia and reperfusion (I/R) injury. Increased cardiomyocyte apoptosis was also seen in unstressed mice in case of overexpression of cardiac BNIP3<sup>116</sup>.

### **1.4.2.2 BNIP3-mediated necrosis**

Some evidence exists for BNIP3-mediated cell death to be necrosis-like. A study by Greenberg et al.<sup>117</sup> showed transfection of cells with *Bnip3* overexpression vector induced cell death independent of nuclear translocation of apoptosis inducing factor, cytochrome c release and caspase activation. Moreover, the cells showed early plasma membrane permeability, mitochondrial damage, extensive cytoplasmic vacuolation and mitochondrial autophagy-morphology typical of necrosis<sup>117</sup>.

### **1.4.2.3 BNIP3-mediated autophagy**

Autophagy is regulated, self-digestion of cellular components that allows for controlled degradation of damaged proteins and organelles into amino acids, fatty acids and nucleotides which can be used for ATP production and synthesis of new macromolecules<sup>118,119</sup>. Autophagy occurs constitutively at low levels and serves to maintain cellular homeostasis. Additionally, cells can increase autophagy levels at times of nutrient starvation to promote cell survival.

Autophagy is classified into three major types- (1) Macroautophagy is the most studied, and well understood autophagy pathway in which a phagophore forms around cellular cargo that needs to be degraded, and engulfs it in a double membrane structure called autophagosome. The autophagosome then fuses with lysosomes where degradation occurs through lysosomal enzymes. (2) Chaperone-mediated autophagy is a highly specific form of autophagy that requires Hsc70 chaperone-complex to bind proteins with motifs that recognize these chaperones. The proteins are directly transferred to the lysosomes through the substrate-chaperone complex. (3) Microautophagy is a non-selective autophagic process, where lysosomes directly engulf cytoplasmic cargo through invaginations of lysosomal membrane<sup>119</sup>.

Autophagy can be induced by many cellular signals, such as hypoxia, lack of nutrients etc. Once induced, an autophagy protein complex forms at a phagophore assembly site (PAS). The initial phagophore complex consists of Unc51-like-kinases 1 and 2 (ULK1/2) and other autophagy proteins (ATGs). The nucleation and elongation of phagophore is mediated by ATG12-ATG5-ATG16L1 complex, class III phosphatidylinositol 3-kinase (PI3K) complex, Beclin 1 (BECN1), LC3-II and ATG9. The PI3K complex and BECN1 are required for the nucleation of the phagophore<sup>118,119</sup>. Normally Beclin is sequestered by BCL-2 in the endoplasmic reticulum (ER).

BNIP3 competes with BECN1 for BCL-2 binding, and allows free BECN1 to participate in autophagy<sup>120,121</sup>.

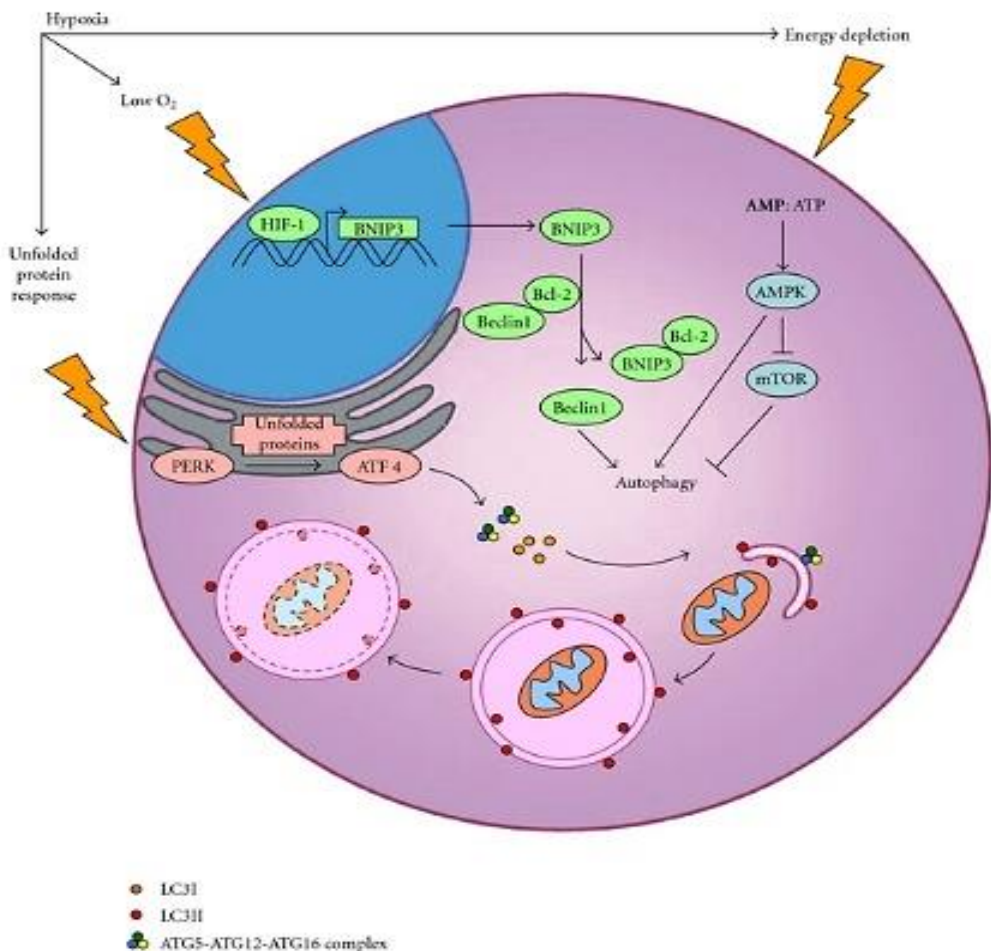


**Figure 1.8 An overview of BNIP3 function in macroautophagy.**

Expression of BNIP3 is increased under hypoxia by HIF1. Increased BNIP3 in the cytoplasm competes with Beclin 1 for BCL-2 binding. This frees Beclin 1 to interact with other autophagy initiating proteins to begin nucleation of phagophore. Mitochondria-localized BNIP3 interacts with adaptor protein LC3-II present in the phagophore via its LC3-interacting region (LIR) and promotes mitophagy, autophagy of mitochondria. (Image taken from International Journal of Cell Biology<sup>120</sup>, open access).

Elongation of the phagophore through formation of autophagy protein complexes, involves lipidation of LC3-I with phosphatidylethanolamine (PE) to form LC3-II which further acts as a scaffolding protein<sup>119</sup>. Mitochondrial BNIP3 can interact with LC3 through its LC3-interacting

region<sup>77</sup>, as previously discussed. This interaction targets phagophore to mitochondria for mitophagy. Once mature, the phagophore (now called the autophagosome) containing cytoplasmic contents fuses with lysosome to form an autolysosome. The cytoplasmic contents are degraded within the autolysosome and released into the cytoplasm<sup>118,119</sup>.

Normally, induction of autophagy through the ULK1/2 complex is inhibited by mammalian target of rapamycin complex (mTORC1)<sup>118,119</sup>. BNIP3 has been shown to inhibit Ras homolog enriched in brain (RHEB), an upstream activator of mTORC1<sup>122,123</sup>.

#### **1.4.3 Nuclear BNIP3 and its role in transcriptional repression**

Although BNIP3 has been shown to localize in the nucleus of glial cells and other cancers, it does not have a nuclear localization signal. The mechanism of nuclear localization of BNIP3 is unknown, however its role in the nucleus has been studied. Nuclear BNIP3 has been shown to be involved in transcriptional repression of apoptosis-inducing factor (AIF) and death receptor 5 (DR5) through a complex with proteins such as histone deacetylase 1 (HDAC1) and polypyrimidine tract-binding protein (PTB)-associated splicing factor (PSF). Inhibition of apoptotic protein AIF and DR5 promotes survival and could be contributing factor in chemotherapy resistance in gliomas<sup>124,125</sup>.

In summary, BNIP3 overexpressed in the cytoplasm can induce mitochondrial dysfunction through different mechanisms, as well as induce different forms of cell death. BNIP3 induced cell death is cell type specific. However, nuclear BNIP3 is involved in transcriptional repression of apoptotic proteins, and promotes cell survival.

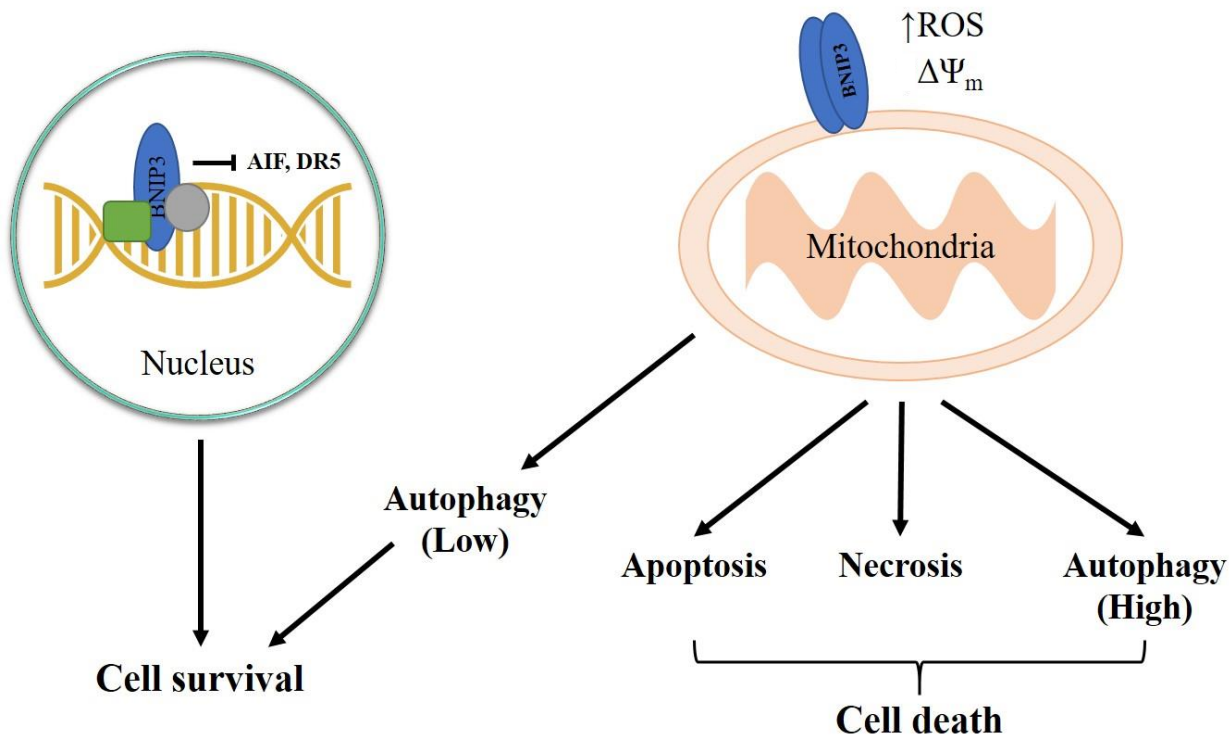


**Figure 1.9 Summary of BNIP3 functions.**

BNIP3 function depends on its localization in the cell. Overexpressed BNIP3 typically localizes in the mitochondria where it can cause mitochondrial dysfunction either directly or by associating with other pro-death proteins such as BAK and BAX. Regardless, mitochondrial dysfunction leads to increase in ROS and loss of mitochondrial potential, which can lead to cell death directly or by induction of cell death mechanisms such as apoptosis, necrosis or other forms of caspase-independent cell death depending on the cell type. Mitochondrial BNIP3 is also associated with autophagy, which serves as a survival mechanism if induced at low levels but can lead to cell death at higher levels. On the other hand, nuclear-localized BNIP3 is involved in transcriptional repression of cell death proteins such as AIF and DR5, which inhibits apoptosis and leads to cell survival.

#### 1.4.4 BNIP3 in human diseases

As previously discussed, expression of BNIP3 is limited to only a few tissues such as brain and skeletal muscle under normal physiological conditions<sup>82</sup>. The function of BNIP3 under normal conditions is not well studied, but may involve transcriptional control of apoptotic proteins<sup>124,125</sup> or regulation of basal autophagy<sup>91</sup>. However, extensive research has been done on the role of BNIP3 in hypoxia-related diseases such as myocardial infarction and cancer.

#### **1.4.4.1 BNIP3 in myocardial infarction**

Myocardial infarction or cardiac ischemia and reperfusion (I/R), commonly referred to as heart attack, is a major cause of heart failure. Blockage of arterial blood flow to the heart leads to lack of oxygen for cardiomyocytes and puts them under hypoxic stress. This condition is clinically known as cardiac ischemia. When blood supply returns to affected tissue, called reperfusion, the cells are further affected by oxidative stress and suffer more damage. During ischemia, the cells may undergo either apoptotic and/or necrotic cell death due to lack of nutrients and a buildup of acid as a result of lack of oxygen<sup>126,127</sup>. Experiments have shown that BNIP3 is overexpressed in cardiomyocytes under hypoxia, and levels of protein stay high until reoxygenation<sup>115,128,129</sup>. BNIP3 has also been shown to be stabilized by the low pH of the cells<sup>128,129</sup>. *In vitro* studies revealed that hypoxia-induced cell death is diminished when BNIP3 expression is inhibited by either RNA interference or co-expression of dominant negative mutant of the protein<sup>115,128,129</sup>. Moreover, overexpression of BNIP3 resulted in increased cell death<sup>115,128</sup>. BNIP3-dependent cell death in I/R injury was also confirmed *in vivo* utilizing animal models. Studies have shown increased levels of BNIP3 in animal models of chronic heart failure<sup>84,115</sup>. Additionally, *Bnip3*-knockout (KO) mice were shown to experience 50% less apoptosis of cardiomyocytes following a surgical I/R injury, compared to wildtype<sup>116</sup>. Forced cardiac expression of BNIP3 in this study resulted in myocardial apoptosis, further indicating the apoptotic cell death in myocardial infarction to be BNIP3 dependent.

#### **1.4.4.2 BNIP3 in cancer**

BNIP3 is often found overexpressed in hypoxic regions of solid tumors. Increased expression has been seen in brain tumors, breast carcinomas, endometrial cancer, cervical tumors, lung tumors, follicular lymphomas, DCIS (ductal carcinoma *in situ*), gastric adenocarcinomas, and prostate

tumors<sup>64</sup>. BNIP3 expression has also been correlated with advanced clinical stage in cervical tumors<sup>109</sup>, tumor grade in DCIS<sup>130</sup>, metastasis in colorectal cancer<sup>131</sup>, and poor patient outcome in ependymomas<sup>132</sup>, endometrial cancer<sup>133</sup> and non-small cell lung cancer<sup>108</sup>. In spite of its strong pro-death function, expression of BNIP3 in cancer often predicts aggressive disease. Hence, cancer cells may have developed mechanisms to escape BNIP3-induced cell death.

As previously mentioned, BNIP3 expression is often increased in hypoxic core of glioblastoma cells, however the majority of protein resides in the nucleus. Nuclear localization of BNIP3 is also seen in non-small cell lung tumors, breast tumors, prostate tumors and cervical tumors. As nuclear BNIP3 is known to inhibit expression of pro-death protein AIF and DR5, this might suggest a possible mechanism by which cancer cells avoid BNIP3-induced cell death<sup>124,125</sup>. BNIP3-induced cell death has also been shown to be inhibited by increased growth factor signalling, which may provide another possible mechanism by which cancer cells avoid cell death<sup>74</sup>. Epigenetic silencing of BNIP3 promoter by hypermethylation has also been observed in several cancers including hematopoietic, colorectal, hepatocellular, pancreatic and gastric tumors<sup>103,134-137</sup>.

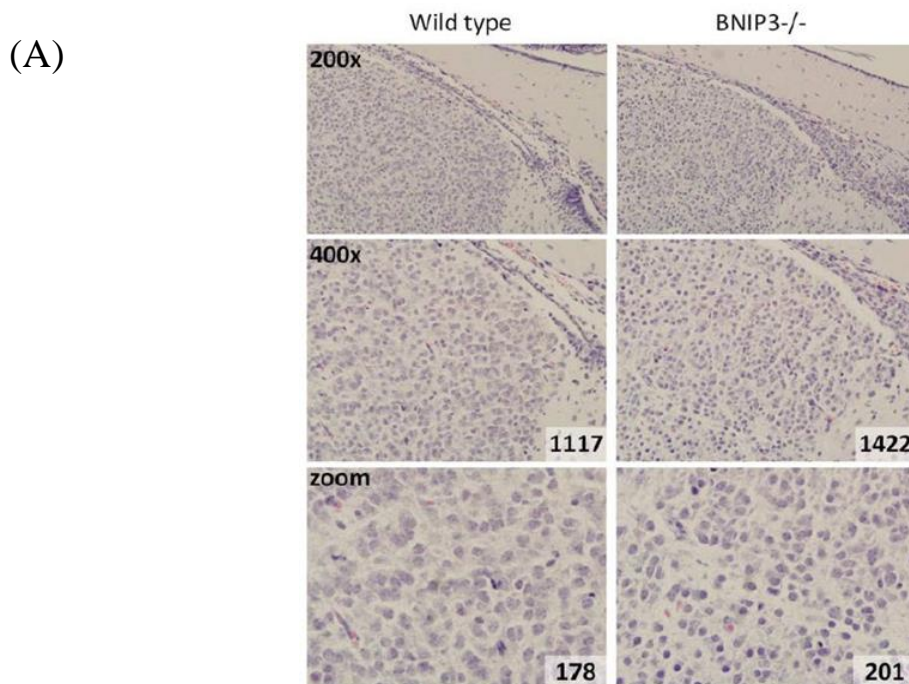
In breast cancer, BNIP3 has been shown to be associated with improved patient survival in invasive breast cancer, but poor outcome in pre-invasive disease<sup>138</sup>. This difference could be associated with the role of BNIP3 in autophagy. BNIP3-induced autophagy could provide increased survival to preinvasive tumors leading to tumor progression, but prolonged autophagy in later stages may lead to autophagic cell death of tumor cells and increased patient survival<sup>138</sup>.

#### **1.4.5 BNIP3 in development**

Studies utilizing mouse models have shown that *Bnip3*-KO mice are born at normal mendelian ratios from heterozygous crosses, and do not differ from wildtype mice in mortality and physical

abnormalities. No detectable defects were identified in cardiac and hematopoietic systems in unstressed *Bnip3*-KO mice<sup>116</sup>. Analysis of gene expression profiles showed an increase in levels of BNIP3 mRNA along with BCL-xL during oligodendrocyte differentiation in an *in vitro* model<sup>139</sup>. Both BNIP3 and BCL-xL may be regulating cell survival and cell death during this process. Another study identified peak BNIP3 expression at postnatal day 6.5 in rats, correlating with cell death that occurs in neonatal rat cortex and hippocampus at this time in development<sup>140</sup>.

Interestingly, when studying the effects of BNIP3 on autophagy, Meghan Azad (a previous member of the Gibson lab) observed a difference in cellularity in the brains of wildtype and *Bnip3*-KO mice<sup>141</sup>. Specifically, immunohistochemistry of mice brain sections revealed a higher number of cells in various parts of the *Bnip3*-KO mice brain (including cerebellum, hippocampus, cortex and inferior colliculus) when compared to wildtype. This difference was 11% on average in E18.5 (embryos at day 18.5) mice brain and statistically significant. However, the difference between adult brains (8 weeks old) was only 5% on average and not statistically significant. Nonetheless, the *Bnip3*-KO mice showed an increase in cellularity of brain during development and this increase persisted in the adult mice.



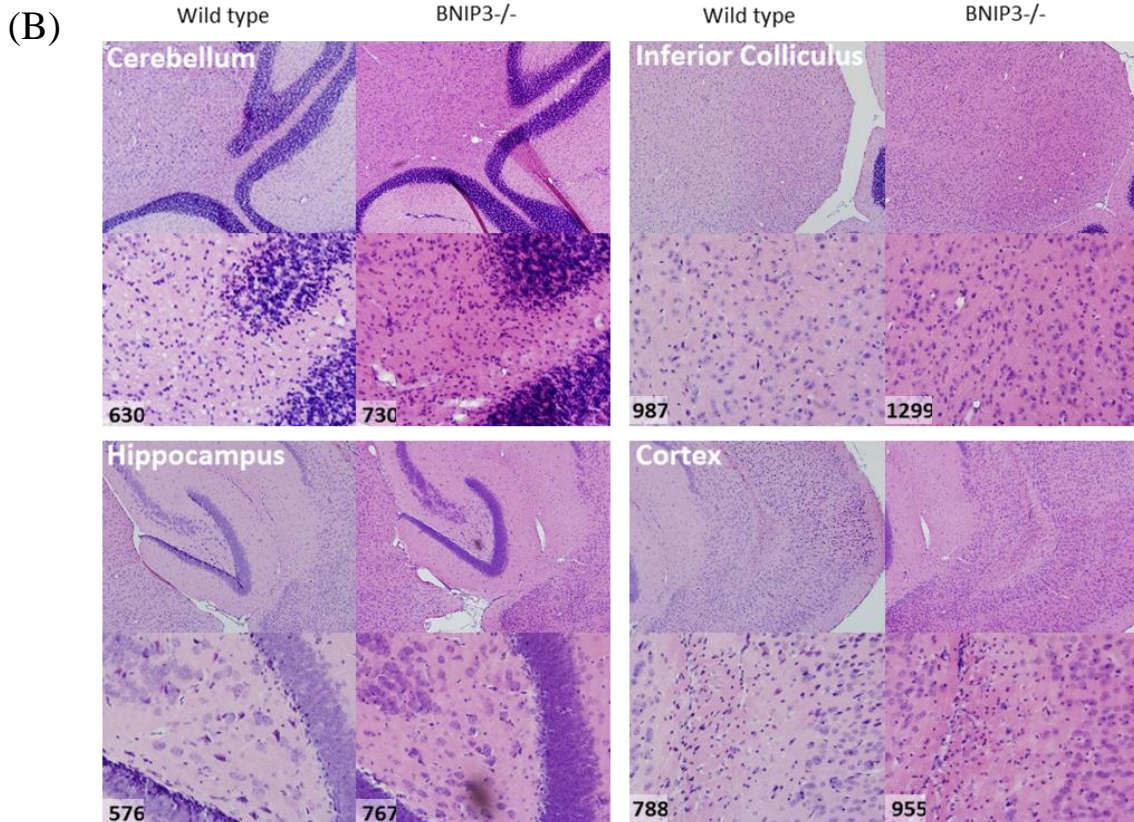


**Figure 1. 10 Cell count differences in wildtype and *Bnip3*-KO mice brain.**

Brains from E18.5 (A) and 8-week old (B) mice were fixed overnight with paraformaldehyde, paraffin embedded, sectioned and stained with hematoxylin and eosin. Images were taken at 200X and 400X magnifications, and cells were counted using Image Pro Plus 5.0 software. Genotype is denoted on top of the images, and the cell number is provided at the bottom of each image. The cell counts are higher in *Bnip3*-KO brains for both E18.5 and adult mice brains. Morphology of cerebellum, inferior colliculus, hippocampus and cortex can be seen in (B). (Images courtesy of Meghan Azad<sup>[41]</sup>).

Apart from increased cell number, the gross brain morphology appeared normal in *Bnip3*-KO mice. Similar to other studies, the mice were also born at normal mendelian ratios from a heterozygous cross and did not show increase in mortality or physical abnormalities.

## **1.5 Thesis Rationale, Hypothesis and Aims**

### **1.5.1 Rationale**

The function of cytoplasmic BNIP3 in mediating various cell death pathways is well studied, and detailed mechanisms have been identified. The role of nuclear BNIP3 in promoting survival by inhibition of cell death proteins has also been established. Studies have also looked at expression profile of *Bnip3* during development, however, information is lacking about the functions of BNIP3 during development.

As previous work in our lab identified differences in cell number between wildtype and *Bnip3*-KO mice brain, this study focuses on quantitative analysis of the effects of *Bnip3* expression on cellular proliferation. Since the initial observations were made in mouse brain, astrocytes and embryonic fibroblasts from wildtype and *Bnip3*-KO mice were used for the study. The mechanism by which BNIP3 may be affecting cellular proliferation will also be explored.

### **1.5.2 Hypothesis**

BNIP3 represses cellular proliferation by regulating the expression of cell cycle progression and/or proliferation genes.

### **1.5.3 Research Aims and Objectives**

This research aims to:

- (1) Determine whether cellular proliferation is affected by presence or absence of BNIP3.
- (2) Determine the mechanism with which BNIP3 may be regulating cellular proliferation.

More specifically, our objective is to:

- (1) Study and quantify the difference in proliferation between wildtype and *Bnip3*-KO cells.
- (2) Determine the differences in proliferation and/or cell cycle signalling pathways between wildtype and *Bnip3*-KO cells, if any.
- (3) Identify the potential target genes involved in cell proliferation and/or cell cycle progression that may be regulated by BNIP3.

## **Chapter 2: Material and Methods**

---

### **2.1 Reagents**

All reagents were of analytical or research grade and were obtained from one of the following sources: Millipore Sigma, ThermoFisher Scientific (Life Technologies, Gibco, Invitrogen) and Sarstedt.

### **2.2 Cell culture**

All cell lines were maintained in a humidified incubator with 5% CO<sub>2</sub> at 37°C. For hypoxia, cells were maintained in a hypoxic chamber (Forma Scientific, Waltham, MA) at 37°C with <1% O<sub>2</sub> and 5% CO<sub>2</sub> balanced with N<sub>2</sub>. For cell cycle synchronization, cells were serum starved overnight in unsupplemented Dulbecco's Modified Eagle Medium (DMEM).

#### **2.2.1 Mouse embryonic fibroblasts**

Mouse embryonic fibroblasts (MEFs) were cultured in DMEM consisting of 4mM L-Glutamine, 4mM Sodium pyruvate, 4.5 µg/mL Glucose and supplemented with 10% fetal bovine serum (FBS) and 100 units/mL penicillin/streptomycin. MEFs were also supplied with 0.1 mM β-mercaptoethanol in culture to help reduce toxic oxygen radicals during regular cell culture maintenance. However, β-mercaptoethanol was not added during proliferation experiments.

#### **2.2.2 Primary mouse astrocytes**

Primary mouse astrocytes were cultured in DMEM/F12 1:1 media (Hyclone) consisting of 2.5 mM L-Glutamine, 0.5 mM Sodium pyruvate, 17.5 mM Glucose and supplemented with 5% Glutamax, 10% FBS, 100 units/mL penicillin/streptomycin and 20 ng/mL mouse epidermal growth factor (EGF).

### **2.2.3 Human embryonic kidney cells, HEK293**

HEK293 cells obtained from American Type Culture Collection (ATCC) were cultured in DMEM media consisting of 4mM L-glutamine, 4mM sodium pyruvate, 4.5 µg/mL glucose and supplemented with 5% FBS and 100 units/ml penicillin/streptomycin.

### **2.2.4 Cell culture plates and flasks**

MEFs and HEK293 cells were cultured and maintained in 100 x 20 mm tissue culture plates (Sarstedt). Primary astrocytes, however, were grown in high attachment T-25/T-75 Primaria™ flasks (Falcon).

### **2.2.5 Cell passaging**

Cells were typically passaged at 80% confluence in varying dilution ratios of 1/4 (astrocytes); 1/5, 1/10 and/or 1/20 (MEFs and HEK293 cells). First, old media was removed via suction and cells were washed once with 1X phosphate buffered saline, PBS (Agilent Technologies). The cells were detached from respective culture plates by adding 2 ml (HEK293), 3 ml (MEFs) and 5 ml (astrocytes) of 0.05% Trypsin, and incubating at 37°C until cells visibly detached (typically 30 seconds for HEK293 cells, 10 minutes for MEFs and 12 minutes for astrocytes). Trypsin is a proteolytic enzyme that helps facilitate detachment of cells by breaking protein linkages between cells and the culture plates. The trypsin was inactivated by adding 8 mL of 5% (HEK293) or 10% (MEFs and astrocytes) FBS containing media. The cells were then transferred to 50 mL tubes and centrifuged at 290 g for 5 minutes. The supernatant was removed and cell pellet was re-suspended in respective cell culture media, and appropriate dilution or number of cells were seeded in new plates.

## **2.2.6 Cell preservation**

All cell lines were stored in liquid nitrogen to preserve for future use. Cells were harvested at 90% confluence by trypsinization and pelleted by centrifugation at 290 g for 5 minutes. The supernatant was removed and cell pellet was re-suspended in 1 mL media consisting of (a) 500 µL of 5% FBS containing DMEM/High Glucose, 300 µL FBS and 200 µL dimethyl sulfoxide (DMSO) for HEK293 cells, (b) 600 µL of 10% FBS containing DMEM/High Glucose, 300 µL FBS and 100 µL DMSO for MEF cells, and (c) 600 µL of 10% FBS containing DMEM/F12 1:1 media with EGF, 300 µL FBS and 100 µL DMSO for primary astrocytes. The cell suspension was transferred to 1.0 mL cryovial (Sarstedt) and placed inside a Nalgene (Mr. Frosty) freezing container (Thermo Scientific) containing isopropanol. The containers were stored at -80°C for a week, and the frozen cryovials were moved to nitrogen tanks for long term storage.

## **2.2.7 Thawing and culturing of frozen cells**

Frozen cryovials were removed from liquid nitrogen tanks and thawed in 37°C incubator. The thawed cells were suspended in 9 mL of appropriate culture media and centrifuged at 290 g for 5 minutes. The supernatant was removed and cell pellet was re-suspended in 10 mL of serum-containing DMEM and transferred to 10 cm plates. The cells were incubated at 37°C for 24 hours and media was replaced. The cells were passaged at 80% confluence at least once before any experiments.

## **2.2.8 Incubation in hypoxia**

For hypoxia induction in MEFs, cells were incubated inside a hypoxic chamber (Forma Scientific). The culture media was removed and plates were transferred to the hypoxic chamber which was then cycled to remove any excess oxygen. Hypoxic media, which had been placed in chamber for more than 5 days to remove oxygen, was used to replace media in the plates and cells were

incubated at 37°C with 5% CO<sub>2</sub>, 10% H<sub>2</sub> and < 1% O<sub>2</sub> balanced with N<sub>2</sub> for 24 hours. The plates were removed from the chamber and immediately harvested by trypsinization as previously explained.

## **2.3 Western blot**

### **2.3.1 Preparation of protein lysates**

Cells were cultured and harvested as previously explained. Harvested cells were spun down in a centrifuge at 290 g for 5 minutes. The supernatant (media) was removed by suction. The resultant cell pellet was then lysed using appropriate lysis buffer.

**Table 2. 1 Composition of lysis buffers used for different cells and tissues.**

<b>Cell lines/ Tissues</b>	<b>Lysis buffer recipe</b>
<b>MEF cells; HEK293 cells</b>	20 mM Tris base (Sigma), 150 mM sodium chloride (NaCl), 10% Glycerol, 2 mM ethylenediaminetetraacetic acid (EDTA), 1% NP-40 (Sigma), 1 mM activated sodium orthovanadate (New England Biolabs), 2 mM phenylmethanesulfonylfluoride (PMSF, Sigma), and SigmaFAST™ protease inhibitor tablet (1 per 10 mL lysis buffer, Sigma). The lysis buffer was aliquoted in 1.5 mL Eppendorf tubes and stored at -20°C. Added fresh before use: 1 µL each of Phosphatase inhibitor cocktails 2 and 3 (Sigma) per mL lysis buffer.
<b>Primary astrocytes; Mice brain</b>	50 mM Tris pH 7.5, 200 mM NaCl, 1% Tween 20, 0.2% NP40, 1 mM NaF, 2 mM PMSF, 1 mM activated sodium orthovanadate, 50 mM beta-Glycerol phosphate (Sigma), and SigmaFAST™ protease inhibitor tablet (1 per 10 mL lysis buffer). The lysis buffer was aliquoted in 1.5 mL Eppendorf tubes and stored at -20°C. Added fresh before use: 1 µL each of Phosphatase inhibitor cocktails 2 and 3 per mL lysis buffer.

The lysates were vortexed for 15 seconds and incubated on ice for 5 minutes. This was repeated two more times and the samples were centrifuged at 16,000 g for 15 minutes at 4°C. The supernatant was transferred to a new tube and stored at -80°C.

The wildtype and *Bnip3*-KO mice brains were homogenized with PowerMasher II (Nippi Inc.). The tissue was homogenized with 20 strokes on ice, followed by 35 minutes incubation on ice, and then re-homogenized with another 10 strokes. The lysates were centrifuged at 16,000 g for 20 minutes at 4°C. The supernatant was transferred to a new tube and stored at -80°C.

### **2.3.2 Protein Quantification, Gel Electrophoresis and Western Blotting**

The concentration of protein lysates was determined by using Pierce BCA (bicinchoninic acid) protein assay kit (Thermo Scientific), using BSA (bovine serum albumin) as a standard control and following manufacturer's instructions. The standard samples were prepared as a series of eight dilutions (2, 1.5, 1.0, 0.8, 0.6, 0.4, 0.2 and 0 µg/µL). The unknown samples were prepared as triplicates with a 1/10 dilution in ddH<sub>2</sub>O. The BCA reagents were added to both standard and unknown samples and incubated 30 minutes in 37°C. The absorbance of samples was then measured at 562 nm using Epoch Microplate Spectrophotometer (BioTek instruments) with Gen 5 v2.09 software. The concentration of each unknown was determined by comparing its absorbance to standard curve generated from BSA samples.

Samples were prepared for gel electrophoresis by equal quantity of protein with 6X loading buffer (375 mM Tris.HCl at pH 6.8, 9% SDS, 50% glycerol, 9% v/v beta-mercaptoethanol, and 0.03% bromophenol blue). Volumes of samples were equalized by adding ddH<sub>2</sub>O to get 1X concentration of loading buffer. Samples were boiled at 98°C for 10 minutes, cooled on ice and centrifuged. Proteins were separated on a 10% acrylamide gel (TGX FastCast Acrylamide kit, Bio-Rad) by SDS-PAGE at 80V for approximately 2 hours. The separated proteins were transferred to 0.45µm nitrocellulose membrane (Bio-Rad) at 24V for 1 hour. The membranes were blocked in 5% skim milk dissolved in PBST (0.1% Tween 20 in 1X PBS), and incubated in primary antibody (in 5%

skim milk in PBST) according to Table 2.2 at 4°C. The membranes were washed three times with PBST (10 minutes per wash), and incubated with HRP (horseradish peroxidase)-linked Immunoglobulin G (IgG) secondary antibodies for 1 hour at room temperature (Table 2.3) and washed three times as above. Finally, the western blots were developed using either Enhanced Chemiluminescence (ECL; Thermo Scientific) or Super Signal West Pico Chemiluminescent Substrate (Thermo Scientific). The blots were imaged using either ImageQuant LAS 500 gel imager (GE Healthcare Life Sciences) or autoradiography film (Fujifilm). The membranes were also probed for Glyceraldehyde 3-phosphate dehydrogenase (GAPDH) as a loading control to correct for loading differences. The protein levels were quantified using ImageJ (an open source image processing program). The membranes were stripped for 45-60 minutes with Western Re-probe agent (Calbiochem) before incubating with additional primary antibodies on the same blot. The membranes were never stripped and re-probed more than two times.

**Table 2. 2 Primary antibodies used for western blot and immunofluorescence.**

Antigen	Host Species	Application	Dilution and incubation time	Source, Catalog #
BNIP3	Mouse	WB	1:1000, overnight	Abcam, ab10433
CASPASE 8	Rabbit	WB	1:1000, overnight	Cell Signaling, 4927
DLX1	Rabbit	WB	1:500, over 3 nights	ThermoFisher, PA5-69058
GAPDH	Chicken	WB	1:20000, 1 hour room temperature	Millipore Sigma, AB2302
GFAP	Mouse	IF	1:1000, overnight	Sigma-Aldrich, G3893
HISTONE 4	Mouse	WB	1:1000, overnight	Abcam, ab10158
IGF2BP1	Rabbit	WB	1:500, over 3 nights	Abcam, ab82968
Ki-67	Rabbit	IF	1:200, overnight	Cell Signaling, 12202
MAPK	Rabbit	WB	1:1000, overnight	Cell Signaling, 4695
phospho-MAPK	Mouse	WB	1:1000, overnight	Abcam, ab50011
PTGS2	Rabbit	WB	1:750, over 3 nights	Abcam, ab15191

**Table 2. 3 Secondary antibodies**

Antigen	Host Species	Conjugate (Dilution)	Source, Catalog #
Rabbit IgG	Goat	HRP (1:5000)	Bio-Rad, 170-6515
Mouse IgG	Goat	HRP (1:5000)	Bio-Rad, 170-6516
Rabbit IgG	Goat	Biotin (1:200)	Vector Labs, BA-1000
Chicken IgG	Donkey	HRP (1:10000)	Millipore Sigma, AP194P
Biotin		Alexa Fluor 488 Streptavidin	Life Technologies, S11223
		Alexa Fluor 633 Streptavidin	Life Technologies, S21375

## **2.4 Reverse Transcription and Quantitative Real-time Polymerase Chain**

### **Reaction (RT-qPCR)**

RNA was extracted using RNeasy kit (QIAGEN) and cDNA was generated using qScript cDNA synthesis kit (Quantabio), according to manufacturer's instructions. Table 2.4 lists the primers used for amplifying mRNA during PCR reactions. The real time PCR was performed in pre-designed 96-well SYBR™ green PCR assay plates (Bio-Rad).

The PCR reaction consisted of initial 2 minutes at 95°C for activation and denaturation, and 40 cycles of [5 seconds at 95°C, 30 seconds at 60°C] for amplification. A melt curve was generated at the end from 65°C to 95°C (0.5°C increments, 5 seconds per step). The data was analyzed using CFX Manager™ software v3.1 (Bio-Rad). PCR products were separated on a 1% agarose gel at 80V for 1.5 hours with EZ-Vision Three™ DNA dye and loading buffer (VWR) and visualized under Ultraviolet (UV) light with Chemidoc XRS+ instrument (Bio-Rad).

**Table 2. 4 Amplicon context sequence and expected product size of Bio-Rad primers.**

<b>Gene</b>	<b>Identity</b>	<b>Amplicon context sequence</b>	<b>Product size, bp</b>
<b><i>Gapdh</i></b>	Reference gene	TGGGAGTTGCTGTTGAAGTCGCAGGAGACAACCTGGCCTCAGTGTAGCCCAAGATGCCCTCAGTGGGCCCTCAGATGCCTGCTTCA CCACCTTCTTGATGTCA	75
<b><i>Tbp</i></b>	Reference gene	TCTGAGTACTGAAGAAAGGGAGAACATGGACCAGAACACAG CCTTCCACCTTATGCTCAGGGCTGGCCTCCCCACAGGGGCCA TGACTCCTGGAATTCCCATCTTAGTCCAATGATGCCCTACGGCA	102
<b><i>Dlx1</i></b>	Target gene	CGAGCTTCTCGGACCAATCCCCGGTATTATGCAAGAGAGCCG ACCAATCAGCTCCACCAGCTCATGAATATTATGACCTTGGCTG AGTCAAAGCTTGAA	72
<b><i>Igf2bp1</i></b>	Target gene	TTGCTCTGTCCTCTGGTGTGCTGTTAACCTGAGCCAGGATG TCTCGGATCTCCGCTGAGCCATCTGGCTGGCATAGAAATGTCC GATGATCTAACATGACTTGGTCGTTCTCATCC	93
<b><i>Ptgs2</i></b>	Target gene	CAAATCCTGCTGTTCCAATCCATGTCAAAACCGTGGGAATGT ATGAGCACAGGATTGACCAGTATAAGTGTGACTGTACCCGGA CTGGATTCTATGGTAAAAC	77

In addition, *neo<sup>r</sup>* (neomycin resistance gene) was amplified in an end-point PCR reaction to validate the *Bnip3*-knockout MEFs and astrocytes. The following primers were used for mRNA amplification: 5'-AGG ATC TCC TGT CAT CTC ACC TTG CTC CTG-3' and 5'-AAG AAC TCG TCA AGA AGG CGA TAG AAG GCG-3'. The  $T_m$  is 72°C and expected size of amplified product is 492 base pairs. The PCR reaction consisted of 2 minutes at 95°C for denaturation followed by 30 cycles of [30 seconds at 95°C, 120 seconds at 72°C] for amplification, and a final 10 minutes hold at 72°C. The product(s) were visualized as previously explained.

## 2.5 Cell proliferation assays

### 2.5.1 Edu cell proliferation assay and Flow cytometry analysis

5-ethynyl-2'-deoxyuridine (Edu) is a nucleoside analog for thymidine, which can be incorporated into DNA by replicating cells. The incorporated Edu contains a free alkyne group which covalently binds to a fluorescent azide dye through “Click” reaction. The fluorescent cells can then be counted with a flow cytometer.

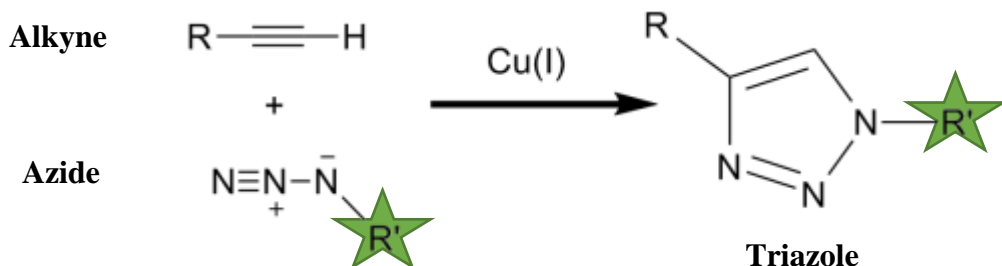


**Figure 2. 1 Copper catalyzed azide-alkyne cycloaddition- “Click” chemistry.**

Alkyne-group containing Edu (R) undergoes Click reaction with Alexa Fluor 488 (R') conjugated Azide-group in a Copper catalyzed reaction. Edu incorporated in cells can then be detected by a flow cytometer with a 488 nm laser.

The cells are seeded in 10cm plates to reach 60% confluence a day before the assay. The cells are then serum starved overnight to synchronize cell cycles. The next morning, serum containing media is added back. The plates are incubated per usual for 3 hours and then Edu is added to the media for a final concentration of 10 µM. No-Edu control plates are made as negative controls. The cells are incubated in Edu for 1 hour (pulse labelling) and harvested for Click labelling. The cells are fixed with 4% paraformaldehyde for 15 minutes and permeabilized with a Saponin-based wash reagent for 15 minutes. The cells are then incubated with fluorescent dye prepared in a proprietary buffer additive per manufacturer's instructions for 30 minutes. The cells are centrifuged and washed with 1% BSA in PBS at every step. The final cell pellet is suspended in 500 µL of Saponin-based permeabilization and wash reagent and transferred to 5 ml FACS tubes (Falcon). The green fluorescence of azide dye is measured using BL1 laser channel of NovoCyte™ Flow Cytometer (ACEA Biosciences) with NovoExpress 1.2.4 software.

### **2.5.2 Real time cellular analysis (RTCA)**

The RTCA instrument gives an indirect measure of cell index in culture in real-time. The instrument uses special 16-well plates coated with electrodes at the bottom. A small amount of electrical current is passed through individual wells from one end and measured at the other end. When no cells are present in the wells, the current measured is the same as the applied current. Once cells attach to the plate, the electrical current is impeded due to inherent resistance of cells and the current measured on the other end is lower than the applied current. This difference in the electrical current increases with an increase in cell number and can be converted to cell index by the accompanying software. Figure 2.2, provided by the manufacturer, summarizes the impedance principle.

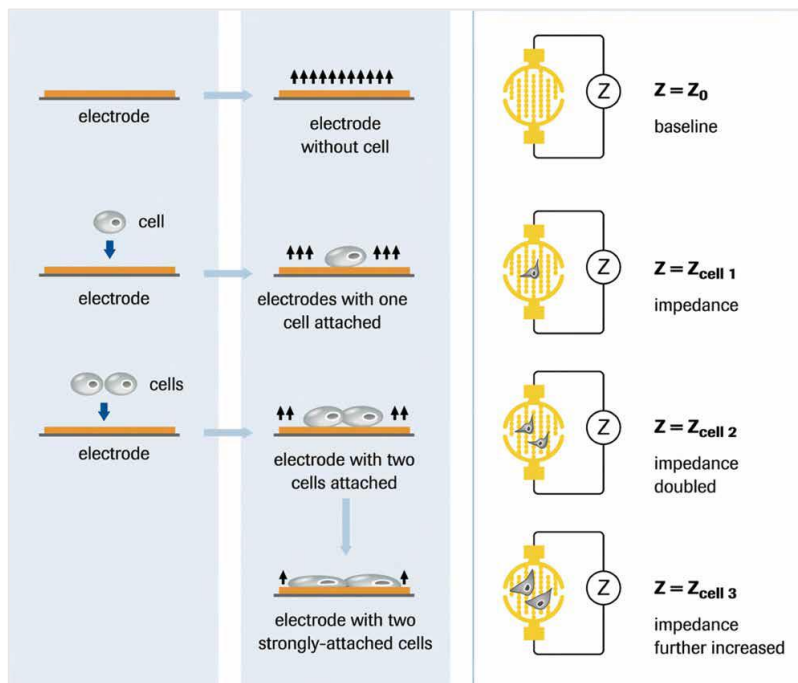


**Figure 2.2 Overview of changes in impedance of electrical current by adherent cells.**

Electrical current passed through electrodes is resisted by attachment of adherent cells at the bottom of RTCA plates. This impedance is proportional to the number and size of cells attached, and can be converted to cell index by the accompanying software. (Image taken from RTCA DP System Operator Manual v3)

The instrument is first blanked with culture media and then 5000 cells are seeded per well. The appropriate cell number was determined by performing an initial experiment for different cell counts from 4000-10,000 cells per well. The plates are incubated undisturbed for 10 days. The instrument was programmed to make measurements every 15 minutes. The cell index curve is generated by the accompanying software, and is normalized to the time where cells initially start proliferating (increase in impedance after an initial lag phase, approximately 15-20 hours).

### 2.5.3 Cytation 5 cell counting

The Cytation 5 Cell Imaging Multi-mode Reader is an electronic imaging device, accompanied by Gen 5 software that can process and analyze captured images. The cells are stained with NucBlue™ Live cell probing reagent (Thermofisher) that stains cell nuclei and imaged using

Cytation 5. The captured images are processed by Gen 5 software, and a “mask” can be generated around the observed nuclei to indicate one cell. The software can then create these masks around all stained nuclei and count the total number of masks in each image to provide a cell count. Figure 2.3A shows the cell image captured by Cytation 5, and figure 2.3B shows the masks generated by Gen 5 to count cells.

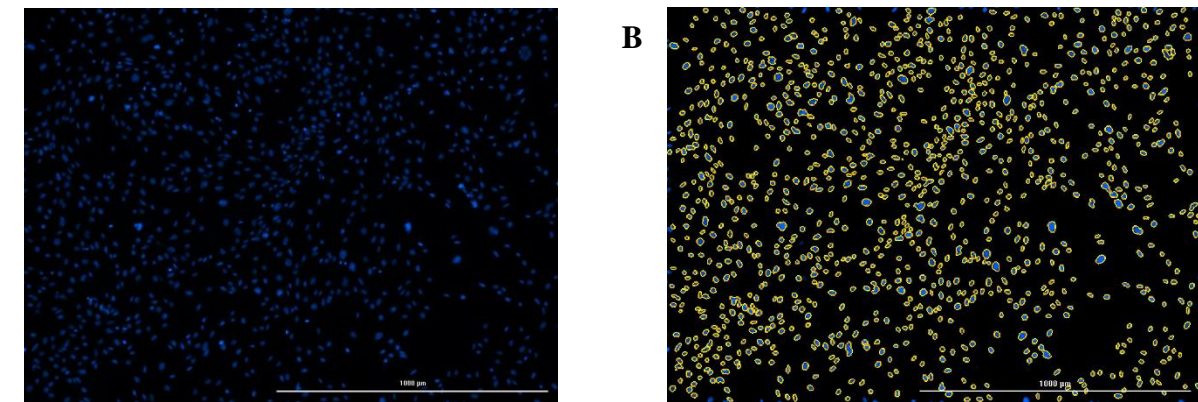


**Figure 2.3 Cell counting analysis performed by Gen 5 software.**

(A) NucBlue™ stained cells imaged by Cytation 5. (B) Gen 5 software creates a mask (yellow) around the blue stained nuclei to count cells. The mask is created by adjusting several size-related parameters (by the user) as defined within Gen 5 software.

We seeded  $1 \times 10^4$  cells per well in a 6-well plate. Enough plates were seeded to count cells in triplicates for each cell line, for six days. We captured four images per well, for a total of 12 images captured per cell line for each day ( $n=4$ ,  $N=3$ ) and counted using Gen 5 software.

## **2.6 Site-directed mutagenesis**

The nuclear localization signal containing *Bnip3* gene (*NLS-Bnip3*) was cloned into pcDNA3.1 vector by a previous member of the Gibson lab. The vector contains neomycin resistance (*neo<sup>r</sup>*) and ampicillin resistance (*amp<sup>r</sup>*) genes. The vector was sequenced (RIOH Sequencing services) to confirm identity and used in site-directed mutagenesis experiments to add human influenza hemagglutinin (HA) and poly-histidine (His) tags on 3' end of *Bnip3* gene.

The mutagenesis was performed using QuikChange Lightning Site-directed mutagenesis kit (Agilent technologies) as per manufacturer's instructions using 100 ng of dsDNA template. The HA-tag was inserted using following primers:

(5'-CACCAAGCACCTTGAATTCTACCCATACGATGTTCCAGATTACGCTATGGCTAGCATGACTG-3';

5'-CAGTCATGCTAGCCATAGCGTAATCTGGAACATCGTATGGTAGAATTCAAAGGTGCTGGT-3')

The His-tag was inserted using following primers:

(5'-GCACCTTGAATTCATGCATCATCACCATCACCACTAGGCTAGCATGACTGGTGG-3';

5'-CCACCAGTCATGCTAGCCTAGTGGTGATGGTATGCATGAATTCAAAGGTGC-3')

The amplified product was digested using *Dpn* I restriction enzyme to digest the non-mutated parental DNA. We transformed XL10-Gold Ultracompetent cells provided by the manufacturer with either amplified vector products or pUC18 control plasmid, as directed. The transformed cells were plated on LB-carbenicillin agar plates (200 µL per plate) containing 80 µg/mL X-gal and 20 mM IPTG. We selected 10 colonies from both HA and His-tag containing vector transformations and inoculated into 2 mL LB broth medium (DIFCO) with 50 µg/mL Carbenicillin and 50 µg/mL Kanamycin overnight. One mL of LB broth per colony was used to isolate plasmids using a mini prep kit (Qiagen) according to manufacturer's protocol. The plasmid preparations from all colonies were sequenced and analyzed for respective HA or His-tags. Successful HA and His-tag containing plasmids were used to transform DH5 $\alpha$ -T1<sup>R</sup> competent bacteria (Sigma), cells were amplified in LB broth and plasmids were isolated using plasmid maxi prep kit (Qiagen), all according to respective manufacturer's instructions. Plasmids were sequenced again and verified for the presence of nuclear localization signal, *Bnip3* gene and the respective HA or His-tags. The plasmid quality and concentrations were measured with Nanodrop 2000 (Thermofisher).

## **2.7 Transient *Bnip3* overexpression in HEK293 cells**

HEK293 cells were seeded in 10 cm dishes at a density of  $2 \times 10^5$  cells per plate and transfected with Lipofectamine 3000 (Invitrogen) at 70-80% confluency. The transfection reaction was prepared by combining 25  $\mu$ L Lipofectamine 3000 diluted in 250  $\mu$ L Opti-MEM (Gibco) with 5  $\mu$ g of either NLS-*Bnip3*-His plasmid DNA or empty pcDNA3.1 vector diluted in 250  $\mu$ L of Opti-MEM and supplied with 10  $\mu$ L of proprietary P3000<sup>TM</sup> reagent. The transfection mix was incubated at room temperature for 30 minutes and then mixed with 4.5 mL plain DMEM to replace the media in plates. The cells were incubated for 6 hours in this reaction mix followed by addition of 5 mL of 10% FBS containing DMEM/High Glucose media. The cells were incubated at least 24 hours before either lysing for western blot to confirm successful transfections or used for Edu cell proliferation assay.

## **2.9 Wildtype and *Bnip3*-null mice**

### **2.9.1 Genotyping**

The mice in animal care facility were regularly genotyped to identify wildtype, heterozygous and *Bnip3*-KO genotypes. The genomic DNA from mice ear punches was extracted using AccuStart II Mouse Genotyping Kit (Quantabio) according to manufacturer's instructions. PCR was performed on the crude DNA using 3 primers: 5'-TGTGGCTGAGAGTCAGTGGTC-3'; 5'-TTGCAAGTCTAGGAGTCAGTT-3'; 5'-GTGGATGTGGAATGTGTGCG-3'. The PCR generated either a 435 bp wildtype allele product or a 220 bp *Bnip3*-null allele product. The following reaction conditions were used for the PCR: (94°C for 4 minutes; 1 cycle), (94°C for 30 seconds, 60°C for 30 seconds, 72°C for 90 seconds; 33 cycles) and (72°C for 7 minutes; 1 cycle). The PCR products were separated on a 1% agarose gel and visualized as previously explained.

### **2.9.2 Isolation of embryonic fibroblasts**

MEFs were prepared by the Animal care facility. Pregnant mice were sacrificed at 13.5 or 14.5 dpc (day post-coitum) by cervical dislocation. The uterine horns were removed, washed with 70% ethanol and placed in falcon tube containing PBS (no  $\text{Ca}^{2+}$ ,  $\text{Mg}^{2+}$ ). Each embryo was separated from its placenta and embryo sac and placed in a petri dish. The head and red organs were dissected and washed with PBS for each embryo. The tissue were chopped with a sterile razor blade until they could be pipetted. The tissue was transferred to a 15 mL tube and incubated in 3 mL of 0.05% Trypsin/EDTA at 37°C for 5 minutes, pipetted and then incubated another 10 minutes. The trypsin was inactivated by adding 10 mL of serum-containing MEF media and cells were pipetted to attain a single cell suspension. The cells were centrifuged at 1000 rpm for 5 minutes. The supernatant was removed and cell pellet was re-suspended in 10 mL warm media. The cell suspension was transferred into a 10 cm dish and passaged at 80% confluency as previously described. The cells were either frozen for future use as primary cells or transfected with pCMVTag vector (SV40 T antigen) to immortalize the cells. The transfected cells were passaged at 80-90% confluency, and were frozen for future use after 5 passages.

### **2.9.3 Isolation of primary astrocytes**

Primary astrocytes were prepared by Dr. Sachin Katyal from mice neonates that were 2-4 days old. The mice were decapitated and both cortices were removed and placed in a 35 mm dish containing 3 mL serum-free media. The cortices were observed under a dissecting microscope and fine needle tweezers were used to remove hippocampus from the bottom, and meninges from the sides of cortices. Both cortices were placed in second 35 mm dish and rinsed with serum-free media and transferred to another 35 mm dish with 3 mL serum-containing media. The cortices were chopped into smaller pieces with fine needle tweezers and transferred to a 50 mL tube with

a pipette. The mixture was pipetted up and down until large chunks of tissue were no longer visible. Additional 10 mL serum-containing media was added to the cell suspension and tubes were centrifuged at 233 g (Allegra X-14R centrifuge, Beckman Coulter) for 5 minutes at room temperature. The supernatant was removed and cell pellet was suspended in 5 mL of astrocytes culture media (section 2.2.2) and transferred to a T-25 Primaria<sup>TM</sup> flask. The cells were incubated at 37°C in 5% CO<sub>2</sub> and media was changed 4-6 days after isolation (when cells were observed to be strongly attached under the microscope), and then once a week until cells were 100% confluent and ready to be passaged. The flasks were vigorously shaken before changing media to remove any less adherent, non-astrocyte cells. Once confluent, cells were harvested as previously explained and 2/3 of cells were transferred to T-75 flasks for expansion, 1 x 10<sup>5</sup> cells were used for immunofluorescence to measure culture purity by staining for astrocytes-specific glial fibrillary acidic protein (GFAP) and the remaining cells were seeded back in the original T-25 flasks. The cells were passaged and preserved as described in sections 2.2.5 and 2.2.6, respectively. All experiments with primary astrocytes were done at passages 1 (immunofluorescence, cell counting) and 2 (lysed for western blot).

## **2.10 Immunofluorescence on cover slips**

Immunofluorescence (IF) was done on cover slips to stain primary astrocytes for GFAP to determine culture purity. Five cover slips were placed per well in 6-well dishes and 30,000 cells were seeded separately from each astrocyte culture. Next day, the cover slips were transferred to 24 well dishes, one cover slip per well. The cells were fixed with 200 µL of 4% paraformaldehyde in PBS for 30 minutes at room temperature. The cover slips were then washed twice with 200 µL of 0.1% NP40 in PBS for 5 minutes (per wash). The primary anti-GFAP antibody was prepared 1:1000 in 0.1% NP 40, 10% FBS, 1X PBS solution. The cover slips were incubated in 200 µL of

primary antibody overnight. The next day cover slips were washed and incubated with red fluorescent secondary antibody diluted 1:5000 for 1.5 hours at room temperature (covered from light) on a shaker. The cover slips were washed twice and incubated with 200 µL of green fluorescent Phalloidin stain (Life Technologies) diluted 1:1000 in PBS for 1.5 hours at room temperature on a shaker. The cover slips were washed again twice and loaded onto a microscope slide with 3 µL of Vectashield Anti-fade mounting medium with DAPI (Vector Laboratories). The slides were observed with Cytation 5 Image reader and cells were counted with Gen 5 software as previously explained.

## **2.11 Immunofluorescence on paraffin-embedded tissue sections**

Paraffin-embedded brain sections from wildtype and *Bnip3*-null mice were prepared previously by a member of the Gibson lab<sup>141</sup>. The slides were baked at 60°C in a Micro Hybridization Incubator (Robbins Scientific) for 20 minutes. The slides were first treated with Xylene for 10 minutes to remove paraffin, followed by two minutes incubation in each of the following reagents (in separate containers, in order): Xylene, Xylene, 100% ethanol, 100% ethanol, 95% ethanol, 85% ethanol, 75% ethanol and 50% ethanol. The slides were left in ddH<sub>2</sub>O for 5 minutes to remove excess ethanol. The slides were then placed in a slow cooker containing 1.2 L of 10 mM Citrate buffer, and heated for 20 minutes on high in a dual wave microwave. The cooker was allowed to cool to room temperature before removing the slides. The slides were then washed three times in PBS, 5 minutes per wash. Immunohistochemistry blocking buffer (1X working solution) was prepared with following reagents: 10 mL of 10X PBS, 5 mL goat serum, 200 µL of 100% Triton X 100, 200 µL of 10% sodium azide, and 100 mg of bovine serum albumin. The final volume was brought to 100 mL with ddH<sub>2</sub>O. The slides were blocked for 2 hours in the blocking buffer at room temperature. After blocking, the slides were transferred to a humid chamber and incubated

overnight with 100 µL of primary antibody diluted to working concentration in blocking buffer, and covered with 22x60 mm coverslips. The next day, slides were washed three times with 1X PBST for 5 minutes (per wash). The slides were then incubated with 100 µL of Biotinylated secondary antibody diluted 1:200 in blocking buffer for 1.5 hours in the humid chamber at room temperature. The slides were again washed three times and incubated with 100 µL of streptavidin conjugated fluorescent tertiary antibody, diluted 1:500 in blocking buffer for 1.5 hours at room temperature. Finally, slides were washed and covered with 22x22 cover slips using 3.5 µL of Vectashield mounting medium.

## **2.12 Statistical Analysis**

All graphs were prepared using Microsoft Excel 2013. The data analysis was performed using Excel, while the Statistical analysis was performed using both Excel 2013 and Graphpad Prism 7. For multiple comparisons in MEF experiments, statistical significance was determined using One way ANOVA followed by tukey's post hoc test in Prism 7. The statistical significance of Astrocytes and HEK293 experiments was determined using Student's t test in Excel 2013. F-value was calculated first to determine whether a paired or unpaired t-test was appropriate. The threshold p-value for statistical significance was 0.05. Statistical significance is noted as follows in the figures: \*  $p < 0.05$ ; \*\*  $p < 0.01$ ; \*\*\*  $p < 0.005$ ; \*\*\*\*  $p < 0.0005$ . An uppercase 'N' denotes the number of times an experiment was independently repeated, while a lowercase 'n' indicates the technical repeats within an experiment.

# Chapter 3: Results

---

## 3.1 AIM 1: To determine whether BNIP3 knockout cells are more proliferative than wildtype cells.

### 3.1.1 Rationale for AIM 1

Increased cellularity in the brain of *Bnip3*-knockout mice indicates a potential role of BNIP3 in regulating cellular proliferation. In order to confirm these differences, we will quantitatively measure proliferation differences between wildtype and *Bnip3*-knockout cells. All experiments will be done with mouse embryonic fibroblasts (MEFs) and primary astrocytes isolated from neonatal mice.

### 3.1.2 Evaluation of purity of Primary Astrocytes cultures.

During the production of primary astrocytes from mice neonates, the cells can often be contaminated with fibroblasts. Therefore, the astrocytes cultures should be evaluated for their purity to find highly pure astrocytes. The Primary Astrocytes were assessed for culture purity by measuring the percentage of cells positive for glial fibrillary acidic protein (GFAP) by immunofluorescence. GFAP is an intermediate filament protein expressed in astrocytes, and is the most widely used astrocyte marker. Immunofluorescence was performed as previously explained (Figure 3.1). We analyzed five wildtype and four *Bnip3*-knockout astrocytes cultures, and their purity is indicated in Table 3.1 as a percentage of GFAP positive cells. The cells were counted with Cytation V as previously explained. The percentage of GFAP positive cells is calculated as:

$$\% \text{ GFAP positive cells} = \frac{\text{number of GFAP positive cells}}{\text{number of DAPI positive cells}}$$

We selected the higher purity wildtype and knockout cultures for all future experiments- WT2, WT3, WT4, KO2, KO3 and KO4. Although these cultures are not pure astrocytes but instead are astrocytes-rich, they will be referred to as astrocytes hereafter.

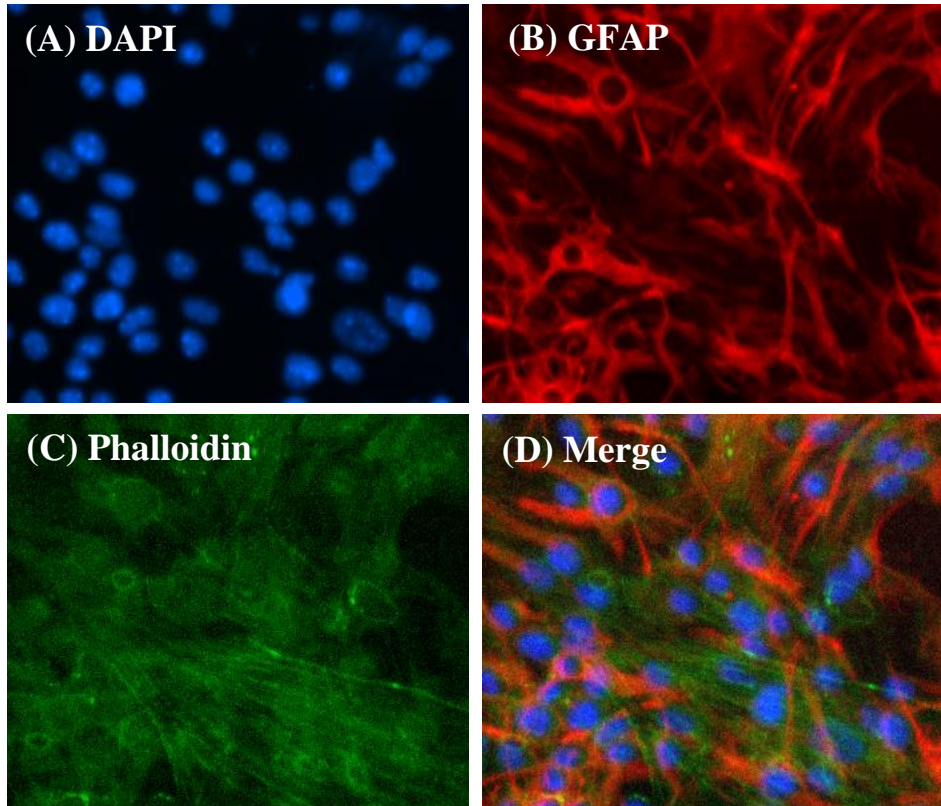


**Figure 3.1** A representative image of immunofluorescence of primary astrocytes to assess culture purity.

Astrocytes were grown on coverslips and immunofluorescence was performed to measure purity of cell cultures. A representative set of images showing (A) DAPI (B) GFAP (C) Phalloidin and (D) Merge staining of astrocytes. The images were taken with Cytation V Cell Imaging device at 10X magnification.

**Table 3. 1 Purity of Astrocytes cultures as a percentage of GFAP positive cells.**

CELL TYPE	% GFAP positive cells
WT1	40 ± 6%
WT2	73 ± 6%
WT3	73 ± 4%
WT4	70 ± 3%
WT5	42 ± 1%
KO1	NA
KO2	74 ± 3%
KO3	63 ± 3%
KO4	88 ± 4%

### 3.1.3 Validation of wildtype and *Bnip3*-knockout MEFs and Primary Astrocytes.

MEFs and Primary Astrocytes were validated for the presence or absence of BNIP3 expression, at both the gene and protein level before further experiments. As the *Bnip3*-null allele was generated by replacing exons 2 and 3 with *neomycin-resistance (neo<sup>r</sup>)* gene cassette (Figure 3.2A), expression of *neo<sup>r</sup>* gene was measured through PCR. Positive expression of *neo<sup>r</sup>* gene is only observed in *Bnip3*-null mice (Figure 3.2B).

MEFs were cultured in hypoxia for 24 hours to overexpress BNIP3. The cells were then lysed for total protein and western blotted for BNIP3. We were able to detect BNIP3 protein in wildtype MEFs but not the knockouts (Figure 3.2C). Unfortunately, the primary astrocytes did not have detectable levels of BNIP3 under normal conditions, and could not be incubated in hypoxia as the cells would not survive.

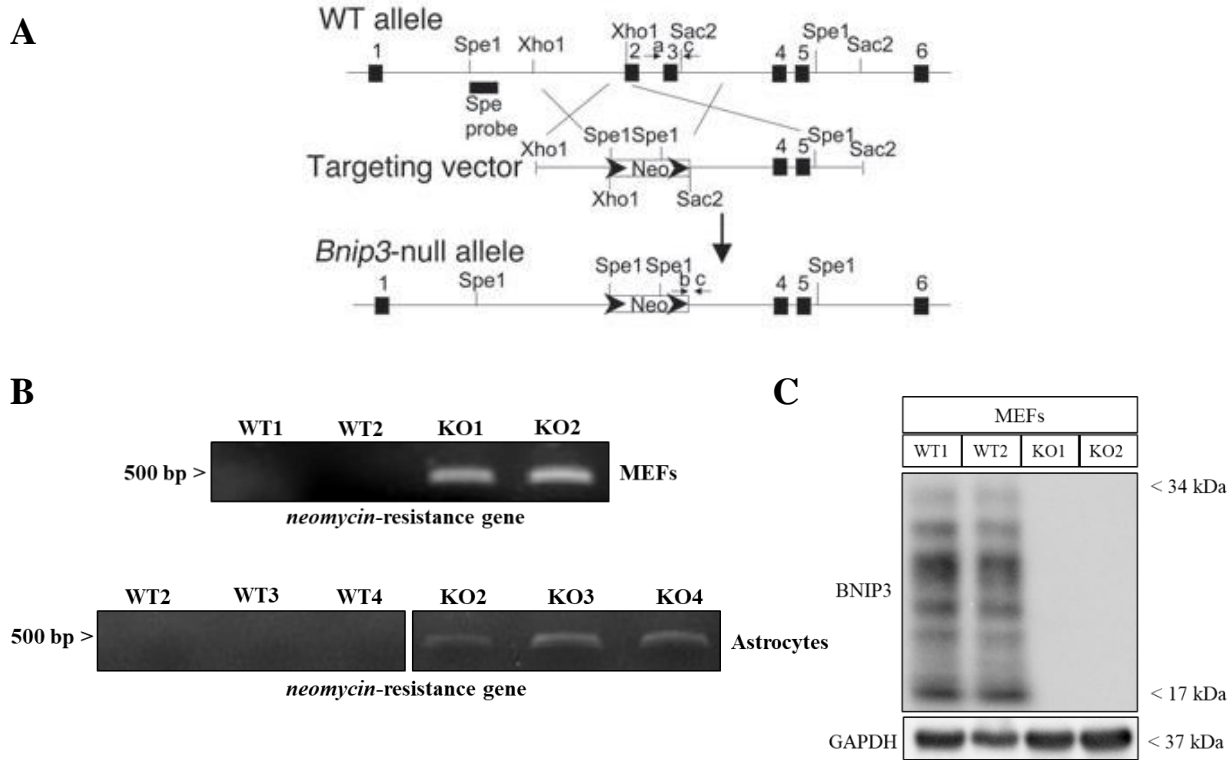


**Figure 3.2 Validation of mouse embryonic fibroblasts (MEFs).**

(A) Bnip3-null allele was created by replacing exons 2 and 3 with a neomycin resistance cassette. (B) RT-PCR was performed on total RNA isolated from MEFs and Astrocytes using primers against neomycin-resistance gene. A single band at ~500bp is observed (expected size is 492 bp). (C) Total lysates from MEFs were western blotted for BNIP3. Cells were incubated under hypoxia for 24 hours before lysing to over-express BNIP3. The blot was stripped and reprobed with GAPDH as loading control. Normally, BNIP3 appears as both a monomer at ~30 kDa and a dimer at ~60 kDa. Our current antibody detects several positive bands of BNIP3 in the expected size range. This could either be due to different isoforms of the protein, post-translational modification or degradation. No protein is detected in the knockout lysates. Unfortunately, BNIP3 protein levels were too low in astrocytes to be detected by western blotting.

### **3.1.4 Optimization of cell proliferation assays.**

The three proliferation assays used in this study were first optimized to identify appropriate experimental conditions. The optimizations were done using wildtype and *Bnip3*-KO MEFs. The MEFs were serum starved overnight to synchronize cell cycles before each assay.

(1) **Edu cell proliferation assay:** Synchronized cells were pulsed with Edu for 1 hour as previously described (section 2.5.1) at 0, 2, 4, 6, 23, 47 and 71 hours after addition of serum containing media. Edu positive cells could be detected at all time intervals measured (Figure 3.2A), however the percentage of Edu positive cells equalized between wildtype and *Bnip3*-KO cells at longer time intervals (24-72 hours). This may be due to a loss of synchronicity between cell cultures after addition of serum-containing media. Based on these results, we used 3 hours incubation in serum-containing media (+ 1-hour Edu pulse) in all future Edu assays.

(2) **RTCA:** Since RTCA is very sensitive to cell number and size, optimal cell seeding density should be determined independently for different types of cells. The assay requires enough cells to observe an initial lag phase with no proliferation of cells, to enable normalization of cell index curves at the first point of observed increase in cell index. In order to determine the optimal density of cells required, different density of cells was seeded from one wildtype and one *Bnip3*-KO MEF cell line, in duplicates. The plates were then incubated in the RTCA apparatus as previously described (section 2.5.2) over 10 days, and a measurement was made every 30 minutes (Figure 3.2B). The cell index curves for 4000 and 6000 cells show an initial lag phase as well as proliferation over a longer time interval compared to 8000 and 10000 cells. From these results, we estimated 5000 cells per well to be the appropriate seeding density for all future RTCA experiments.

**(3) Cytation V cell counting:** The Gen5 software (that accompanies Cytation V) can accurately count cells in a captured image until a threshold. At higher density of cells, the software is unable to distinguish between overlapping cell nuclei. In order to determine the highest number of cells that could be accurately counted by Gen 5, we seeded five different densities-2, 4, 8, 16 and 20 ( $\times 10^4$ ) of cells per well in a 6 well plate and counted them using Cytation V apparatus as described in section 2.5.3. As the cells were seeded in relative ratios of 1:2:4:8:10, the ratios of cells counted by Cytation V were compared to the known ratios (assuming lowest density of cells to be an accurate 1:1 cell count). As seen in Figure 3.2C, Cytation V cell counting matches the expected count until cell density goes beyond roughly 2300 cells per image, or  $8 \times 10^4$  cells per well. Based on these results, we estimated  $1 \times 10^4$  cells per well to be an appropriate initial seeding density to be able to accurately count cells for at least 5 days.

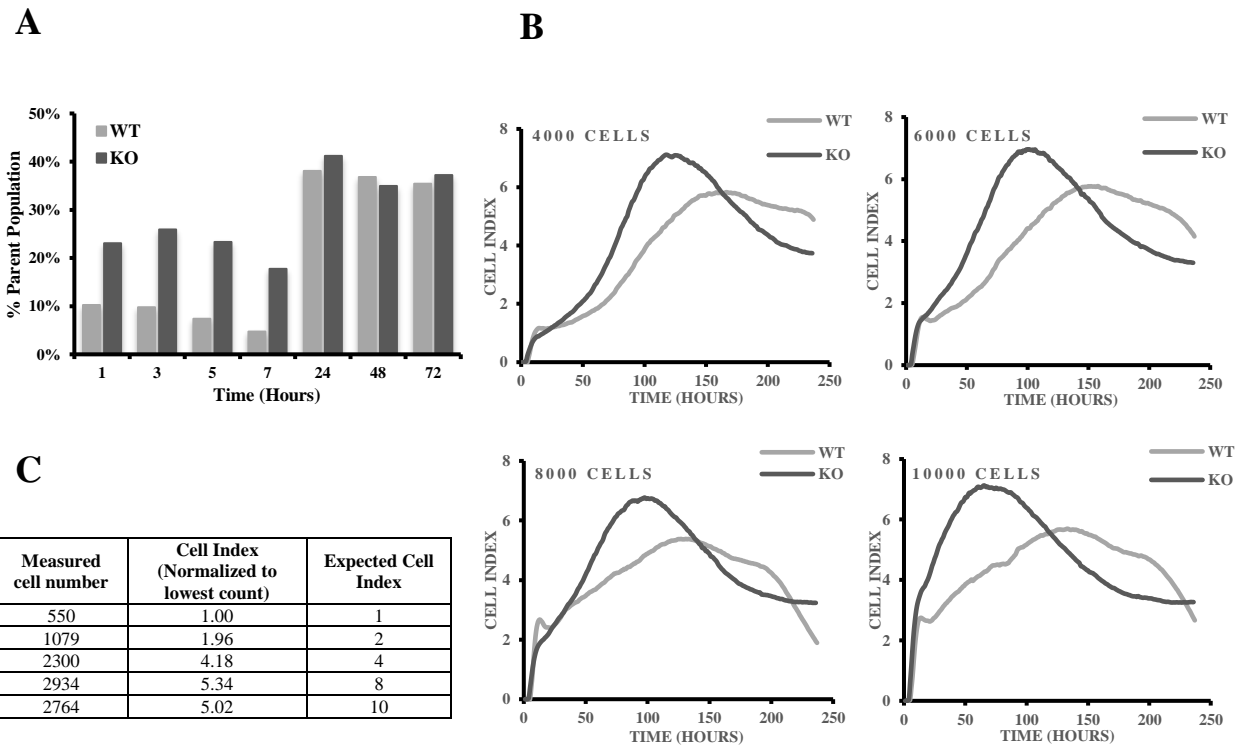


**Figure 3.3 Optimization of the three cell proliferation assays that were used in this study.**

(A) Edu cell proliferation assay was performed as previously explained at different time intervals after addition of serum containing media to synchronized cell cultures. Edu positive cells were counted using flow cytometer and are presented as a percentage of total cell count. This experiment was only done once to identify the best time point for Edu analysis. (B) RTCA plates were set up with different initial cell numbers to find appropriate seeding density of MEFs in E16 RTCA plates. The results are an average of two repeats ( $n=2$ ,  $N=1$ ). (C) Cells were seeded at different initial densities in 6 well plates and counted using Cytation V. The cell counts were divided by the lowest count to find the cell index ratios. These ratios were compared to expected cell index (based on initial seeding densities) to find the maximum number of cells that can be counted accurately by Cytation V. The results are an average of four readings per well ( $n=4$ ,  $N=1$ ).

### **3.1.5 *Bnip3*-knockout cells are more proliferative than *Bnip3*-expressing cells.**

To determine whether *Bnip3*-KO cells are more proliferative than *Bnip3*-expressing cells, the proliferation differences in wildtype and *Bnip3*-KO MEFs were measured with three different assays- Edu cell proliferation assay, Real time cellular analysis (RTCA) and Cytation V cell counting. The proliferation differences in primary astrocytes were only measured through Cytation V cell counting. MEF cell cycles were synchronized by serum starvation overnight before every assay.

For Edu cell proliferation assay, synchronized MEFs were supplied with serum-containing media for 3 hours before addition of 10 mM Edu for 1 hour. The cells were then harvested and labelled as previously explained. The Edu assay shows higher incorporation of Edu in *Bnip3*-KO MEFs compared to wildtype (Figure 3.4A). The wildtype MEFs had 27.0% and 28.7% Edu positive cells, whereas the *Bnip3*-KO MEFs had 35.8% and 43.3% Edu positive cells.

The RTCA assay was setup as previously explained- 5000 cells were seeded per well and measurements were taken every 15 minutes for >160 hours. As seen in Figure 3.4B, *Bnip3*-KO MEFs reached a higher cell index compared to wildtype MEFs. Moreover, the peak cell index was attained faster by *Bnip3*-KO MEFs. The *Bnip3*-KO MEFs reached peak cell indices of 6.37 and 4.20 in 83.06 and 93.07 hours, respectively. Whereas, wildtype MEFs reached peak cell indices of 3.76 and 3.01 in 107.84 and 128.11 hours, respectively.

The Cytation V cell counting experiments were setup identically with both MEFs and primary astrocytes-  $1 \times 10^4$  cells were seeded per well in 6 well dishes. The cells were counted each day as previously explained. Similar to RTCA, *Bnip3*-KO cells proliferate faster than wildtype cells and reach higher cell counts. The cell count differences between wildtype (130 and 133) and *Bnip3*-

KO MEFs (191 and 252) become significant at day 3 (Figure 3.4C) whereas these differences are significant as early as day 2 (Figure 3.4D) in primary astrocytes. As described in section 3.1.4, the Cytation V cell counting is not accurate past 2300 cells per image due to high cell density. Since the *Bnip3*-KO MEFs reach this limit at day 6, the actual cell count may be higher than reported.

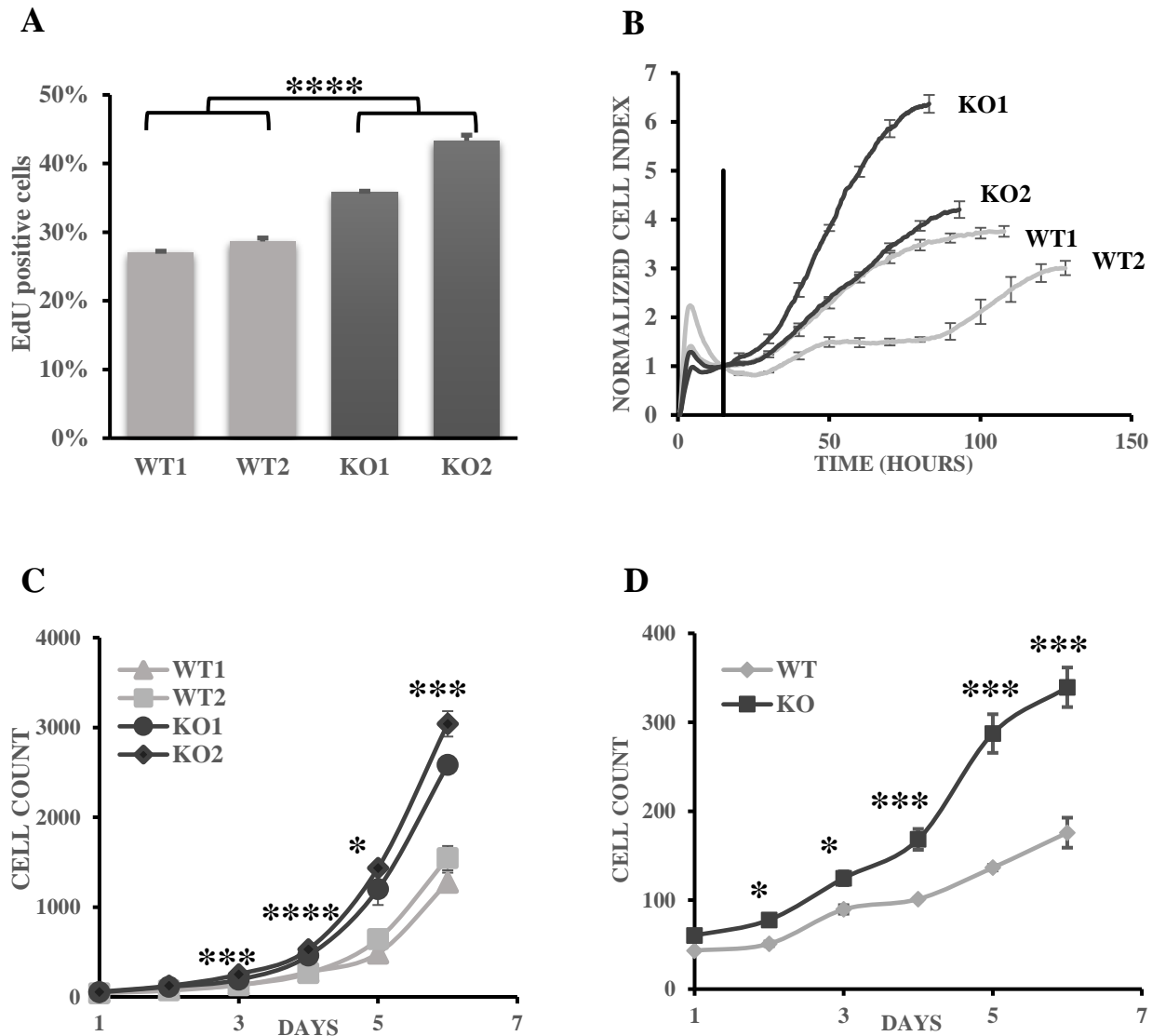


**Figure 3.4** *Bnip3*-knockout cells are more proliferative than wildtype cells expressing BNIP3.

(A) Click iT<sup>TM</sup> EdU cell proliferation assay was performed and Edu positive cells were counted using flow cytometer. The results show Edu positive cells as a percentage of total cells in the sample, and are an average of three replicates (n=3). These results are representative of three independent experiments (N=3). The error bars show standard error of mean. The statistical significance was tested with One way ANOVA, followed by Tukey's post hoc analysis. (\*\*\*\*p<0.0001). (B) Cell count was monitored using RTCA instrument over 5 days. The results shown are an average of three replicates (n=3), and representative of three independent experiments (N=3). The error bars show standard deviation. (C) Cells were incubated under normal conditions and counted with Cytation V instrument over 6 days. The cell count shown is an average of three independent wells (4 measurements per well; n=4, N=3). The error bars show standard error of mean. Statistical significance was tested with One way ANOVA followed by Tukey's post hoc analysis (\* p<0.05, \*\* p<0.005, \*\*\*\* p<0.0005). (D) Similar to (C), Cytation V was used to measure the differences in proliferation between wildtype and *Bnip3*-knockout astrocytes (n=4, N=3). Student's t-test was used to measure the statistical significance (\* p < 0.05, \*\*\* p < 0.005).

### **3.1.6 HEK293 cells overexpressing nuclear *Bnip3* have lower proliferation capacity than cells lacking *Bnip3* expression.**

Since our previous results indicated an increase in cell proliferation in *Bnip3*-knockout cells, we wanted to test whether reintroduction or overexpression of *Bnip3*/BNIP3 would lead to an opposite effect, i.e. reduced proliferation. We used HEK293 cell line for these experiments as it is a highly efficient transfection cell line. It also provides us a human cell line model to validate the results from mouse cells. BNIP3 is expressed at low levels in HEK293 cells and is not detectable by western blotting under normal oxygen conditions.

We transfected HEK293 cells with either *Bnip3*-expression vector or an empty vector as explained in section 3.7. Before measuring cell proliferation, we wanted to confirm the time at which BNIP3 is detectable at protein levels. The cells were lysed 24- and 48-hours post-transfection and western blotted for BNIP3. The protein was detectable at high levels at both time points (Figure 3.5A).

The proliferation differences between empty and *Bnip3*-vector transfected cells were measured by Edu cell proliferation assay. The cells were transfected in 10 cm dishes in triplicates and incubated for 24 hours. After 24 hours, cells were serum starved overnight for cell cycle synchronization. After overnight incubation, cells were harvested from each plate for western blot (Figure 3.5C), and  $2 \times 10^6$  were seeded back in plates for Edu analysis (Figure 3.5B). The cells overexpressing BNIP3 have a lower percentage of Edu positive cells (11.85%) compared to cells lacking significant BNIP3 expression (15.26%). The cells were also lysed using NEPER<sup>TM</sup> protein extraction kit to isolate nuclear and cytoplasmic proteins. As expected, due to the presence of the nuclear localization signal in the vector, the majority of BNIP3 protein is seen in the nuclear extract (Figure 3.5D).

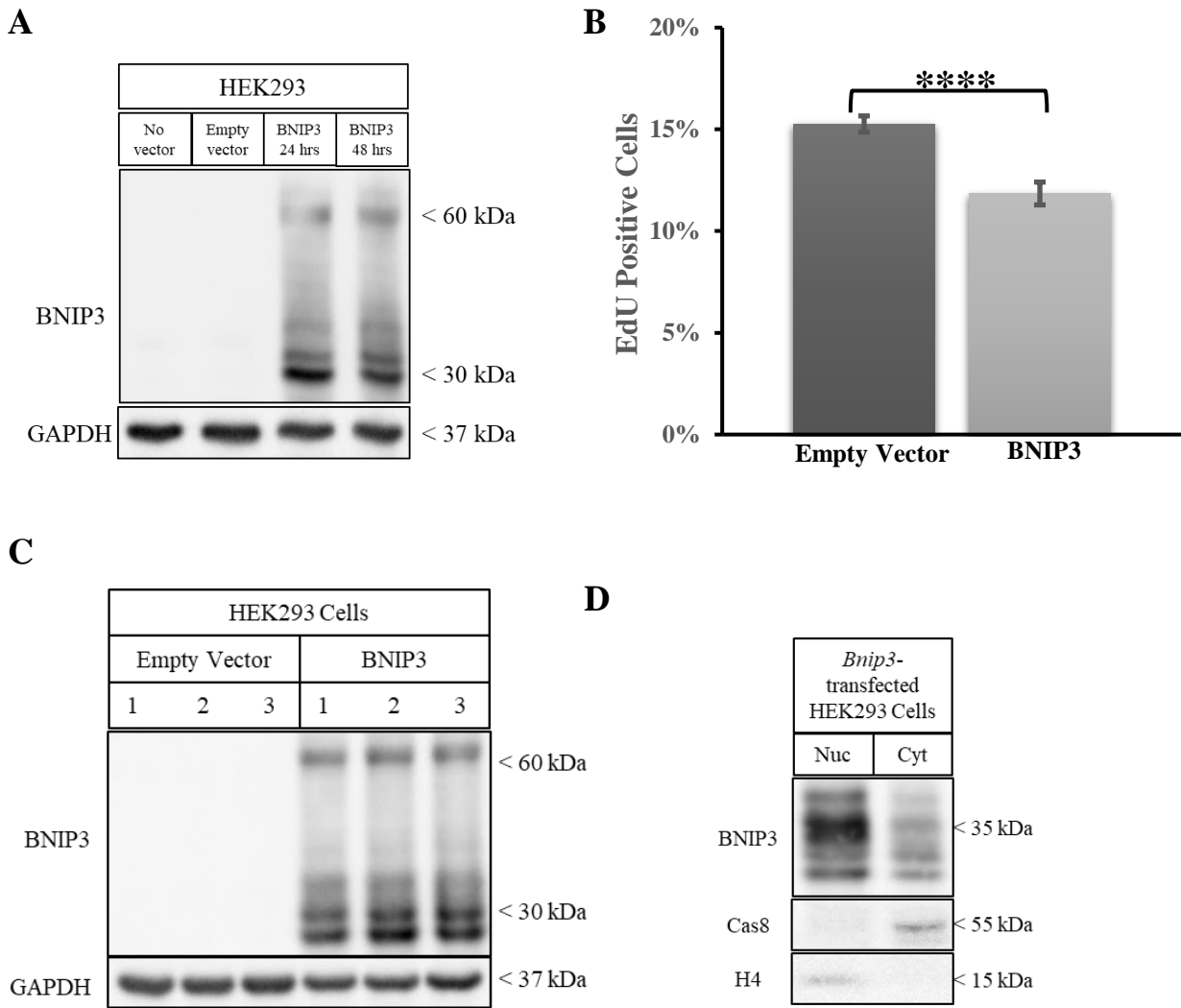


**Figure 3. 5 HEK293 cells overexpressing nuclear *Bnip3* have lower proliferation capacity than cells lacking *Bnip3*.**

(A) HEK293 cells transfected with either *Bnip3*-expression vector, empty vector or no vector control were lysed at 24 and 48 hours post transfection, and western blotted for BNIP3. The western blot indicates successful transfection and expression of protein at both 24 and 48 hours. GAPDH was used as the loading control. (B) Edu analysis of cells shows a decrease in percentage of cells actively synthesizing DNA when transfected with *Bnip3*-expression vector. The results are an average of three independent experiments, with three replicates each (N=3, n=3). Student's t-test was used to measure statistical significance of the differences (\*\*\*\* p< 0.0005). (C) A fraction of transfected cells used in Edu analysis were lysed for western blot analysis to confirm if the transfections were successful. GAPDH was used as loading control. (D) The transfected cells were also lysed using NEPER™ protein extraction kit to isolate nuclear and cytoplasmic proteins. Caspase 8 and Histone 4 were used as cytoplasmic and nuclear loading controls.

### **3.1.7 *Bnip3*-KO mice brain show increased levels of Ki-67 protein compared to wildtype brain.**

In addition to cell line models, we also investigated the difference in the proliferation marker protein Ki-67 in paraffin-embedded brain sections from wildtype and *Bnip3*-KO mice that first showed increased cellularity in *Bnip3*-KO brain (section 1.4.5). The slides were prepared for immunostaining as described in section 2.11, and probed with antibodies against Ki-67. A representative image of hippocampus is shown in Figure 3.6. The *Bnip3*-KO mice brain have increased nuclear positive staining for Ki-67 compared to wildtype, further confirming increased proliferation in *Bnip3*-KO cells.

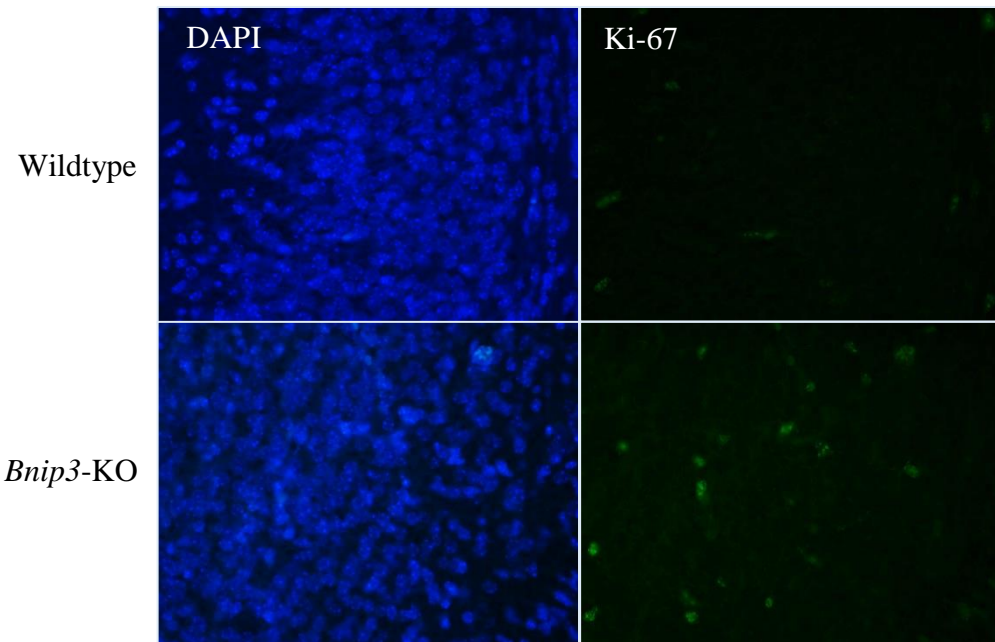


**Figure 3. 6 Immunostaining of brain sections shows higher positive staining for Ki-67 in *Bnip3*-KO mice brains.**

Paraffin-embedded mice brain sections were immunostained for Ki-67 and DAPI. The slides were observed with a Olympus BX51 microscope equipped with Coolsnap cf camera at 40X magnification. A representative image of hippocampus is shown here. The *Bnip3*-KO mice show increased positive staining for Ki-67 proliferation marker, indicating higher proliferation in these mice compared to wildtype.

### **3.1.8 Summary of AIM 1**

In summary, results for AIM 1 indicate that cells lacking BNIP3 are more proliferative than cells expressing BNIP3. These differences are consistent across different cell lines- MEFs, astrocytes and HEK293, as well as in mouse brain tissues.

## **3.2 AIM 2: To identify potential target genes through which BNIP3 may be repressing proliferation.**

### **3.2.1 Rationale for AIM 2**

The increased proliferation in cells lacking BNIP3 indicates a potential repressive effect of BNIP3 on cell proliferation. This could be achieved through involvement of BNIP3 in either cell proliferation and/or cell cycle pathways. We will investigate the differences in activation of important proliferation pathways, as well as the differences in expression of important cell proliferation and/or cell cycle genes between wildtype and *Bnip3*-KO cells.

### 3.2.2 *Bnip3*-knockout MEFs have increased expression and/or activation of proliferation proteins compared to wildtype MEFs.

Due to the proliferation differences observed between *Bnip3*-expressing and lacking cells, we investigated the levels of two well-studied proliferation proteins- MAPK and Cyclin D1. We western blotted the MEF lysates for activated p-(phosphorylated) and total MAPK. The *Bnip3*-KO MEFs show higher levels of p-MAPK compared to wildtype MEFs (Figure 3.7A). As seen in Figure 3.7B, protein levels of p-MAPK normalized to total MAPK in wildtype MEFs is 0.12 and 0.08 whereas this ratio is 1.00 and 0.48 in *Bnip3*-KO MEFs.

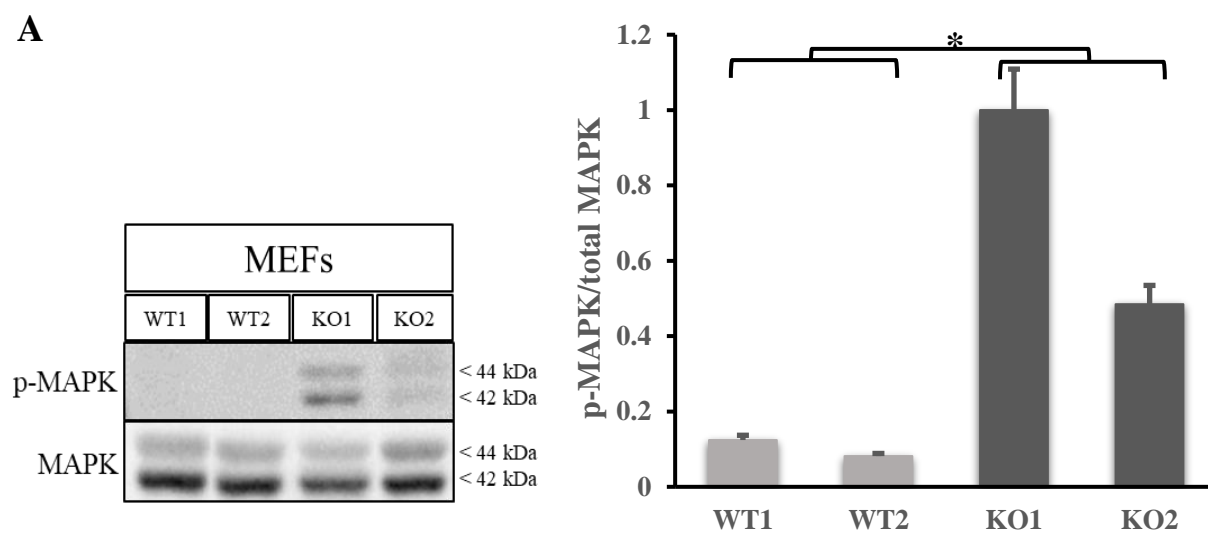


**Figure 3. 7 *Bnip3*-KO MEFs show higher activation of MAPK compared to wildtype MEFs.**  
(A) Total cell lysates from wildtype and *Bnip3*-null MEFs were western blotted for phospho-MAPK. The blot was then stripped and reprobed for total MAPK. (B) The levels of protein were quantified using ImageJ, and plotted as a ratio of p-MAPK to total MAPK. The statistical significance was tested using one way ANOVA, followed by Tukey's post hoc analysis (n=3, \* p< 0.05).

Furthermore, as shown in Figure 3.8, the *Bnip3*-KO MEFs also show higher levels of Cyclin D1 protein (1.00) as compared to wildtype (0.36).

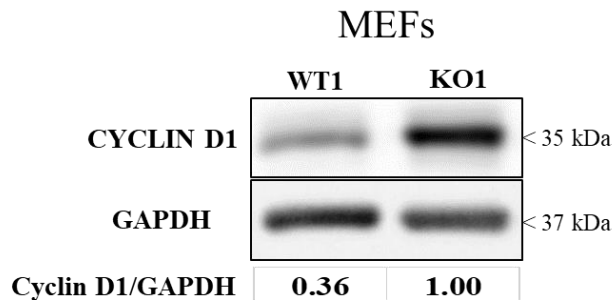


**Figure 3. 8 MEF cells lacking BNIP3 show higher levels of Cyclin D1 compared to cells expressing BNIP3.**

Total lysates from wild-type and *Bnip3*-KO MEFs were western blotted for Cyclin D1. The blot was stripped and reprobed with GAPDH as loading control. The protein levels were quantified using ImageJ software. The ratio of Cyclin D1 to GAPDH was calculated and normalized to the highest level of protein.

Interestingly, when Cyclin D1 protein levels were measured in synchronized MEF cell lysates (Figure 3.9), wildtype cells showed a higher level of Cyclin D1 (0.76) as compared to *Bnip3*-KO cells (0.07). Synchronized cells were incubated in serum-containing media for 4 hours before harvesting the cells for western blot analysis. This time coincides with Edu proliferation analysis of MEFs (Figure 3.4A), where higher percentage of *Bnip3*-KO MEFs are in S-phase of cell cycle compared to wildtype MEFs. Although Cyclin D1 level is positively correlated with cell proliferation capacity, it is degraded during S phase of cell cycle. Based on this knowledge, the observed lack of Cyclin D1 in *Bnip3*-KO synchronized MEFs complements our results from Edu cell proliferation assay.

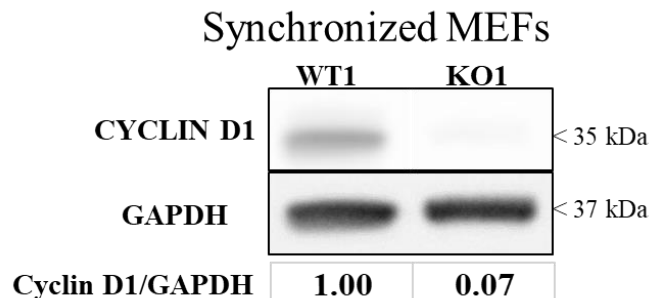


**Figure 3. 9 MEF cells lacking BNIP3 have diminished levels of Cyclin D1 compared to MEF cells expressing BNIP3 after cell cycle synchronization.**

Similar to EdU assay, MEF cells expressing or lacking BNIP3 were serum starved overnight to synchronize cell cycle. After overnight incubation, cells were supplied with 10% serum for 4 hours, and lysed for total protein. The lysates were western blotted for Cyclin D1. The blot was stripped and reprobed with GAPDH as loading control. The protein levels were quantified with ImageJ software, and are presented as a ratio of Cyclin D1 to GAPDH (normalized to the highest ratio).

### **3.2.2 *Bnip3*-KO astrocytes have altered expression of cell cycle and proliferation genes which could be involved in the observed increase in proliferation in these cells.**

The differences in activation of MAPK indicate potential changes in the cell proliferation and/or cell cycle signalling pathways. As previously mentioned, RNA-Seq of wildtype and *Bnip3*-KO mice astrocytes identified 100 differentially expressed genes. We analyzed this data through Ingenuity pathway analysis (IPA) to identify potential target genes that are known to be involved in either cell cycle or proliferation signalling.

Table 3.2 lists the three potential target genes identified through IPA of RNA-Seq data. The fold change refers to changes in gene expression in the *Bnip3*-KO astrocytes compared to wildtype.

**Table 3. 2 Three potential target genes identified through IPA of RNA-Seq data.**

#	Gene Name	Encoded Protein	Fold change	Function of encoded protein
1	<i>Dlx1</i>	Distal-less Homeobox 1 (DLX1)	↓ 18 fold	Suppresses several cytokine signalling pathways
2	<i>Igf2bp1</i>	Insulin-like growth factor 2 mRNA binding protein 1 (IGF2BP1)	↑ 7 fold	Oncofetal RNA-binding protein, involved in proliferation
3	<i>Ptgs2</i>	Prostaglandin-endoperoxidase synthase 2 (PTGS2)	↓ 3 fold	Important in biosynthesis of prostaglandins; implicated in progression of cancer

### 3.2.3 RT-qPCR of identified target genes shows differences in expression that are not consistent with RNA-Seq data.

To validate the RNA-Seq data for the three identified genes, we performed RT-qPCR on RNA isolated from primary astrocytes. The qPCR was performed in 96-well predesigned plates. The wildtype and *Bnip3*-KO samples were analyzed in pairs, one pair per plate- WT2 and KO2; WT3 and KO3; WT4 and KO4. The final PCR products for each gene, from one wildtype and one *Bnip3*-KO well, were run on an agarose gel to validate the primers used (Figure 3.10A). The PCR products were observed at the expected size for each gene (Table 3.2), and only one band was seen for every gene eliminating the presence of any non-specific products or primer dimers. The relative quantity and stability values for reference genes, *Tbp* and *Gapdh*, are shown in Figure 3.10B and C, respectively.

As seen in Figure 3.10(D-F), the expression levels of all genes differ between wildtype and *Bnip3*-KO cells but the differences are not consistent between all cells. For example, *Igf2bp1* expression is higher in KO2 and KO3 cells when compared to WT2 and WT3, and this result is consistent with RNA-Seq. However, WT4 shows higher expression of the gene compared to KO4. Similar

results are seen for other genes where differences between wildtype and *Bnip3*-KO cells are highly variable.

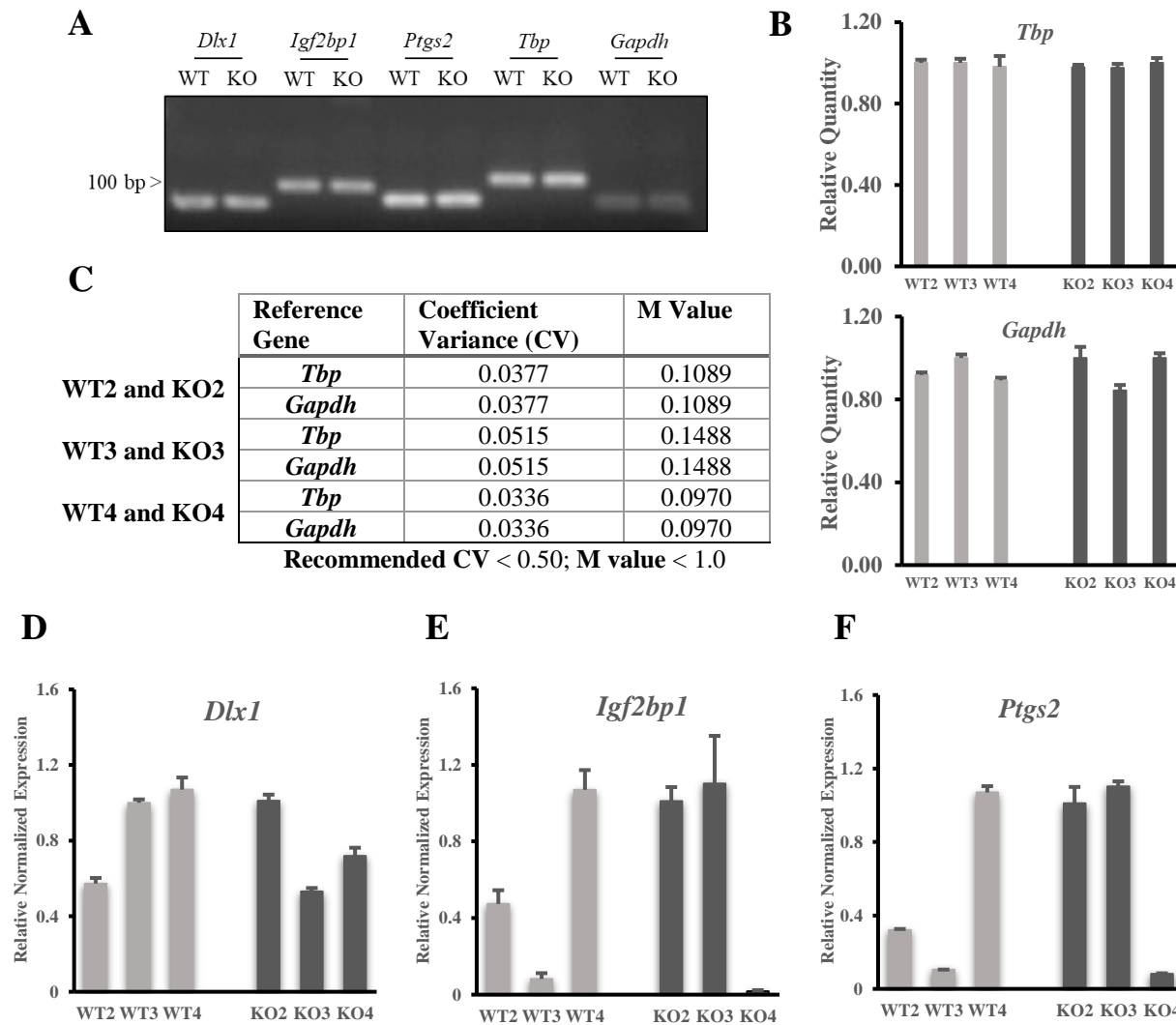


**Figure 3. 10 RT-qPCR analysis of primary astrocytes to quantify the expression of identified target genes.**

(A) The PCR products for each gene were run on a 2% agarose gel and visualized as previously explained. Only one band was seen for each gene at the expected size (Table 3.2). (B) The relative quantity of *Tbp* and *Gapdh* is shown as bar graphs as reported by CFX 3.1 manager software. These genes were used to normalize the gene expression data. (C) This table reports the Coefficient of Variance (CV) and M value for both reference genes, measured for each PCR plate. Recommended values are reported at the bottom of the table. (D-F) The gene expression data for targets *Dlx1*, *Igf2bp1*, and *Ptgs2* was normalized to both reference genes and has been represented as bar graphs. The results are an average of three repeats (n=3, N=1).

### **3.2.4 Determination of levels of proteins encoded by identified target genes.**

Although the gene expression data was inconclusive, we were interested in measuring the levels of proteins encoded by the target genes. We western blotted total protein lysates from primary astrocytes as well as mice whole brains. The protein levels were quantified with ImageJ analysis software.

The protein levels of DLX1 were mostly similar between wildtype and *Bnip3*-KO lysates for both whole brain lysates (Figure 3.11A) and primary astrocytes lysates (Figure 3.11C) with an exception to KO4 which had much lower levels of DLX1 (0.38 ratio compared to >0.50 in other astrocytes). The protein levels of IGF2BP1 were higher in *Bnip3*-KO brain (0.98) compared to wildtype (0.74) (Figure 3.11B). However, similar to RT-qPCR, protein levels were highly variable in primary astrocytes lysates (Figure 3.11D). The protein levels of PTGS2 were also highly variable in primary astrocytes lysates (Figure 3.11E) and mirrored the gene expression data from RT-qPCR. The protein levels of PTGS2 could not be detected in whole brain lysates.

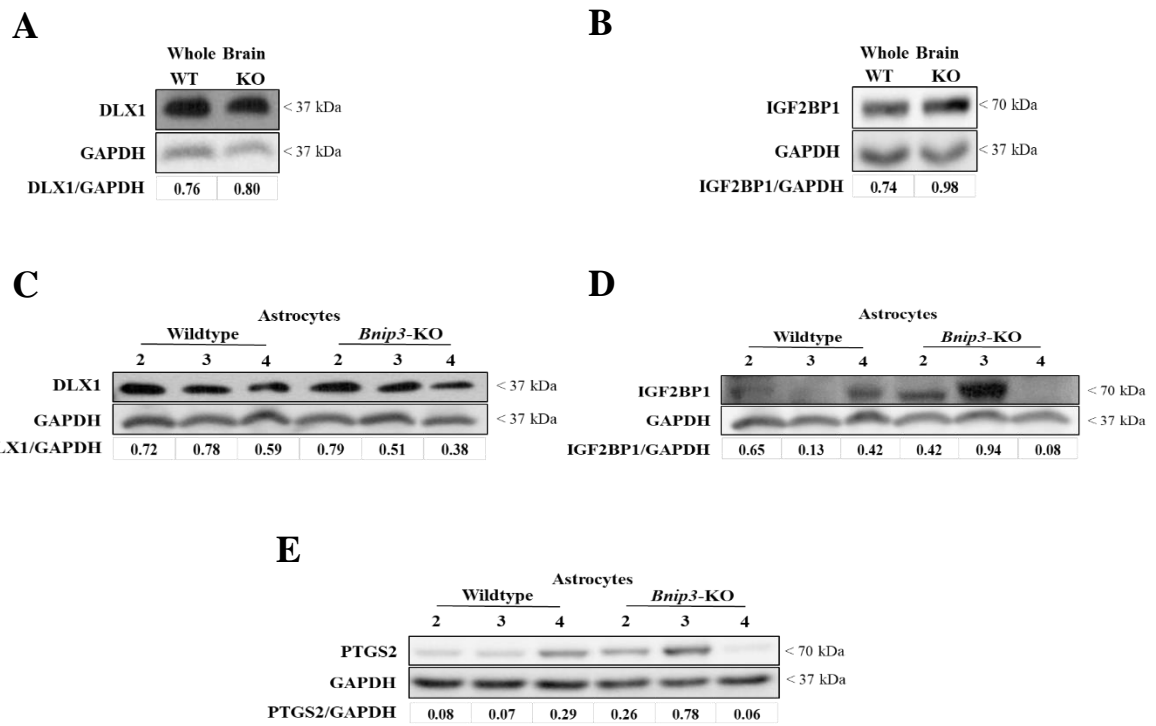


**Figure 3. 11 Western blot analysis of identified target proteins in both mice whole brain and primary astrocytes lysates.**

Mice whole brain lysates and primary astrocytes total cell lysates from wildtype and *Bnip3*-KO mice were western blotted and probed for identified targets- DLX1, IGF2BP1 and PTGS2. The membranes were stripped and reprobed for GAPDH as loading control. (A) and (B) show western blots for DLX1 and IGF2BP1, resp. in whole brain lysates. (C), (D) and (E) show western blots for DLX1, IGF2BP1 and PTGS2, resp. in primary astrocytes lysates. PTGS2 was not detectable in whole brain lysates. These western blots are representative of three independent repeats. The protein levels were quantified using ImageJ, and normalized to the loading control, GAPDH. The normalized protein level ratios are provided under respective western blot.

### **3.2.5 Summary of AIM 2**

In summary, results for AIM 2 confirm increased proliferation signalling in *Bnip3*-KO cells compared to wildtype. Gene expression analysis revealed potential target genes which may have altered expression in *Bnip3*-KO cells. However, further investigations into these targets did not reveal consistent differences between wildtype and *Bnip3*-KO cells.

Overall our results confirm that cells lacking BNIP3 are more proliferative than cells expressing BNIP3, with an increased activation of proliferation signalling. However, we were unable to identify specific proliferation and/or cell cycle gene(s) which may potentially be regulated by BNIP3.

# Chapter 4: Discussion and Conclusion

---

## 4.1 Discussion

The role of BNIP3 in cell death has been well established over the years. BNIP3 has been shown to be involved in all three major types of cell death- necrosis<sup>117</sup>, apoptosis<sup>112,115,116</sup> and autophagy<sup>77,120,121</sup>. In addition to cell death, its role in causing mitochondrial dysfunction has also been well studied<sup>72,111-114</sup>. Overexpression of BNIP3 is required for all the aforementioned functions. HIF1α, master regulator of hypoxia, is the chief activator of *Bnip3* expression<sup>74,84</sup>. The overexpressed BNIP3 localizes in the cytoplasm which might explain why initial research focused on the cell death function of BNIP3<sup>64</sup>. Recently however, studies have focused on the role of BNIP3 in cells with nuclear localization of the protein, such as glial cells. Nuclear localization of BNIP3 has also been seen in many cancers such as glioblastoma, non-small cell lung tumors, cervical tumors, breast tumors, and prostate tumors<sup>64</sup>. Even in the hypoxic core of glioblastoma tumor, overexpressed BNIP3 shows heavy nuclear localization. Nuclear BNIP3 has been shown to inhibit transcriptional expression of some cell death proteins, which might explain the survival of tumor cells<sup>124,125</sup>.

While studying the effects of nuclear BNIP3 through a *Bnip3*-KO mouse model, our lab observed an increase in cell number in the brains of *Bnip3*-KO mice compared to wildtype<sup>141</sup>. Evaluation of these cell number differences formed the basis of my research.

We used the same model of *Bnip3*-KO mice in which the initial observations were made. The *Bnip3*-KO allele was generated by replacing exons 2 and 3 of the gene with a *neomycin-resistance* (*neo*<sup>r</sup>) gene cassette<sup>116</sup>. Expression of *neo*<sup>r</sup> was used to validate both MEF and primary astrocyte cell lines prepared from these mice. We also wanted to confirm the presence of BNIP3 protein in

wildtype MEFs and primary astrocytes, but the protein levels were undetectable in cells cultured under normal conditions, with the current antibodies. However, the presence of BNIP3 in the nucleus of astrocytes under normal conditions has previously been shown by our lab<sup>82</sup>. We were able to induce overexpression of BNIP3 in wildtype MEFs through 24-hour incubation in hypoxic chamber. Western blot results further confirmed the identity of wildtype MEFs. Due to the sensitive nature of primary astrocytes, however, they could not be cultured in hypoxia to induce overexpression.

As measuring the difference in proliferation between wildtype and *Bnip3*-KO cells was the main focus of this research, we employed a number of different techniques/assays to measure cell proliferation. Although all these assays directly or indirectly measure cell proliferation, they all have different strengths and weaknesses associated with them. (1) The Edu cell proliferation assay measures incorporation of thymidine analog Edu into DNA. This enabled us to measure the percentage of cells replicating DNA in both wildtype and *Bnip3*-KO cultures as DNA synthesis is an important aspect of cell cycle. However, DNA synthesis is also required to repair DNA damage. This assay does not differentiate between DNA synthesized during cell cycle and cellular damage. Moreover, it is possible for *Bnip3*-KO MEFs to be arrested in G2 phase despite having a higher percentage of cells replicating DNA. Therefore, these results need to be verified through other methods before drawing any conclusions. (2) Real time cellular analysis measures electric current impeded by cells and converts it into cell index. As the instrument can be directed to make readings at any time interval e.g. every 15 minutes, the increase in cell index could be measured in real time. Additionally, as cell cultures are left undisturbed in the incubation chamber, the cell proliferation is not affected by any external stimuli such as temperature variations or handling issues. However, as previously pointed in section 3.5.2, the electrical impedance of cells in plates

is affected both by cell number and cell size, as well as how strongly cells are attached to the plates.

(3) Cytation 5 was the third, and final instrument used to measure cell proliferation. In theory, this technique is similar to traditional methods of counting cells with a hemocytometer. However, as live cells can be imaged directly in culture for counting with Cytation 5, this assay is superior since any human errors related to cell harvesting are avoided. All three assays show higher proliferation in *Bnip3*-KO MEFs, but there are inconsistencies within the two wildtype and *Bnip3*-KO cell lines. Specifically, WT2 and KO2 show higher proliferation than WT1 and KO1, respectively with Edu cell proliferation assay as well as Cytation 5 cell counting. However, the trend is reversed with RTCA as WT1 and KO1 are more proliferative than their counterparts. These inconsistencies could be due to inherent differences between the assays as RTCA is more sensitive to cell morphology and initial cell number. Moreover, as the MEFs are transformed cell lines, aberrations can arise over extended passaging of cells resulting in observed inconsistencies. We also measured the proliferation differences in primary astrocytes isolated from wildtype and *Bnip3*-KO neonatal mice as the initial cellularity differences were observed in mice brain. Since all three assays showed similar results in MEFs, only Cytation 5 cell counting was used to measure proliferation difference in astrocytes. Similar to MEFs, *Bnip3*-KO astrocytes are more proliferative than wildtype MEFs. BNIP3 mRNA has previously been shown to be upregulated in oligodendroglial lineage cells (OLCs) during oligodendrocyte differentiation, along with other BCL-2 family proteins<sup>139</sup>. Although this upregulation has previously been speculated to be required for cell death, it is possible that BNIP3 expressed and/or upregulated in the nucleus may play a role (in conjunction with its pro-survival function) to repress proliferation of developing glial cells in the brain before differentiation.

We also investigated if reintroduction of BNIP3 in *Bnip3*-KO cells would result in lower proliferation. Initially, we tried to transfect *Bnip3*-KO MEFs with an overexpression vector, but transfections in MEFs were not successful. We then switched to HEK293 cells as they present a human cell line model as well as have a really high transfection efficiency. HEK293 cells were transiently transfected with either empty pcDNA3.1 vector or NLS-*Bnip3* pcDNA3.1 expression vector. As the expression of transfected plasmid decays over 1 to 7 days, RTCA and Cytation 5 assays were not appropriate to measure the proliferation differences. Instead we used Edu proliferation assay as it can be done within a few hours at the peak expression of protein (24-48 hours post-transfection). Our results show higher incorporation of Edu in cells transfected with empty vector compared to nuclear BNIP3 overexpressing cells, further confirming our hypothesis that cells lacking BNIP3 are more proliferative than cells expressing BNIP3. It was important to confirm the nuclear localization of BNIP3 in these experiments because an increase in cytoplasmic (or mitochondrial) localization of BNIP3 may result in increased cell death, amplifying the effects of proliferation differences between the cells.

The proliferation results in cell lines were also verified by higher positive staining for Ki67, a key proliferation marker<sup>168</sup>, on paraffin-embedded frozen brain tissue sections from *Bnip3*-KO mice compared to wildtype. We also western blotted MEF lysates for Cyclin D1, a key cell cycle protein required for G1 to S phase progression of cell cycle<sup>169</sup>. For total cell lysates from unsynchronized cells, Cyclin D1 protein levels were higher in *Bnip3*-KO MEFs than wildtype, however the differences were variable as might be expected considering Cyclin D1 is degraded during S phase of cell cycle<sup>169</sup>, and unsynchronized cell cultures often have varying percentages of cells in different cell cycle phases. Interestingly, however, synchronized cell lysates showed much lower levels of Cyclin D1 in *Bnip3*-KO MEFs. This result can be explained by our Edu proliferation

assay results in MEFs as these cells were harvested at the same time point (4 hours after adding serum free media) as the Edu cell proliferation assay. Edu assay showed a higher percentage of *Bnip3*-KO MEFs in DNA synthesis phase of cell cycle. Since Cyclin D1 is degraded during S-phase of cell cycle, we would expect *Bnip3*-KO MEFs to show lower levels of protein when more cells in culture are in S-phase, compared to wildtype MEFs. Hence, Edu cell proliferation assay results complement the findings from analysis of Cyclin D1 levels in MEFs. Collectively, these results show that cells expressing *Bnip3* have lower proliferation than cells lacking *Bnip3*.

Studies have shown that BCL-2 family member BAX promotes cell proliferation by modulating CDKN1A expression in the nucleus<sup>142</sup>, and nuclear BID is involved in cell cycle checkpoint response following DNA damage<sup>143</sup>. The anti-apoptotic MCL-1 member has also been shown to have nuclear localization. Shortened nuclear fragment of MCL-1 (snMCL-1) has been shown to interact with CDK1, affecting its ability to bind Cyclin B1. This affects G2 to S transition of cell cycle and results in lower proliferation<sup>144</sup>. MCL-1 has also been shown to localize at sites of DNA damage, and has been shown to play important role in DNA damage checkpoint response through gene knockout studies<sup>145</sup>. It is possible that BNIP3, another BCL-2 member, may be involved in regulation of cell cycle and/or proliferation pathways in the nucleus. We investigated the differences in signalling pathways between wildtype and *Bnip3*-KO cells in order to understand the mechanism by which BNIP3 may be affecting proliferation. We identified increased level of activated MAPK proteins in *Bnip3*-KO MEFs compared to wildtype, via western blot. The antibodies were directed against ERK1/2 (or classic MAPK), two best characterized members of MAPK family. As described previously, activated ERKs are transcription factors that turn on gene expression for proteins involved in cell growth, differentiation and proliferation<sup>16,17</sup>. MAPK

signalling cascades are key regulators of proliferation, and any differences in activated ERKs indicates a difference in proliferation signalling between wildtype and *Bnip3*-KO MEFs.

Our lab had initially performed an RNA sequencing study on wildtype and *Bnip3*-KO mouse astrocytes, and identified 100 target genes with differential gene expression between the two cell types. The RNAseq data was later analyzed through Ingenuity pathway analysis (IPA). IPA is a web-based functional analysis tool capable of analyzing and interpreting omics data to identify signalling and molecular pathways as well as biological functions of differentially expressed genes. IPA analysis of RNAseq data identified three target genes- Distal-less Homeobox 1 (*Dlx1*), Insulin-like growth factor 2 mRNA binding protein 1 (*Igf2bp1*), and Prostaglandin-endoperoxidase Synthase 2 (*Ptgs2*).

DLX1 belongs to DLX family homeobox proteins which are transcription factors, required for the development of brain, blood, bones, sensory organs, craniofacial features as well as appendages. They are homologous to Drosophila distal-less genes (*Dll*)<sup>146</sup>. Although these proteins are essential for development, their aberrant expression has been implicated in many cancers. DLX1 plays a role in terminal differentiation of interneurons<sup>147,148</sup> and ganglion cells in developing retina<sup>149</sup>. It also inhibits several cytokine signalling pathways by repressing the activity of other stimulatory pathways. DLX1 directly interacts with SMAD4 in the nucleus to upregulate Transforming growth factor-β (TGFβ) signalling<sup>150</sup>, and may be responsible for increased cell growth and metastasis in ovarian cancer where DLX1 is upregulated by Forkhead box M1 (FOXM1), another developmentally important transcriptional regulator<sup>151</sup>. However, lack of DLX1 expression in acute myeloid leukemia (AML) was shown to cause cell cycle arrest at G0 phase which slowed down proliferation *in vitro*, and prolonged cell survival *in vivo*<sup>152,153</sup>. Hence, the role of DLX1 in

proliferation may be cell dependent. In our RNA-Seq analysis, the *DlxI* expression was 18-fold lower in *Bnip3*-KO mice astrocytes compared to wildtype.

Similar to DLX1, IGF2BP1 is important during early development. It is an oncofetal protein, normally expressed during embryogenesis<sup>154-156</sup> and the expression in adults is limited to ovaries/testes and intestinal crypts<sup>154,157,158</sup>. However, its expression has been seen in many cancers where it often serves as a poor prognostic marker<sup>155-160</sup>. Normally, IGF2BP1 binds to 5'-UTR (untranslated region) and regulates translation of mRNAs from several genes, most notably Insulin-like growth factor 2 (IGF2)<sup>154</sup>. IGF2 plays an essential role in pre-natal cell proliferation, differentiation, growth, migration and survival<sup>161</sup>. Inhibition of IGF2BP1 in glioblastoma via regulation by microRNA-506 (miR-506) was shown to repress cell growth, block G1/S transition and suppress cell invasion<sup>162</sup>. We found a 7-fold increase in *Igf2bp1* expression in *Bnip3*-KO astrocytes through RNA-Seq.

*Ptgs2* was the last target gene analyzed in this study. The encoded protein Prostaglandin-endoperoxidase synthase 2 (PTGS2), also known as Cyclooxygenase 2 (COX2) is an enzyme that is involved in the conversion of arachidonic acid to prostaglandin H2, an important precursor to other biologically important molecules such as Prostacyclin, Thromboxane, and other Prostaglandins. Humans have two active cyclooxygenase enzymes, COX1 and COX2. Of these, COX1 is constitutively produced by cells, whereas COX2 is an inducible enzyme<sup>163,164</sup>. Some known activators of COX2 expression include inflammatory molecules including cytokines, mitogens and endotoxins<sup>164</sup>. PTGS2 overexpression is seen in cancers such as breast<sup>165</sup> and colorectal<sup>166</sup>, where expression levels of the protein could also serve as potential prognostic marker. Some knockdown studies of PTGS2 with miRNA have shown reduced proliferation in

both breast and cervical cancers<sup>165,167</sup>. Our RNA-Seq results showed a 3-fold decrease in expression of *Ptgs2* in *Bnip3*-KO cells.

Although we identified differences in both gene expression and protein levels of the three identified targets, these differences are variable between and within the wildtype and *Bnip3*-KO cells. Increased levels of IGF2BP1 and PTGS2 in 2/3 *Bnip3*-KO astrocytes are in accordance to the known functions of these proteins in promoting proliferation, however their expression is very low in the third knockout cell line, and vice versa. As all three genes are highly regulated either during development (*Dlx1* and *Igf2bp1*) or have inducible expression (*Ptgs2*), it is possible that the expression differences seen in RNA-Seq could be due to the time at which the cells were harvested, and not be a result of regulation by BNIP3.

## **4.2 Conclusion**

In conclusion, this study has shown that expression of *Bnip3* results in lower cellular proliferation in MEFs, mice astrocytes as well as HEK293 cells transfected with a *Bnip3*-expression vector. As described in section 1.7, our lab also previously showed that mice lacking *Bnip3* show increased cellularity in brain, *in vivo*. Taken together, we may have discovered a new function for BNIP3 in regulating cellular proliferation. This observed repression of proliferation by BNIP3 in the brain may play a role in proper development of brain by inhibiting the proliferation of cells before differentiation, in conjunction with survival advantages provided by other BCL-2 members<sup>57</sup>. However, further research is required to confirm these claims. We also identified several differentially expressed genes between wildtype and *Bnip3*-KO astrocytes through RNA-Seq analysis, however the expression of potential BNIP3 target genes failed to be confirmed by mRNA or protein levels in the astrocytes.

## **Chapter 5: Future Directions**

---

This research sought to investigate the role of BNIP3 in regulating cellular proliferation. The results of our present studies confirm that cells expressing BNIP3 are less proliferative than cells lacking BNIP3, indicating a new function of BNIP3 in repressing proliferation of cells.

Future studies will aim to understand the mechanism through which BNIP3 may be regulating cellular proliferation. Although RNA-Seq identified 100 differentially expressed genes between wildtype and *Bnip3*-KO mice astrocytes, we were unable to find a target gene whose expression may be affected by BNIP3. Since we identified increased activation of MAPK in *Bnip3*-KO MEFs, future experiments should also analyze the expression of other genes involved in Ras-MAPK proliferation signalling pathway. Commercial cell cycle arrays might also serve as important tools to identify BNIP3-target genes.

Moreover, although BNIP3 appears to repress cellular proliferation in the cell lines and tissue samples employed in this research, it would also be interesting to study other organ systems and animal models to confirm if this function of BNIP3 is cell line, organ or animal dependent.

## Chapter 6: References

---

1. Golias, C. , Charalabopoulos, A. and Charalabopoulos, K. (2004), Cell proliferation and cell cycle control: a mini review. *International Journal of Clinical Practice*, 58: 1134-1141. doi:10.1111/j.1742-1241.2004.00284.x.
2. Karp, G. (2010). *Cell and molecular biology* (6th ed., Chapter 14: Cellular Reproduction). Hoboken, NJ: John Wiley.
3. Cooper, G. (2000). *The cell* (2nd ed., Chapter 14: The Cell Cycle). Washington, D.C.: ASM Press.
4. Reece, J., & Campbell, N. (2013). *Campbell biology* (10th ed., Chapter 12: The Cell). Boston: Pearson.
5. Gorbsky, G. (2001). The mitotic spindle checkpoint. *Current Biology*, 11(24), R1001-R1004. doi:10.1016/s0960-9822(01)00609-1.
6. Nigg, E. A. (1995), Cyclin-dependent protein kinases: Key regulators of the eukaryotic cell cycle. *Bioessays*, 17: 471-480. doi:10.1002/bies.950170603.
7. OpenStax College, Biology. (2018). Control of the cell cycle. Retrieved from <http://cnx.org/contents/185cbf87-c72e-48f5-b51e-f14f21b5eabd@9.87:53/Control-of-the-Cell-Cycle>
8. Nigg, E. (2001). Mitotic kinases as regulators of cell division and its checkpoints. *Nature Reviews Molecular Cell Biology*, 2(1), 21-32. doi:10.1038/35048096.
9. McDonald, E. and El-Deiry, W. (2001), Checkpoint genes in cancer. *Annals of Medicine*, 33:2, 113-122. doi:10.3109/07853890109002066.
10. Ronco, C., Martin, A., Demange, L., & Benhida, R. (2017). ATM, ATR, CHK1, CHK2 and WEE1 inhibitors in cancer and cancer stem cells. *Medchemcomm*, 8(2), 295-319. doi:10.1039/c6md00439c.
11. Hanahan, D., & Weinberg, R. (2011). Hallmarks of Cancer: The Next Generation. *Cell*, 144(5), 646-674. doi:10.1016/j.cell.2011.02.013.
12. Lodish, H., Berk, A., Zipursky, S. L., Matsudaira, P., Baltimore, D., and Darnell, J. (2000). Proto-oncogenes and tumor suppressor genes. *Molecular cell biology* (4th ed., section 24.2). New York, NY: W. H. Freeman.

13. Chow, A. Y. (2010) Cell cycle control by oncogenes and tumor suppressors: driving the transformation of normal cells into cancerous cells. *Nature Education*, 3(9), 7. Retrieved from: <http://www.nature.com/scitable/topicpage/cell-cycle-control-by-oncogenes-and-tumor-14191459>.
14. Cell division and cancer. (2014). In *Scitable*. Retrieved from: <http://www.nature.com/scitable/topicpage/cell-division-and-cancer-14046590>
15. Vogelstein, B., & Kinzler, K. (2004). Cancer genes and the pathways they control. *Nature Medicine*, 10(8), 789-799. doi:10.1038/nm1087.
16. Roberts, P., & Der, C. (2007). Targeting the Raf-MEK-ERK mitogen-activated protein kinase cascade for the treatment of cancer. *Oncogene*, 26(22), 3291-3310. doi:10.1038/sj.onc.1210422.
17. Santarpia, L., Lippman, S. L., & El-Naggar, A. K. (2012). Targeting the Mitogen-Activated Protein Kinase RAS-RAF Signaling Pathway in Cancer Therapy. *Expert Opinion on Therapeutic Targets*, 16(1), 103–119. doi:10.1517/14728222.2011.645805.
18. Vogelstein, B., Sur, S. & Prives, C. (2010) p53: The Most Frequently Altered Gene in Human Cancers. *Nature Education* 3(9):6. Retrieved from: <https://www-nature-com.uml.idm.oclc.org/scitable/topicpage/p53-the-most-frequently-altered-gene-in-14192717>
19. Galluzzi L, Maiuri MC, Vitale I, et al. Cell death modalities: Classification and pathophysiological implications. *Cell Death Differ*, 2007; 14(7):1237-43. doi:10.1038/sj.cdd.4402148.
20. Edinger AL, Thompson CB. Death by design: Apoptosis, necrosis and autophagy. *Curr Opin Cell Biol*, 2004; 16(6):663-9. doi:10.1016/j.ceb.2004.09.011.
21. Brill A, Torchinsky A, Carp H, Toder V. The Role of Apoptosis in Normal and Abnormal Embryonic Development. *Journal of Assisted Reproduction and Genetics* (1999);16(10):512-519. doi:10.1023/A:1020541019347.
22. Meier, P., Finch, A., & Evan, G. (2000). Apoptosis in development. *Nature*, 407(6805), 796-801. doi:10.1038/35037734.
23. Hotchkiss RS, Strasser A, McDunn JE, Swanson PE. Cell death. *N Engl J Med* (2009); 361(16):1570-83. doi:10.1056/NEJMra0901217.

24. Fulda S, Debatin KM. Extrinsic versus intrinsic apoptosis pathways in anticancer chemotherapy. *Oncogene* (2006); 25(34):4798-811. doi:10.1038/sj.onc.1209608.
25. Carswell, E. A., Old, L. J., Kassel, R. L., Green, S., Fiore, N., & Williamson, B. (1975). An endotoxin-induced serum factor that causes necrosis of tumors. *Proceedings of the National Academy of Sciences of the United States of America*, 72(9), 3666–3670. doi:10.1073/pnas.72.9.3666.
26. Karp, G. (2010). *Cell and molecular biology* (6th ed., Chapter 15, section 15.8: Apoptosis (Programmed cell death)). Hoboken, NJ: John Wiley.
27. Rath, P., & Aggarwal, B. (1999). TNF-induced signaling in apoptosis. *Journal Of Clinical Immunology*, 19(6), 350-364. doi:10.1023/a:1020546615229.
28. Elmore, S. (2007). Apoptosis: A Review of Programmed Cell Death. *Toxicologic Pathology*, 35(4), 495–516. doi:10.1080/01926230701320337.
29. Ichim, G., & Tait, S. (2016). A fate worse than death: apoptosis as an oncogenic process. *Nature Reviews Cancer*, 16(8), 539-548. doi:10.1038/nrc.2016.58.
30. Chipuk JE, Moldoveanu T, Llambi F, Parsons MJ, Green DR (2010). The BCL-2 family reunion. *Mol Cell*; 37(3):299-310. doi:10.1016/j.molcel.2010.01.025.
31. Proskuryakov, S., Konoplyannikov, A., & Gabai, V. (2003). Necrosis: a specific form of programmed cell death?. *Experimental Cell Research*, 283(1), 1-16. doi:10.1016/s0014-4827(02)00027-7.
32. Raffray, M., & Gerald M., C. (1997). Apoptosis and necrosis in toxicology: A continuum or distinct modes of cell death?. *Pharmacology & Therapeutics*, 75(3), 153-177. doi:10.1016/s0163-7258(97)00037-5.
33. Rock, K. L., & Kono, H. (2008). The inflammatory response to cell death. *Annual Review of Pathology*, 3, 99–126. doi:10.1146/annurev.pathmechdis.3.121806.151456.
34. Festjens, N., Vanden Berghe, T., & Vandenabeele, P. (2006). Necrosis, a well-orchestrated form of cell demise: Signalling cascades, important mediators and concomitant immune response. *Biochimica Et Biophysica Acta (BBA) - Bioenergetics*, 1757(9-10), 1371-1387. doi:10.1016/j.bbabiobio.2006.06.014.
35. Levine, B. (2005). Eating Oneself and Uninvited Guests. *Cell*, 120(2), 159-162. doi:10.1016/j.cell.2005.01.005.

36. Maiuri, M., Zalckvar, E., Kimchi, A., & Kroemer, G. (2007). Self-eating and self-killing: crosstalk between autophagy and apoptosis. *Nature Reviews Molecular Cell Biology*, 8(9), 741-752. doi:10.1038/nrm2239.
37. Siddiqui WA, Ahad A, Ahsan H. (2015). The mystery of BCL2 family: Bcl-2 proteins and apoptosis: an update. *Arch Toxicol*, 89(3), 289-317. doi:10.1007/s00204-014-1448-7.
38. Lomonosova E, Chinnadurai G. (2008) BH3-only proteins in apoptosis and beyond: an overview. *Oncogene*. 27(Suppl 1), S2-19. doi:10.1038/onc.2009.39.BH3-only.
39. Shamas-Din A, Kale J, Leber B, Andrews DW. (2013). Mechanisms of Action of Bcl-2 Family Proteins. *Cold Spring Harb Perspect Biol*. 5(4), a008714. doi:10.1101/cshperspect.a008714.
40. Patingre S, Levine B. (2006) Bcl-2 inhibition of autophagy: A new route to cancer? *Cancer Res.*, 66(6), 2885-8. doi:10.1158/0008-5472.CAN-05-4412.
41. Shimizu S, Kanaseki T, Mizushima N, et al. (2004). Role of Bcl-2 family proteins in a non-apoptotic programmed cell death dependent on autophagy genes. *Nat Cell Biol*. 6(12), 1221-8. doi:10.1038/ncb1192.
42. Wong, W., & Puthalakath, H. (2008). Bcl-2 family proteins: The sentinels of the mitochondrial apoptosis pathway. *IUBMB Life*, 60(6), 390-397. doi:10.1002/iub.51.
43. Giménez-Cassina, A., & Danial, N. N. (2015). Regulation of mitochondrial nutrient and energy metabolism by BCL-2 family proteins. *Trends in Endocrinology and Metabolism: TEM*, 26(4), 165–175. doi:10.1016/j.tem.2015.02.004.
44. Zhang, H.M., Cheung, P., Yanagawa, B., McManus, B.M., Yang, D.C. (2003). BNips: A group of pro-apoptotic proteins in the bcl-2 family. *Apoptosis*, 8(3), 229-36. doi:10.1023/A:1023616620970.
45. Boyd, J.M., Malstrom, S., Subramanian, T., et al. (1994). Adenovirus E1B 19 kDa and bcl-2 proteins interact with a common set of cellular proteins. *Cell*, 79(2), 341-51. doi:10.1016/0092-8674(94)90202-X.
46. Subramanian, T., Boyd, J.M., Chinnadurai, G. (1995) Functional substitution identifies a cell survival promoting domain common to adenovirus E1B 19 kDa and Bcl-2 proteins. *Oncogene*. 11(11), 2403-9.

47. Hahn, P., Lindsten, T., Ying, G., Bennett, J., et al. (2003). Proapoptotic Bcl-2 family members, Bax and Bak, are essential for developmental photoreceptor apoptosis. *Investigative Ophthalmology & Visual Science*, 44(8), 3598. doi:10.1167/iovs.02-1113.
48. Lindsten, T., Ross, A. J., King, A., Zong, W.-X., et al. (2000). The Combined Functions of Proapoptotic Bcl-2 Family Members Bak and Bax Are Essential for Normal Development of Multiple Tissues. *Molecular Cell*, 6(6), 1389–1399.
49. Krajewska, M., Mai, J., Zapata, J., Ashwell, K., Schendel, S., Reed, J., & Krajewski, S. (2002). Dynamics of expression of apoptosis-regulatory proteins Bid, Bcl-2, Bcl-X, Bax and Bak during development of murine nervous system. *Cell Death & Differentiation*, 9(2), 145-157. doi:10.1038/sj.cdd.4400934.
50. Abedohmae, S., Harada, N., Yamada, K., & Tanaka, R. (1993). bcl-2 Gene Is Highly Expressed during Neurogenesis in the Central Nervous System. *Biochemical And Biophysical Research Communications*, 191(3), 915-921. doi:10.1006/bbrc.1993.1304.
51. Merry, D., Veis, D., Hickey, W., & Korsmeyer, S. (1994). bcl-2 protein expression is widespread in the developing nervous system and retained in the adult PNS. *Development*, 120(2), 301-311.
52. Motoyama, N., Wang, F., Roth, K., Sawa, H., Nakayama, K., & Nakayama, K. et al. (1995). Massive cell death of immature hematopoietic cells and neurons in Bcl-x-deficient mice. *Science*, 267(5203), 1506-1510. doi:10.1126/science.7878471.
53. Veis, D., Sorenson, C., Shutter, J., & Korsmeyer, S. (1993). Bcl-2-deficient mice demonstrate fulminant lymphoid apoptosis, polycystic kidneys, and hypopigmented hair. *Cell*, 75(2), 229-240. doi:10.1016/0092-8674(93)80065-m.
54. Yamamura, K., Kamada, S., Ito, M., Nakagawa, Y., Ichihashi, & Tsujimoto. (1996). Accelerated disappearance of melanocytes in bcl-2-deficient mice. *Cancer Research*, 56(15), 3546-3550.
55. Ross, A., Waymire, K., Moss, J., Parlow, A., Skinner, M., Russell, L., & MacGregor, G. (1998). Testicular degeneration in Bclw-deficient mice. *Nature Genetics*, 18(3), 251-256. doi:10.1038/ng0398-251.

56. Wang, X., Bathina, M., Lynch, J., Koss, B., Calabrese, C., & Frase, S. et al. (2013). Deletion of MCL-1 causes lethal cardiac failure and mitochondrial dysfunction. *Genes & Development*, 27(12), 1351-1364. doi:10.1101/gad.215855.113.
57. Opferman, J. T., & Kothari, A. (2018). Anti-apoptotic BCL-2 family members in development. *Cell Death and Differentiation*, 25(1), 37–45. doi:10.1038/cdd.2017.170.
58. Ghobrial, I., Witzig, T., & Adjei, A. (2005). Targeting Apoptosis Pathways in Cancer Therapy. *CA: A Cancer Journal For Clinicians*, 55(3), 178-194. doi:10.3322/canjclin.55.3.178.
59. Yip, K., & Reed, J. (2008). Bcl-2 family proteins and cancer. *Oncogene*, 27(50), 6398-6406. doi:10.1038/onc.2008.307.
60. Tsujimoto, Y., Cossman, J., Jaffe, E., & Croce, C. (1985). Involvement of the bcl-2 gene in human follicular lymphoma. *Science*, 228(4706), 1440-1443. doi:10.1126/science.3874430.
61. Gross MB. Personal Communication in OMIMR Online Mendelian Inheritance in Man. MIM number: {603293} Johns Hopkins University, Baltimore, MD. <https://omim.org/>. Published 2011.
62. Gang, H., Dhingra, R., Lin, J., Hai, Y., Aviv, Y., & Margulets, V. et al. (2015). PDK2-mediated alternative splicing switches Bnip3 from cell death to cell survival. *The Journal Of Cell Biology*, 210(7), 1101-1115. doi:10.1083/jcb.201504047.
63. Chen, G., Ray, R., Dubik, D., Shi, L., Cizeau, J., Bleackley, R. C., ... Greenberg, A. H. (1997). The E1B 19K/Bcl-2–binding Protein Nip3 is a Dimeric Mitochondrial Protein that Activates Apoptosis. *The Journal of Experimental Medicine*, 186(12), 1975–1983.
64. Burton, T., & Gibson, S. (2009). The role of Bcl-2 family member BNIP3 in cell death and disease: NIPping at the heels of cell death. *Cell Death & Differentiation*, 16(4), 515-523. doi:10.1038/cdd.2008.185.
65. Lawrie, C., Sulistijo, E., & MacKenzie, K. (2010). Intermonomer Hydrogen Bonds Enhance GxxxG-Driven Dimerization of the BNIP3 Transmembrane Domain: Roles for Sequence Context in Helix–Helix Association in Membranes. *Journal Of Molecular Biology*, 396(4), 924-936. doi:10.1016/j.jmb.2009.12.023.

66. Vasagiri, N., & Kutala, V. (2014). Structure, function, and epigenetic regulation of BNIP3: a pathophysiological relevance. *Molecular Biology Reports*, 41(11), 7705-7714. doi:10.1007/s11033-014-3664-x.
67. Yasuda, M., Theodorakis, P., Subramanian, T., Chinnadurai, G. (1998). Adenovirus E1B-19K/BCL-2 Interacting Protein BNIP3 Contains a BH3 Domain and a Mitochondrial Targeting Sequence. *J Biol Chem.* 273(20), 12415-12421.
68. Ray, R., Chen, G., Vande Velde, C., et al. (2000). BNIP3 Heterodimerizes with Bcl-2/Bcl-X L and Induces Cell Death Independent of a Bcl-2 Homology 3 (BH3) Domain at Both Mitochondrial and Nonmitochondrial Sites. *J Biol Chem*, 275(2), 1439-1448. doi:10.1074/jbc.275.2.1439.
69. Sulistijo, E.S., Jaszewski, T.M., Mackenzie, K.R. (2003). Sequence-specific Dimerization of the Transmembrane Domain of the “BH3-only” Protein BNIP3 in Membranes and Detergent. *J Biol Chem.*, 278(51), 51950-51956. doi:10.1074/jbc.M308429200.
70. Vereshaga, Y.A., Volynsky, P.E., Pustovalova, J.E., Nolde, D.E., Arseniev, A.S., Efremov, R.G. (2007). Specificity of helix packing in transmembrane dimer of the cell death factor BNIP3: A molecular modeling study. *Proteins*, 69(2), 309-325. doi:10.1002/prot.21555.
71. Kim, J., Cho, J., Ha, J., Park, J. (2002). The Carboxy Terminal C-Tail of BNip3 Is Crucial in Induction of Mitochondrial Permeability Transition in Isolated Mitochondria. *Arch Biochem Biophys.* 398(2), 147-152. doi:10.1006/abbi.2001.2673.
72. Bocharov, E., Pustovalova, Y., Pavlov, K., Volynsky, P., Goncharuk, M., & Ermolyuk, Y. et al. (2007). Unique Dimeric Structure of BNip3 Transmembrane Domain Suggests Membrane Permeabilization as a Cell Death Trigger. *Journal Of Biological Chemistry*, 282(22), 16256-16266. doi:10.1074/jbc.M701745200.
73. Kubli, D., Quinsay, M., Huang, C., Lee, Y., & Gustafsson, Å. (2008). Bnip3 functions as a mitochondrial sensor of oxidative stress during myocardial ischemia and reperfusion. *American Journal Of Physiology-Heart And Circulatory Physiology*, 295(5), H2025-H2031. doi:10.1152/ajpheart.00552.2008.
74. Kothari, S., Cizeau, J., McMillan-Ward, E., Israels, S., Bailes, M., & Ens, K. et al. (2003). BNIP3 plays a role in hypoxic cell death in human epithelial cells that is inhibited by growth factors EGF and IGF. *Oncogene*, 22(30), 4734-4744. doi: 10.1038/sj.onc.1206666.

75. Chinnadurai, G., Vijayalingam, S., & Gibson, S. B. (2008). BNIP3 subfamily BH3-only proteins - mitochondrial stress sensors in normal and pathological functions. *Oncogene*, 27(Suppl 1), S114–S127. doi:10.1038/onc.2009.49.
76. Cizeau, J., Ray, R., Chen, G., Gietz, R., & Greenberg, A. (2000). The *C. elegans* orthologue ceBNIP3 interacts with CED-9 and CED-3 but kills through a BH3- and caspase-independent mechanism. *Oncogene*, 19(48), 5453-5463. doi:10.1038/sj.onc.1203929.
77. Zhu, Y., Massen, S., Terenzio, M., Lang, V., Chen-Lindner, S., Eils, R., et al. (2013). Modulation of Serines 17 and 24 in the LC3-interacting Region of Bnip3 Determines Pro-survival Mitophagy *versus* Apoptosis. *The Journal of Biological Chemistry*, 288(2), 1099–1113. doi:10.1074/jbc.M112.399345.
78. Bristow, N., Burton, T., Henson, E., Ong-Justiniano, C., Brown, M., & Gibson, S. (2011). Truncated forms of BNIP3 act as dominant negatives inhibiting hypoxia-induced cell death. *Biochimica Et Biophysica Acta (BBA) - Molecular Basis Of Disease*, 1812(3), 302-311. doi:10.1016/j.bbadi.2010.11.013.
79. Rogers, S., Wells, R., & Rechsteiner, M. (1986). Amino acid sequences common to rapidly degraded proteins: the PEST hypothesis. *Science*, 234(4774), 364-368. doi:10.1126/science.2876518.
80. Yasuda, M., Han, J., Dionne, C.A., Boyd, J.M., Chinnadurai, G. (1999). BNIP3 $\alpha$ : A Human Homolog of Mitochondrial Proapoptotic Protein BNIP3. *Cancer Res.* 59(3), 533-537.
81. Sowter, H.M., Ratcliffe, P.J., Watson, P., Greenberg, A.H., Harris, A.L. (2001). HIF-1-dependent regulation of hypoxic induction of the cell death factors BNIP3 and NIX in human tumors. *Cancer Res.*, 61(18), 6669-6673.
82. Burton, T., Henson, E., Baijal, P., Eisenstat, D., & Gibson, S. (2006). The pro-cell death Bcl-2 family member, BNIP3, is localized to the nucleus of human glial cells: Implications for glioblastoma multiforme tumor cell survival under hypoxia. *International Journal Of Cancer*, 118(7), 1660-1669. doi:10.1002/ijc.21547.
83. Hamacher-Brady, A., Brady, N., Logue, S., Sayen, M., Jinno, M., & Kirshenbaum, L. et al. (2006). Response to myocardial ischemia/reperfusion injury involves Bnip3 and autophagy. *Cell Death And Differentiation*, 14(1), 146-157. doi:10.1038/sj.cdd.4401936.

84. Bruick, R. K. (2000). Expression of the gene encoding the proapoptotic Nip3 protein is induced by hypoxia. *Proceedings of the National Academy of Sciences of the United States of America*, 97(16), 9082–9087.
85. Muz, B., de la Puente, P., Azab, F., & Azab, A. K. (2015). The role of hypoxia in cancer progression, angiogenesis, metastasis, and resistance to therapy. *Hypoxia*, 3, 83–92. doi:10.2147/HP.S93413.
86. Wheaton, W., & Chandel, N. (2011). Hypoxia. 2. Hypoxia regulates cellular metabolism. *American Journal Of Physiology-Cell Physiology*, 300(3), C385-C393. doi: 10.1152/ajpcell.00485.2010.
87. Niecknig, H., Tug, S., Reyes, B., Kirsch, M., Fandrey, J., & Berchner-Pfannschmidt, U. (2012). Role of reactive oxygen species in the regulation of HIF-1 by prolyl hydroxylase 2 under mild hypoxia. *Free Radical Research*, 46(6), 705-717. doi:10.3109/10715762.2012.669041.
88. Zhang, L., Li, L., Liu, H., Prabhakaran, K., Zhang, X., Borowitz, J. L., & Isom, G. E. (2007). HIF-1alpha Activation by a Redox-Sensitive Pathway Mediates Cyanide-induced BNIP3 Upregulation and Mitochondrial Dependent Cell Death. *Free Radical Biology & Medicine*, 43(1), 117–127. doi:10.1016/j.freeradbiomed.2007.04.005.
89. Yurkova, N., Shaw, J., Blackie, K., Weidman, D., Jayas, R., Flynn, B., & Kirshenbaum, L. (2008). The Cell Cycle Factor E2F-1 Activates Bnip3 and the Intrinsic Death Pathway in Ventricular Myocytes. *Circulation Research*, 102(4), 472-479. doi:10.1161/circresaha.107.164731.
90. Yang, Y.-S., Yang, M.-C. W., Guo, Y., Williams, O. W., & Weissler, J. C. (2009). PLAGL2 expression-induced lung epithelium damages at bronchiolar alveolar duct junction in emphysema: bNip3- and SP-C-associated cell death/injury activity. *American Journal of Physiology - Lung Cellular and Molecular Physiology*, 297(3), L455–L466. doi:10.1152/ajplung.00144.2009.
91. Mammucari, C., Milan, G., Romanello, V., Masiero, E., Rudolf, R., & Del Piccolo, P. et al. (2007). FoxO3 Controls Autophagy in Skeletal Muscle In Vivo. *Cell Metabolism*, 6(6), 458-471. doi:10.1016/j.cmet.2007.11.001.

92. Chaanine, A. H., Kohlbrenner, E., Gamb, S. I., Guenzel, A. J., Klaus, K., Fayyaz, A. U., ... Redfield, M. M. (2016). FOXO3a regulates BNIP3 and modulates mitochondrial calcium, dynamics, and function in cardiac stress. *American Journal of Physiology - Heart and Circulatory Physiology*, 311(6), H1540–H1559. doi:10.1152/ajpheart.00549.2016.
93. An, H., Maeng, O., Kang, K., Lee, J., Kim, Y., Paik, S., & Lee, H. (2006). Activation of Ras Up-regulates Pro-apoptotic BNIP3 in Nitric Oxide-induced Cell Death. *Journal Of Biological Chemistry*, 281(45), 33939-33948. doi:10.1074/jbc.m605819200.
94. Prabhakaran, K., Chapman, G., & Gunasekar, P. (2009). BNIP3 up-regulation and mitochondrial dysfunction in manganese-induced neurotoxicity. *Neurotoxicology*, 30(3), 414-422. doi:10.1016/j.neuro.2009.02.012.
95. Kanzawa, T., Zhang, L., Xiao, L., Germano, I., Kondo, Y., & Kondo, S. (2004). Arsenic trioxide induces autophagic cell death in malignant glioma cells by upregulation of mitochondrial cell death protein BNIP3. *Oncogene*, 24(6), 980-991. doi:10.1038/sj.onc.1208095.
96. Daido, S., Kanzawa, T., Yamamoto, A., Takeuchi, H., Kondo, Y., & Kondo, S. (2004). Pivotal Role of the Cell Death Factor BNIP3 in Ceramide-Induced Autophagic Cell Death in Malignant Glioma Cells. *Cancer Research*, 64(12), 4286-4293. doi:10.1158/0008-5472.can-03-3084.
97. Zhang, S., Zhang, Z., Sandhu, G., Ma, X., Yang, X., Geiger, J., & Kong, J. (2007). Evidence of oxidative stress-induced BNIP3 expression in amyloid beta neurotoxicity. *Brain Research*, 1138, 221-230. doi:10.1016/j.brainres.2006.12.086.
98. Shaw, J., Yurkova, N., Zhang, T., Gang, H., Aguilar, F., Weidman, D., ... Kirshenbaum, L. A. (2008). Antagonism of E2F-1 regulated Bnip3 transcription by NF-κB is essential for basal cell survival. *Proceedings of the National Academy of Sciences of the United States of America*, 105(52), 20734–20739. doi:10.1073/pnas.0807735105.
99. Mahon, P., Baril, P., Bhakta, V., Chelala, C., Caulee, K., Harada, T., & Lemoine, N. (2007). S100A4 Contributes to the Suppression of BNIP3 Expression, Chemoresistance, and Inhibition of Apoptosis in Pancreatic Cancer. *Cancer Research*, 67(14), 6786-6795. doi:10.1158/0008-5472.can-07-0440.

100. Farrall, A., & Whitelaw, M. (2009). The HIF1 $\alpha$ -inducible pro-cell death gene BNIP3 is a novel target of SIM2s repression through cross-talk on the hypoxia response element. *Oncogene*, 28(41), 3671-3680. doi:10.1038/onc.2009.228.
101. Tracy, K., Dibling, B. C., Spike, B. T., Knabb, J. R., Schumacker, P., & Macleod, K. F. (2007). BNIP3 Is an RB/E2F Target Gene Required for Hypoxia-Induced Autophagy. *Molecular and Cellular Biology*, 27(17), 6229–6242. doi:10.1128/MCB.02246-06.
102. Okami, J., Simeone, D., & Logsdon, C. (2004). Silencing of the Hypoxia-Inducible Cell Death Protein BNIP3 in Pancreatic Cancer. *Cancer Research*, 64(15), 5338-5346. doi:10.1158/0008-5472.can-04-0089.
103. Murai, M., Toyota, M., Satoh, A., Suzuki, H., Akino, K., Mita, H., ... Imai, K. (2005). Aberrant DNA methylation associated with silencing BNIP3 gene expression in haematopoietic tumours. *British Journal of Cancer*, 92(6), 1165–1172. doi:10.1038/sj.bjc.6602422.
104. Bacon, A., Fox, S., Turley, H., & Harris, A. (2006). Selective silencing of the hypoxia-inducible factor 1 target gene BNIP3 by histone deacetylation and methylation in colorectal cancer. *Oncogene*, 26(1), 132-141. doi:10.1038/sj.onc.1209761.
105. Manka, D., & Millhorn, D. (2006). A Potential Molecular Link Between Aerobic Glycolysis and Cancer. *Cell Cycle*, 5(4), 343-344. doi:10.4161/cc.5.4.2474.
106. Liu, K. E., & Frazier, W. A. (2015). Phosphorylation of the BNIP3 C-Terminus Inhibits Mitochondrial Damage and Cell Death without Blocking Autophagy. *PLoS ONE*, 10(6), e0129667. doi:10.1371/journal.pone.0129667.
107. Park, C. W., Hong, S. M., Kim, E.-S., Kwon, J. H., Kim, K.-T., Nam, H. G., & Choi, K. Y. (2013). BNIP3 is degraded by ULK1-dependent autophagy via MTORC1 and AMPK. *Autophagy*, 9(3), 345–360. doi:10.4161/auto.23072.
108. Giatromanolaki, A. (2004). BNIP3 Expression Is Linked with Hypoxia-Regulated Protein Expression and with Poor Prognosis in Non-Small Cell Lung Cancer. *Clinical Cancer Research*, 10(16), 5566-5571. doi:10.1158/1078-0432.ccr-04-0076.
109. Leo, C., Horn, L., & Hockel, M. (2006). Hypoxia and expression of the proapoptotic regulator BNIP3 in cervical cancer. *International Journal Of Gynecological Cancer*, 16(3), 1314-1320. doi:10.1111/j.1525-1438.2006.00394.x.

110. Schmidt-Kastner, R., Aguirre-Chen, C., Kietzmann, T., Saul, I., Bustos, R., & Ginsberg, M. (2004). Nuclear localization of the hypoxia-regulated pro-apoptotic protein BNIP3 after global brain ischemia in the rat hippocampus. *Brain Research*, 1001(1-2), 133-142. doi:10.1016/j.brainres.2003.11.065.
111. Kim, J., Cho, J., Ha, J., & Park, J. (2002). The Carboxy Terminal C-Tail of BNip3 Is Crucial in Induction of Mitochondrial Permeability Transition in Isolated Mitochondria. *Archives Of Biochemistry And Biophysics*, 398(2), 147-152. doi:10.1006/abbi.2001.2673.
112. Kubli, D. A., Ycaza, J. E., & Gustafsson, Å. B. (2007). Bnip3 mediates mitochondrial dysfunction and cell death through Bax and Bak. *The Biochemical Journal*, 405(Pt 3), 407–415. doi:10.1042/BJ20070319.
113. Landes, T., Emorine, L. J., Courilleau, D., Rojo, M., Belenguer, P., & Arnauné-Pelloquin, L. (2010). The BH3-only Bnip3 binds to the dynamin Opa1 to promote mitochondrial fragmentation and apoptosis by distinct mechanisms. *EMBO Reports*, 11(6), 459–465. doi:10.1038/embor.2010.50.
114. Lee, Y., Lee, H.-Y., Hanna, R. A., & Gustafsson, Å. B. (2011). Mitochondrial autophagy by Bnip3 involves Drp1-mediated mitochondrial fission and recruitment of Parkin in cardiac myocytes. *American Journal of Physiology - Heart and Circulatory Physiology*, 301(5), H1924–H1931. doi:10.1152/ajpheart.00368.2011.
115. Regula, K., Ens, K., & Kirshenbaum, L. (2002). Inducible Expression of BNIP3 Provokes Mitochondrial Defects and Hypoxia-Mediated Cell Death of Ventricular Myocytes. *Circulation Research*, 91(3), 226-231. doi:10.1161/01.res.0000029232.42227.16.
116. Diwan, A., Krenz, M., Syed, F. M., Wansapura, J., Ren, X., Koesters, A. G., ... Dorn, G. W. (2007). Inhibition of ischemic cardiomyocyte apoptosis through targeted ablation of Bnip3 restrains postinfarction remodeling in mice. *The Journal of Clinical Investigation*, 117(10), 2825–2833. doi:10.1172/JCI32490.
117. Vande Velde, C., Cizeau, J., Dubik, D., Alimonti, J., Brown, T., Israels, S., ... Greenberg, A. H. (2000). BNIP3 and Genetic Control of Necrosis-Like Cell Death through the Mitochondrial Permeability Transition Pore. *Molecular and Cellular Biology*, 20(15), 5454–5468.

118. Yin, Z., Pascual, C., & Klionsky, D. J. (2016). Autophagy: machinery and regulation. *Microbial Cell*, 3(12), 588–596. doi:10.15698/mic2016.12.546.
119. Parzych, K. R., & Klionsky, D. J. (2014). An Overview of Autophagy: Morphology, Mechanism, and Regulation. *Antioxidants & Redox Signaling*, 20(3), 460–473. doi:10.1089/ars.2013.5371.
120. Schlie, K., Spowart, J. E., Hughson, L. R. K., Townsend, K. N., & Lum, J. J. (2011). When Cells Suffocate: Autophagy in Cancer and Immune Cells under Low Oxygen. *International Journal of Cell Biology*, 2011, 470597. doi:10.1155/2011/470597.
121. Decuypere, J.-P., Parys, J. B., & Bultynck, G. (2012). Regulation of the Autophagic Bcl-2/Beclin 1 Interaction. *Cells*, 1(3), 284–312. doi:10.3390/cells1030284.
122. Quinsay, M. N., Thomas, R. L., Lee, Y., & Gustafsson, Å. B. (2010). Bnip3-mediated mitochondrial autophagy is independent of the mitochondrial permeability transition pore. *Autophagy*, 6(7), 855–862. doi:10.4161/auto.6.7.13005.
123. Li, Y., Wang, Y., Kim, E., Beemiller, P., Wang, C., & Swanson, J. et al. (2007). Bnip3 Mediates the Hypoxia-induced Inhibition on Mammalian Target of Rapamycin by Interacting with Rheb. *Journal Of Biological Chemistry*, 282(49), 35803-35813. doi:10.1074/jbc.m705231200.
124. Burton, T. R., Eisenstat, D. D., & Gibson, S. B. (2009). Bcl-2 Nineteen kilodalton Interacting Protein (BNIP3) acts as transcriptional repressor of Apoptosis Inducing Factor (AIF) expression preventing cell death in human malignant gliomas. *The Journal of Neuroscience : The Official Journal of the Society for Neuroscience*, 29(13), 4189–4199. doi:10.1523/JNEUROSCI.5747-08.2009.
125. Burton, T. R., Henson, E. S., Azad, M. B., Brown, M., Eisenstat, D. D., & Gibson, S. B. (2013). BNIP3 acts as transcriptional repressor of death receptor-5 expression and prevents TRAIL-induced cell death in gliomas. *Cell Death & Disease*, 4(4), e587–. doi:10.1038/cddis.2013.100.
126. Frank, A., Bonney, M., Bonney, S., Weitzel, L., Koeppen, M., & Eckle, T. (2012). Myocardial ischemia reperfusion injury - from basic science to clinical bedside. *Seminars in Cardiothoracic and Vascular Anesthesia*, 16(3), 123–132. doi:10.1177/1089253211436350.

127. Dorn, G., & Kirshenbaum, L. (2008). Cardiac reanimation: targeting cardiomyocyte death by BNIP3 and NIX/BNIP3L. *Oncogene*, 27(S1), S158-S167. doi:10.1038/onc.2009.53.
128. Kubasiak, L. A., Hernandez, O. M., Bishopric, N. H., & Webster, K. A. (2002). Hypoxia and acidosis activate cardiac myocyte death through the Bcl-2 family protein BNIP3. *Proceedings of the National Academy of Sciences of the United States of America*, 99(20), 12825–12830. doi:10.1073/pnas.202474099.
129. Graham, R. (2004). A unique pathway of cardiac myocyte death caused by hypoxia-acidosis. *Journal Of Experimental Biology*, 207(18), 3189-3200. doi:10.1242/jeb.01109.
130. Sowter, H., Ferguson, M., Pym, C., Watson, P., Fox, S., Han, C., & Harris, A. (2003). Expression of the cell death genes BNip3 and NIX in ductal carcinomain situ of the breast; correlation of BNip3 levels with necrosis and grade. *The Journal Of Pathology*, 201(4), 573-580. doi:10.1002/path.1486.
131. Koukourakis, M., Giatromanolaki, A., Polychronidis, A., Simopoulos, C., Gatter, K., Harris, A., & Sivridis, E. (2006). Endogenous markers of hypoxia/anaerobic metabolism and anemia in primary colorectal cancer. *Cancer Science*, 97(7), 582-588. doi:10.1111/j.1349-7006.2006.00220.x.
132. Lukashova-v.Zangen, I., Kneitz, S., Monoranu, C., Rutkowski, S., Hinkes, B., & Vince, G. et al. (2007). Ependymoma gene expression profiles associated with histological subtype, proliferation, and patient survival. *Acta Neuropathologica*, 113(3), 325-337. doi:10.1007/s00401-006-0190-5.
133. Giatromanolaki, A., Koukourakis, M., Gatter, K., Harris, A., & Sivridis, E. (2007). BNIP3 expression in endometrial cancer relates to active hypoxia inducible factor 1 pathway and prognosis. *Journal Of Clinical Pathology*, 61(2), 217-220. doi:10.1136/jcp.2007.046680.
134. Murai, M., Toyota, M., Suzuki, H., Satoh, A., Sasaki, Y., Akino, K., Ueno, M. et. al. (2005). Aberrant methylation and silencing of the BNIP3 gene in colorectal and gastric cancer. *Clin Cancer Res.*, 11(3), 1021–1027.
135. Calvisi, D. F., Ladu, S., Gorden, A., Farina, M., Lee, J.-S., Conner, E. A., ... Thorgeirsson, S. S. (2007). Mechanistic and prognostic significance of aberrant methylation in the molecular pathogenesis of human hepatocellular carcinoma. *The Journal of Clinical Investigation*, 117(9), 2713–2722. doi:10.1172/JCI31457.

136. Erkan, M., Kleeff, J., Esposito, I., Giese, T., Ketterer, K., & Büchler, M. et al. (2005). Loss of BNIP3 expression is a late event in pancreatic cancer contributing to chemoresistance and worsened prognosis. *Oncogene*, 24(27), 4421-4432. doi:10.1038/sj.onc.1208642.
137. Akada, M. (2005). Intrinsic Chemoresistance to Gemcitabine Is Associated with Decreased Expression of BNIP3 in Pancreatic Cancer. *Clinical Cancer Research*, 11(8), 3094-3101. doi:10.1158/1078-0432.ccr-04-1785.
138. Tan, E., Campo, L., Han, C., Turley, H., Pezzella, F., & Gatter, K. et al. (2007). BNIP3 as a Progression Marker in Primary Human Breast Cancer; Opposing Functions in In situ Versus Invasive Cancer. *Clinical Cancer Research*, 13(2), 467-474. doi:10.1158/1078-0432.ccr-06-1466.
139. Itoh, T., Itoh, A., & Pleasure, D. (2003). Bcl-2-related protein family gene expression during oligodendroglial differentiation. *Journal Of Neurochemistry*, 85(6), 1500-1512. doi:10.1046/j.1471-4159.2003.01795.x.
140. Sandau, U., & Handa, R. (2006). Localization and developmental ontogeny of the pro-apoptotic Bnip3 mRNA in the postnatal rat cortex and hippocampus. *Brain Research*, 1100(1), 55-63. doi:10.1016/j.brainres.2006.05.006.
141. Azad, M. (2010). *The Role of BNIP3 in Proliferation and Hypoxia-Induced Autophagy: Implications for Cancer Therapy* (Doctoral dissertation). University of Manitoba.
142. Brayer, S., Joannes, A., Jaillet, M., Gregianin, E., Mahmoudi, S., Somm  , J. M., . . . Mailleux, A. A. (2017). The pro-apoptotic BAX protein influences cell growth and differentiation from the nucleus in healthy interphasic cells. *Cell Cycle*, 16(21), 2108-2118. doi:10.1080/15384101.2017.1371882.
143. Zinkel, S., Gross, A., & Yang, E. (2006). BCL2 family in DNA damage and cell cycle control. *Cell Death & Differentiation*, 13(8), 1351-1359. doi:10.1038/sj.cdd.4401987.
144. Jamil, S., Sobouti, R., Hojabrpor, P., Raj, M., Kast, J., & Duronio, V. (2005). A proteolytic fragment of Mcl-1 exhibits nuclear localization and regulates cell growth by interaction with Cdk1. *Biochemical Journal*, 387(Pt 3), 659-667. doi:10.1042/BJ20041596.
145. Jamil, S., Stoica, C., Hackett, T.-L., & Duronio, V. (2010). MCL-1 localizes to sites of DNA damage and regulates DNA damage response. *Cell Cycle*, 9(14), 2843-2855. doi:10.4161/cc.9.14.12354.

146. Merlo, G.R., Zerega, B., Paleari, L., Trombino, S., Mantero, S., & Levi, G. (2000). Multiple functions of Dlx genes. *The International journal of developmental biology*. 44(6), 619-26.
147. Cobos, I., Calcagnotto, M., Vilaythong, A., Thwin, M., Noebels, J., Baraban, S., & Rubenstein, J. (2005). Mice lacking Dlx1 show subtype-specific loss of interneurons, reduced inhibition and epilepsy. *Nature Neuroscience*, 8(8), 1059-1068. doi:10.1038/nn1499.
148. Wonders, C., & Anderson, S. (2005). Beyond migration: Dlx1 regulates interneuron differentiation. *Nature Neuroscience*, 8(8), 979-981. doi:10.1038/nn0805-979.
149. de Melo, J. (2005). Dlx1 and Dlx2 function is necessary for terminal differentiation and survival of late-born retinal ganglion cells in the developing mouse retina. *Development*, 132(2), 311-322. doi:10.1242/dev.01560.
150. Chiba, S., Takeshita, K., Imai, Y., Kumano, K., Kurokawa, M., Masuda, S., ... Hirai, H. (2003). Homeoprotein DLX-1 interacts with Smad4 and blocks a signaling pathway from activin A in hematopoietic cells. *Proceedings of the National Academy of Sciences of the United States of America*, 100(26), 15577–15582. doi:10.1073/pnas.2536757100.
151. Chan, D., Hui, W., Wang, J., Yung, M., Hui, L., & Qin, Y. et al. (2016). DLX1 acts as a crucial target of FOXM1 to promote ovarian cancer aggressiveness by enhancing TGF- $\beta$ /SMAD4 signaling. *Oncogene*, 36(10), 1404-1416. doi:10.1038/onc.2016.307.
152. Starkova, J., Gadgil, S., Qiu, Y. H., Zhang, N., Hermanova, I., Kornblau, S. M., & Drabkin, H. A. (2011). Up-regulation of homeodomain genes, *DLX1* and *DLX2*, by *FLT3* signaling. *Haematologica*, 96(6), 820–828. doi:10.3324/haematol.2010.031179.
153. Rejlova, K., Kardosova, M., Slamova, M., Zaliova, M., Alberich-Jorda, M., Trka, J., & Starkova, J. (2016). DLX1 Affects Cell Cycle and Proliferation of Myeloid Leukemia Cells *In Vitro* and *In Vivo*. *Blood*, 128(22), 1666.
154. Nielsen, J., Christiansen, J., Lykke-Andersen, J., Johnsen, A. H., Wewer, U. M., & Nielsen, F. C. (1999). A Family of Insulin-Like Growth Factor II mRNA-Binding Proteins Represses Translation in Late Development. *Molecular and Cellular Biology*, 19(2), 1262–1270.

155. Ioannidis, P., Trangas, T., Dimitriadis, E., Samiotaki, M., Kyriazoglou, I., & Tsipalis, C. et al. (2001). C-MYC and IGF-II mRNA-binding protein (CRD-BP/IMP-1) in benign and malignant mesenchymal tumors. *International Journal Of Cancer*, 94(4), 480-484. doi:10.1002/ijc.1512.
156. Ioannidis, P., Mahaira, L., Perez, S., Gritzapis, A., Sotiropoulou, P., & Kavalakis, G. et al. (2005). CRD-BP/IMP1 Expression Characterizes Cord Blood CD34+Stem Cells and Affects c-myc and IGF-II Expression in MCF-7 Cancer Cells. *Journal Of Biological Chemistry*, 280(20), 20086-20093. doi:10.1074/jbc.m410036200.
157. Hammer, N., Hansen, T., Byskov, A., Rajpert-De Meyts, E., Grøndahl, M., & Bredkjær, H. et al. (2005). Expression of IGF-II mRNA-binding proteins (IMPs) in gonads and testicular cancer. *Reproduction*, 130(2), 203-212. doi:10.1530/rep.1.00664.
158. Dimitriadis, E., Trangas, T., Milatos, S., Foukas, P., Gioulbasanis, I., & Courtis, N. et al. (2007). Expression of oncofetal RNA-binding protein CRD-BP/IMP1 predicts clinical outcome in colon cancer. *International Journal Of Cancer*, 121(3), 486-494. doi:10.1002/ijc.22716.
159. Huang, X., Zhang, H., Guo, X., Zhu, Z., Cai, H., & Kong, X. (2018). Insulin-like growth factor 2 mRNA-binding protein 1 (IGF2BP1) in cancer. *Journal of Hematology & Oncology*, 11, 88. doi:10.1186/s13045-018-0628-y.
160. Mahaira, L., Katsara, O., Pappou, E., Iliopoulou, E., Fortis, S., & Antsaklis, A. et al. (2014). IGF2BP1 Expression in Human Mesenchymal Stem Cells Significantly Affects Their Proliferation and Is Under the Epigenetic Control of TET1/2 Demethylases. *Stem Cells And Development*, 23(20), 2501-2512. doi:10.1089/scd.2013.0604.
161. Shimizu, M. (2016). Insulin-Like Growth Factor-II. *Handbook Of Hormones*, 164-e19C-5. doi:10.1016/b978-0-12-801028-0.00150-1.
162. Luo, Y., Sun, R., Zhang, J., Sun, T., Liu, X., & Yang, B. (2015). miR-506 inhibits the proliferation and invasion by targeting IGF2BP1 in glioblastoma. *American Journal of Translational Research*, 7(10), 2007–2014.
163. Smith, W., DeWitt, D., & Garavito, R. (2000). Cyclooxygenases: Structural, Cellular, and Molecular Biology. *Annual Review Of Biochemistry*, 69(1), 145-182. doi:10.1146/annurev.biochem.69.1.145.

164. Kurumbail, R. (2001). Cyclooxygenase enzymes: catalysis and inhibition. *Current Opinion In Structural Biology*, 11(6), 752-760. doi:10.1016/s0959-440x(01)00277-9.
165. Li, J., Kong, X., Zhang, J., Luo, Q., Li, X., & Fang, L. (2013). MiRNA-26b inhibits proliferation by targeting PTGS2 in breast cancer. *Cancer Cell International*, 13, 7. doi:10.1186/1475-2867-13-7.
166. Wang, D., Xia, D., & DuBois, R. N. (2011). The Crosstalk of PTGS2 and EGF Signaling Pathways in Colorectal Cancer. *Cancers*, 3(4), 3894–3908. doi:10.3390/cancers3043894.
167. Huang, F., Lin, C., Shi, Y., & Kuerban, G. (2013). MicroRNA-101 Inhibits Cell Proliferation, Invasion, and Promotes Apoptosis by Regulating Cyclooxygenase-2 in Hela Cervical Carcinoma Cells. *Asian Pacific Journal Of Cancer Prevention*, 14(10), 5915-5920. doi:10.7314/apjcp.2013.14.10.5915.
168. Scholzen, T., & Gerdes, J. (2000). The Ki-67 protein: From the known and the unknown. *Journal Of Cellular Physiology*, 182(3), 311-322. doi:10.1002/(sici)1097-4652(200003)182:3<311::aid-jcp1>3.0.co;2-9.
169. Stacey, D. (2003). Cyclin D1 serves as a cell cycle regulatory switch in actively proliferating cells. *Current Opinion In Cell Biology*, 15(2), 158-163. doi:10.1016/s0955-0674(03)00008-5.